Infrared Spectroscopy of Gas Phase Ions: Using Infrared Multi-photon Spectroscopy to Investigate Ionization Sites and Hydrogen Bonding in Gaseous Ions.

A DISSERTATION
SUBMITTED TO THE FACULTY OF THE GRADUATE SCHOOL
OF THE UNIVERSITY OF MINNESOTA
BY

Jacob C. Schmidt

IN PARTIAL FULFILLMENT OF THE REQUIREMENTS
FOR THE DEGREE OF
DOCTOR OF PHILOSOPHY

Dr. Steven R. Kass, Advisor

July, 2013

Acknowledgments

I'd like to thank my advisor, Professor Steven Kass, for taking me into his research group and giving me the opportunity to work on the projects documented here. Without his teachings, advice, and enthusiasm none of this would have been possible. I'd also like to thank the members of the Kass group I was fortunate to work with: Dr. Zhixin Tian and Dr. Matthew Meyer for introducing me to the mass spectrometers; Dr. Kris Murphy for keeping the Kass group lively; and Dr. Lev Lis, Mr. Evgeniy Beletskiy, Mr. Alireza Shokri, and Mr. Masoud Samet for their expertise at producing synthetic compounds.

I'd like to thank the past and present members of the mass spectrometry facility at the University of Minnesota whom I was able to work with: Dr. Dana Reed, Dr. Joseph Dalluge, and Mr. Sean Murray. They greatly broadened my experiences with mass spectrometry, analytical chemistry, and customer service.

I'd like to thank my parents for supporting me and giving me a loving home to always return to. My brothers Zach, Jeremy, Andrew, Simon, and Patrick are thanked for giving me encouragement and people to look up to.

Finally, I'd like to thank my wife, Mallory. Because of her I strive to be the best person I can be.

Abstract

In this work a novel instrument was developed to obtain infrared multiphoton dissociation (IRMPD) spectra of gas phase ions. This was done by coupling a tunable infrared laser with a Fourier transform mass spectrometer (FTMS). Gas phase ions were trapped in the FTMS cell and irradiated with infrared light for a period of time, typically 1-60 seconds, and the fragmentation of the parent ions was observed. Fragmentation was plotted vs. infrared wavelength to generate infrared action spectra. Experimental spectra were compared to computational spectra to gain insight into the gas phase structure of the irradiated ions. Some species were then derivatized to experimentally assign infrared absorption bands.

The first objective was the determination of the ionization site of the $(M+H)^+$ ion of *p*-aminobenzoic acid (1) formed during positive mode electrospray ionization (ESI) from either methanol/water or acetonitrile solutions. The two most likely protonation sites are at the amino or carboxyl functional groups. Protonated *p*-aminobenzoic acid ions were irradiated for 20 seconds from 2800-4000 cm^{-1}. Computational predictions for both amino-protonated and carboxy-protonated ions were generated. When methanol/water was used as the ESI solvent there was an excellent match between experimental and the carboxy-protonated computational spectra, indicating that the carboxy-protonated structure was generated. When acetonitrile was used as the ESI solvent the experimental spectrum is identical to the carboxy-protonated structure, however, only 70% of the ions fragment. This indicates that a 70 : 30 ratio of carboxy : amino protonated structures were generated.

A series of poly-hydroxy hydrocarbons (polyols) were investigated via IRMPD. Of particular interest is the extent of intramolecular hydrogen bonding in polyols containing as many as seven hydroxyl groups (i.e. **2**), as well as the binding characteristics of a series of

anions to triol **3**. The infrared action spectrum of polyol **2** clustered with chloride anion shows the presence of several hydroxyl groups with varying hydrogen bond strengths indicating that a second, and even third, solvation shell forms around the chloride anion. Chlorine and sulfur anions prefer a geometry with the maximum of three hydrogen bonds while oxygen anions are presumably too small and thus only utilizes two of the three possible hydrogen bonds.

Finally, the ionic structure of proline clustered to chloride anion was examined by IRMPD. Whether proline exists in its zwitterionic or neutral structure is not well understood. An exhaustive computational analysis was conducted on multiple neutral and zwitterionic conformers and the computed spectra were compared to the experimental infrared action spectrum. Furthermore, infrared action spectra of proline-d_2 and proline-d_7 were obtained to empirically assign infrared absorption features. It was determined that while the observed IRMPD spectrum suggests the neutral structure was generated as the sole ion, a more in depth study of the photokinetic data and computations indicate that both the neutral and zwitterionic structures are generated in approximately equal proportions.

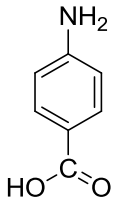

1

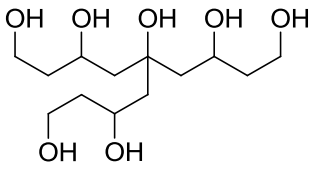

2

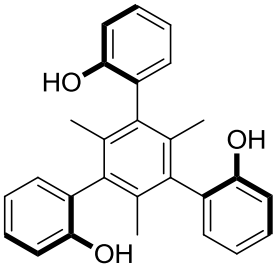

3

Table of Contents

List of Tables

Chapter 2:

Chapter 3:

Chapter 5:

List of Figures

Chapter 1:

Chapter 2:

Chapter 3:

Chapter 4:

Chapter 5:

List of Abbreviations

B3LYP	Becke three-parameter hybrid exchange plus Lee-Yang-Parr correlation density functional
CCSD(T)	Coupled cluster theory with single, double, and triple excitations
CID	Collision-induced dissociation
DC	Direct current
DFT	Density functional theory
DMSO	Dimethyl sulfoxide
ESI	Electrospray ionization
FT	Fourier transform
H/D	Hydrogen / deuterium
ICR	Ion cyclotron resonance
IR	Infrared
IRMPD	Infrared multiphoton photodissociation
IRPD	Infrared photodissociation
IVR	Intramolecular vibrational relaxation
KTA	Potassium titanyl arsenate
KTP	Potassium titanyl phosphate
LBHB	Low barrier hydrogen bond
MMFF	Molecular mechanics force field
MS	Mass spectrometry
M06-2X	Minnesota 2006 suite of density functionals
N	Neutral
Nd:YAG	Neodymium doped yttrium aluminum garnet
NMR	Nuclear magnetic resonance
OPO/OPA	Optical parametric oscillator / optical parametric amplifier
PA	Proton Affinity
*p*AB	*para*-aminobenzoic acid
PVC	Polyvinyl chloride
RF	Radio frequency
SWIFT	Stored waveform inverse Fourier transform
ZW	Zwitterion

Chapter 1

Introduction

Ionization Site

Electrospray ionization mass spectrometry (ESI-MS) constitutes a large, and still growing, portion of the analytical, pharmaceutical, and academic sciences. The versatility of ESI-MS, discussed in more depth later on, is what makes it a very powerful tool. In essence, molecules are transferred from bulk solution to the gas phase and they are ionized so they can be detected with a mass spectrometer. The exact mechanism for this process, however, is not well understood, but the most widely accepted explanations are called the ion evaporation model[1] and the charge residue model.[2] In both models, ESI droplets are formed containing ionized analyte molecules. These droplets continuously decrease in size through solvent evaporation, concentrating the amount of charged species in the droplet. According to the ion evaporation model, the droplet will reach a threshold in which the coulombic repulsion of the ions overcomes the solvation energy and ions are ejected from the droplet. In the charge residue model, the droplet will undergo fission, creating smaller daughter ions which continue to lose solvent to evaporation. These processes continue until only the naked ion remains.

Experimentally distinguishing between these two models has not yet been accomplished, though they may affect the structure of the resulting ion differently. However, there is evidence that the observed ionization site under similar electrospray conditions can be altered by simply changing the solvent composition.[3]

The question of ionization site arises due to the difference between the gas phase and solution phase structures for some ions. For example, *p*-hydroxybenzoic acid is known to be deprotonated at the carboxylic acid in solution to generate the carboxylate ion, but in the gas phase deprotonation occurs at the phenol to generate the phenoxide (scheme 1.1).[4] During the ESI process, the analyte is transported from bulk solution to the gas phase and is exposed to a gradient of solvating conditions during evaporation of the ESI droplet. Whether the solution phase structure is retained or changes during the ESI process has been shown to be dependent on the electrospray solvent used.[3]

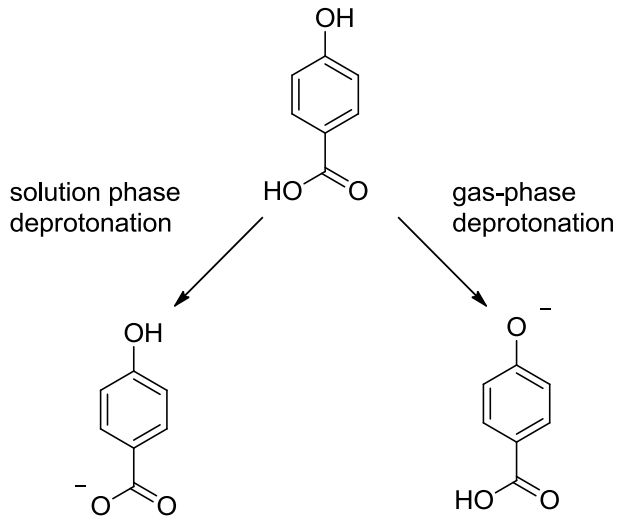

Scheme 1.1. Thermodynamic deprotonation sites of *p*-hydroxybenzoic acid in solution and in the gas phase.

In chapter two the effect of the solvent used on the ionization site of *p*-aminobenzoic acid during electrospray ionization will be investigated. A 3:1 ratio of methanol to water will be compared to acetonitrile. The gas phase structures of ions generated from the respective solvent mixtures will be probed by infrared multiphoton spectroscopy (IRMPD).

Neutral vs. Zwitterionic Structures

It is well known that in a neutral pH aqueous solution the twenty natural amino acids exist as zwitterionic compounds. That is, species that have both a positive and negative charge site (figure 1.1). In the gas phase, however, it is well accepted that all 20 amino acids adopt their neutral (i.e. nonzwitterionic) forms.[5] This difference indicates that the environment around amino acids is extremely important in determining their

structure. While the effect of water molecules on the form of the amino acid has been well studied,[6] the effect of charged species is less well understood. This is an important distinction because the local environment in an enzymatic active site is highly charged.

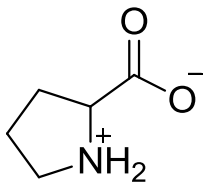

Figure 1.1 Zwitterionic structure of proline.

In chapter five the gas phase structures of proline clustered to chloride will be studied. Gas phase ions were generated via electrospray ionization by subjecting a solution of the amino acid with ammonium chloride. Ionization conditions were optimized to favor generation of the clustered anion. Infrared multiphoton dissociation was then used to probe the structure of the complex by monitoring the dissociation of the ion as a function of the wavelength of the infrared light.

Hydrogen Bonded Networks

Hydrogen bonding has become an increasingly important scientific topic. While hydrogen bonding is, of course, essential for life as we know it, it has also become a powerful tool for catalysis[7], and yet there is still much room for innovation.[8] A new class of hydrogen bonding catalysts involving multiple hydroxyl groups arranged in an intramolecular hydrogen bonding network may prove to be extremely useful for synthetic chemists.

Understanding hydrogen bonding is also central to understanding how enzymatically catalyzed processes occur. For example, the strength of hydrogen bonds measured in solution are <10 kcal mol^{-1},[9] but this does not account for enzymatic processes that require stabilizations of 20 kcal mol^{-1}or more.[10] To account for this discrepancy, low barrier hydrogen bonds (LBHB) were proposed. This class of hydrogen bonds consists of an unusually short hydrogen bond distance of less than 2.5 Å,[11] but this idea is controversial due to the lack of sufficient experimental evidence[12]; no hydrogen bond has been measured in solution stronger than 10 kcal/mol.[13]

Another explanation has been proposed that consists of a multiple hydrogen bond network to account for the large stabilizations seen in nature.[14] Rather than one or two unusually strong hydrogeon bonds, a network of otherwise ordinary intramolecular hydrogen bonds may collectively stabilize transition state energies in enzymatic processes. This can be seen in the crystal structure of the Charcot-Leyden chloride(ClC) channel (figure 1.2) where the chloride anion is interacting with four hydrogen bond donors.[15]

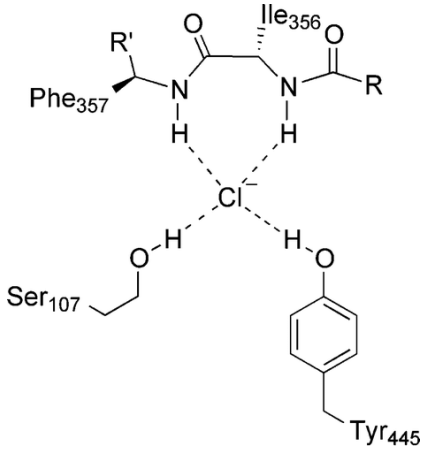

Figure 1.2. Diagram of Charcot-Leyden chloride channel depicting the binding of chloride anion via multiple hydrogen bonds.

In chapter three the interaction between triphenol **1** and related compounds with multiple anions will be probed. In particular, the infrared absorption, measured by IRMPD, of these triphenol anion clusters can give insight into the hydrogen bonding nature of the hydroxyl groups. By modifying triphenol **1** we can also constrain its geometry to directly control the number of hydrogen bonds in the lowest energy conformer.

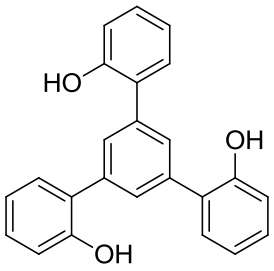

1

In chapter four the effect of multiple hydrogen bonds between chloride anion and a novel polyol possesing seven hydroxyl groups will be investigated to determine the effect of a network of hydrogen bonds in a single complex. This will be done by monitoring the IRMPD spectrum of the polyol cluster ion for distinct hydroxyl absorptions and assigning them to the different hydrogen bonds in the hydrogen bonding network.

Infrared Multiphoton Dissociation

Infrared spectroscopy is the study of molecules based on the absorption of infrared light by individual or combinations of chemical bonds. In order for these bonds to be IR active, their vibrational mode must constitute a change in the dipole moment of the

molecule. Some of these vibrational modes include stretching, bending, scissoring, rocking, wagging, and twisting. These vibrational modes correspond to the infrared portion of the electromagnetic spectrum (i.e. 500-4000 cm^{-1}). Because of this, these chemical bonds will absorb infrared light at resonant frequencies in this energy range. In a typical Fourier transform infrared (FT-IR) experiment, infrared light is passed through a compound of interest and the resulting absorbance/transmission spectrum is obtained. Such an approach typically cannot be used for the study of gas phase ions, however, because the effective concentration of the charged particles is far too small to induce a significant infrared absorption. This has led researchers around the world to develop IR action spectroscopy.[16] In this approach the absorption of infrared light is reported or made apparent by inducing fragmentation of an ion, a process that is readily detected with a mass spectrometer.

Infrared multiphoton dissociation (IRMPD) is the fragmentation of gas phase ions via irradiation with multiple sequential infrared photons. If the frequency of a vibrational mode matches the frequency of infrared light emitted, the photon will be absorbed and the ion will be excited into a more energetic vibrational state. The vibrationally excited ion must relax to the ground vibrational state before absorbing a second photon, due to the anharmonicity of the excited ion. This anharmonicity results in vibrational modes that are no longer resonant with the IR photon, and thus IR absorption is much less efficient. This relaxation is done through a fast process called intramolecular vibrational relaxation (IVR) and effectively converts the vibrational energy into thermal energy. When a sufficient number of absorption/relaxation processes occur, the ion may gain enough internal energy to overcome the barrier to ion fragmentation.

Instrument Design

A commercial optical parametric oscillator / optical parametric amplifier (OPO/OPA) laser system was chosen as the source of infrared light due to its ability to produce infrared frequencies from 2500 cm^{-1} to 4000 cm^{-1} as well as its bench-top nature. OPO/OPA lasers require a pump source of 532 nm which can be achieved by frequency doubling the fundamental frequency (1064 nm) of readily available neodymium doped yttrium aluminum garnet (Nd:YAG) IR lasers. Through non-linear optical processes, the OPO stage of the tunable laser generates IR light from 2500 cm^{-1} to 4000 cm^{-1} which targets O-H (3200-3600 cm^{-1}), N-H (3300-3500 cm^{-1}), and C-H (2850-3300 cm^{-1}) stretches. The intensity of this IR light, however, is not powerful enough to induce IRMPD of the gas phase ions of interest, and thus the OPA stage is required. By frequency mixing the tunable IR with the fundamental frequency of the Nd:YAG laser, the IR photons are multiplied, and thus the resulting IR power is of analytical significance. (The measured infrared power was 1 mJ/pulse at 2500 cm^{-1} followed by a sharp increase to 6 mJ/pulse at 2800 cm^{-1} then a roughly linear increase to 26 mJ/pulse at 4000 cm^{-1}.)

Infrared light is strongly absorbed by water at many wavelengths such that even atmospheric water vapor significantly reduces the effective IR power of our system. Because of this, interfacing an OPO/OPA laser with a mass spectrometer requires actively drying the atmosphere that the laser light travels. This was accomplished using a Parker FT-IR purge gas generator which lowered the relative humidity to effectively 0% as read by a Fisher model 06-664-37 hygrometer. The entire path length of the laser

was enclosed by acrylic boxes and PVC pipe and purged with dry air for >30 minutes to ensure no infrared absorption by gaseous water.

Mass spectrometry is a natural tool for studying IRMPD of gas phase ions. Fourier transform ion cyclotron resonance mass spectrometry (FT-ICR-MS) provides flexible ion trapping to allow for long IR irradiation times, if desired, and is also capable of high sensitivity and very high resolution mass detection which is useful in identifying fragmentation products. Many ionization techniques are compatible with FT-ICR-MS, including electron impact ionization, chemical ionization, and the technique of interest; electrospray ionization. By generating ions via ESI, trapping them in an ICR cell, irradiating with tunable infrared light, and detecting fragmentation products, infrared action spectra can be obtained which provide a great deal of insight into the structures of the gas phase ions.

References

1. Iribarne, J.V., Thomson, B.A., *J. Chem. Phys.***1976**, 64, 2287-2294.
2. Dole, M., Mack, L.L., Hines, R.L. Mobley, R.C., Ferguson, L.D., Alice, M.B., *J. Chem. Phys.* **1968,** 49, 2240-2249.
3 . (a) Tian, Z.; Kass, S. R. *Angew. Chemie, Int. Ed. Engl*. **2009**, *48*, 1321-1323.
(b) Schmidt, J.; Meyer, M.M.; Spector, I.; Kass, S.R. *J. Phys. Chem. A.* **2011,** *115*, 7625-7632.
4. Kebarle, P., McMahon, T. B. *J. Am. Chem. Soc.* **1977,** 99, 2222-2230.
5. (a) Godfrey, P.D., Brown, R.D., *J. Am. Chem. Soc*. 117 **1995**, 2019.
(b) Chapo, C. J.; Paul, J. B.; Provencal, R. A.; Roth, K.; Saykally, R. J. *J. Am. Chem. Soc*. **1998**, 120, 12956.
6. Gordon, M.; Jensen, J., *J. Am. Chem. Soc.* **1995,** *117*, 8159-8170.
7. (a) Schreiner, P. R.; Wittkopp, A. *Org. Lett.* **2002**, *4*, 217-220.
(b) Takemoto, Y. *Org. Biomol. Chem*. **2005**, *3*, 4299-4306.
(c) Taylor, M. S., Jacobsen, E. N., *Angew. Chem. Int. Ed.* **2006**, *45*, 1520-1543.
8. Shokri, A., Schmidt, J., Wang, X., Kass, S. *J. Am. Chem. Soc.*, **2012**, 134 (4), 2094–2099.
7. Guthrie, J. P. *Chem. Biol.* **1996**, 3, 163– 170.
8. (a) Jencks, W. P. *Adv. Enzymol. Relat. Areas Mol. Biol.* **1975**, 43, 219– 410.
(b) Jencks, W. P. *Acc. Chem. Res.* **1976**, 9, 425– 432.
9. (a) Cleland, W. W. *Biochemistry* **1992**, 31, 317– 319.
(b) Gerlt, J. A.; Gassman, P. G. *Biochemistry* **1993**, 32, 11943– 11952.
(c) Gerlt, J. A.; Gassman, P. G. *J. Am. Chem. Soc.* **1993**, 115, 11552– 11568.
12. Schutz, C.N., Warshel, A., *Proteins*. **2004**, 55, 711-723.
13. Guthrie, J.P., *Chem. Biol.*, **1996**, 3, 163-170.
11. Shokri, A., Abedin, A., Fattahi, A., Kass, R. *J. Am. Chem. Soc.*, **2012**, 134 (25), 10646–10650
15. (a) Dutzler, R., Campbell, E. B., Cadene, M., Chait, B. T., MacKinnon, R. *Nature* **2002**, 415, 287−294. (b) Dutzler, R., Campbell, E. B., MacKinnon, R. *Science* **2003**, 300, 108−112.
(c) Accardi, A., Miller, C. *Nature* **2004**, 427, 803−807.
(d) Miller, C., *Nature* **2006**, 440, 484−489.
16. (a) Duncan, M.A*.,* Int. Rev. Phys. Chem. **2003***,* 22, 407*.*
(b) Oomens*, J.,* van Roij*, A.J.A.,* Meijer*, G.,* von Helden, G.*,* Astrophys. J. **2000***,* 542, 404–410*.*
(c) Price, W.D., Schnier, P.D., Williams, E.R., *Anal. Chem.*, **1996**, 68 (5), 859–866.

Chapter 2

Reprinted with permission from *The Journal of Physical Chemistry A* **2011** *115* (26), 7625-7632.

An Infrared Multiphoton Dissociation Spectroscopy Study of Protonated *p*-Aminobenzoic Acid: Does Electrospray Ionization Afford the Amino- or Carboxy-Protonated Ion?

Introduction

Acid-base reactions are among the most important in all of chemistry and play a particularly critical role in biochemical transformations.[1] The structures of protonated and deprotonated ions, consequently, are of tremendous significance in many reactions including enzyme-catalyzed processes. Ionization sites, however, may vary with the presence or absence of a substituent, the solvent, and the local environment.[2] As a result, it is not surprising that the most stable charged-site in a bi- or polyfunctional molecule may be different in liquid media and the gas phase.[2b,3,4] This possibility is typically ignored when carrying out electrospray ionization (ESI) mass spectrometry studies. That is, it is commonly assumed that the location of the charge is preserved upon ESI even though the position and the nature of the charged group can have a direct bearing on the resulting structural information that is obtained.

We recently reported that the most basic site of *p*-aminobenzoic acid (*p*AB) in the gas- phase is the carboxyl group whereas it is well-known to be the amino substituent in aqueous media.[4] The structure of the resulting $(M + 1)^+$ ion was interrogated by hydrogen-deuterium (H/D) exchange and collision-induced dissociation (CID). The *O*-

protonated ion was found to incorporate two deuterium atoms upon exposure to ethanol-OD in accord with the carboxy-protonated structure whereas the *N*-protonated ion only underwent one charge-remote H/D exchange of the carboxy group ~25 times less rapidly. This enabled us to determine that a structural reversal occurred upon ESI from a methanol/water solution and that the more stable gas-phase structure was obtained. When an acetonitrile/water mixture was used the liquid-phase ion was detected.

Similar structural results were also found for the $(M - 1)^-$ ions of tyrosine and *p*-hydroxybenzoic acid using reactivity studies and photoelectron spectroscopy.[3] In the latter case, however, the assignments of the ionization sites were reversed, and this led us to suggest that the electrospray source conditions can alter the isomeric composition of the sprayed ion. A wavelength-dependent infrared multiphoton photodissociation (IRMPD) study by Oomens et al. on the same anions led to similar results, but they concluded (erroneously) that only liquid-phase species are produced by ESI.[5] That is, the change in the ionization site upon going from CH_3OH/H_2O to CH_3CN or DMSO reflects the structure of the ions in these solvents. Given this discrepancy, and the widespread use of ESI for obtaining structural information, we decided to reinvestigate the isomeric structure of protonated *p*-aminobenzoic acid. Herein, we present the infrared action spectra of this ion generated by ESI from two different solvents. The experimental results are supplemented with DFT calculations, and an unwarranted assumption in the work by Oomens et al. is pointed out.

Experimental Section

A Fourier transform mass spectrometer (FTMS) consisting of a 3 T superconducting magnet, an IonSpec ESI cart with a modified (more flexible) inlet system which has previously been described,[6] and the Omega ver. 9 data system was used for these studies. The 2.75" blank flange at the end of the instrument was replaced by one with a 1" CaF_2 window (Kurt Lesker) to enable IR radiation to enter into the 6" long by 2.5" diameter gold-plated cylindrical ion cyclotron resonance (ICR) cell. To reduce scattering and IR light losses, the wire mesh attached to the end plate of the ICR cell by the electron ionization filament was removed.

A Surelite II unseeded Nd:YAG laser (Continuum) that produced 7 ns pulses of 1064 nm light with a 7 mm beam diameter and a smoothed beam profile to avoid hot spots provided 510 mJ/pulse of power at a repetition rate of up to 10 Hz. Two dielectric mirrors were used to steer the light into a telescope at the entrance of an optical parametric oscillator/optical parametric amplifier laser (OPO/OPA, Laser Vision) to reduce the spot size by 10%. The resulting beam was split into two paths and the reflected portion (40%) was passed through a potassium titanyl phosphate ($KTiOPO_4$, KTP) doubling crystal to generate 532 nm (green) photons. This light was brought into an OPO cavity containing a larger KTP crystal on a motor mount where the intensity is built up, optical parametric generation takes place, and photons with two new wavelengths are produced. Their frequencies vary as a function of the incident light on the moveable KTP crystal over a range in the visible (710 – 885 nm) and the infrared (1334 – 2122 nm or 4712 – 7498 cm^{-1}). The latter radiation is sometimes referred to as the idler component and it is combined with the transmitted 1064 nm photons through a series of four rotatable potassium titanyl arsenate ($KTiOAsO_4$, KTA) crystals. This results in the transformation of 1064 nm photons via difference frequency generation into

near (4712 – 7498 cm^{-1}) and mid (1900 – 4686 cm^{-1}) IR light and its subsequent amplification. A stack of silicon wave plates mounted at Brewster's angle filters out the undesired wavelengths and enables the mid-IR radiation to pass out of the instrument. The energy of the resulting IR light was 26 mJ/pulse at 4000 cm^{-1} but this power diminishes in an approximately linear fashion to 6 mJ/pulse at 2800 cm^{-1} and then falls off rapidly to 1 mJ/pulse at 2500 cm^{-1}; it was a bit less (~0.8 mJ/pulse) at 2000 cm^{-1}. All of the IR power measurements were carried out using a Spectra Physics model 407A thermopile and analog reader whereas an Ophir thermal head (model 30A-P) and meter was used for the Nd:YAG laser.

To obtain IR action spectra, the IR light emerging from the OPO/OPA laser (which sits on a 6' long laser table) was directed with a 1" silver mirror past an on/off mechanical shutter with a 15 ms response time (Electrical-Optical Products Co., model SH10) to a series of two 2" silver mirrors where the height of the beam was adjusted before being passed on to a chromium/gold-coated 2" focusing mirror (Janos) with a 100 cm focal length (Figure 2.1). The converging IR light was guided through the middle of the CaF_2 window so that the focal point was located at the center of the ICR cell; a lens was not used because their focal length typically changes with wavelength. At the laser exit the IR beam was ~3/16" in diameter and it expanded to ~1" x 1/2" after traveling ~2.5 m to the concave mirror, but was reduced to a pencil thin line (~1/32") about 1/8" in length at the focal point; this was determined outside of the FTMS by placing a 2" silver mirror into the light path and reflecting the beam to a convenient location. Alternatively, if an image rotator consisting of 3 mirrors was inserted between the OPO and OPA stages, then a smaller beam was produced at the focusing mirror (~7/8" x 7/16") and a rounder spot was obtained at the focal point (~1/16" x 1/16"). The latter arrangement was ultimately used to obtain all of the spectra reported in this work.

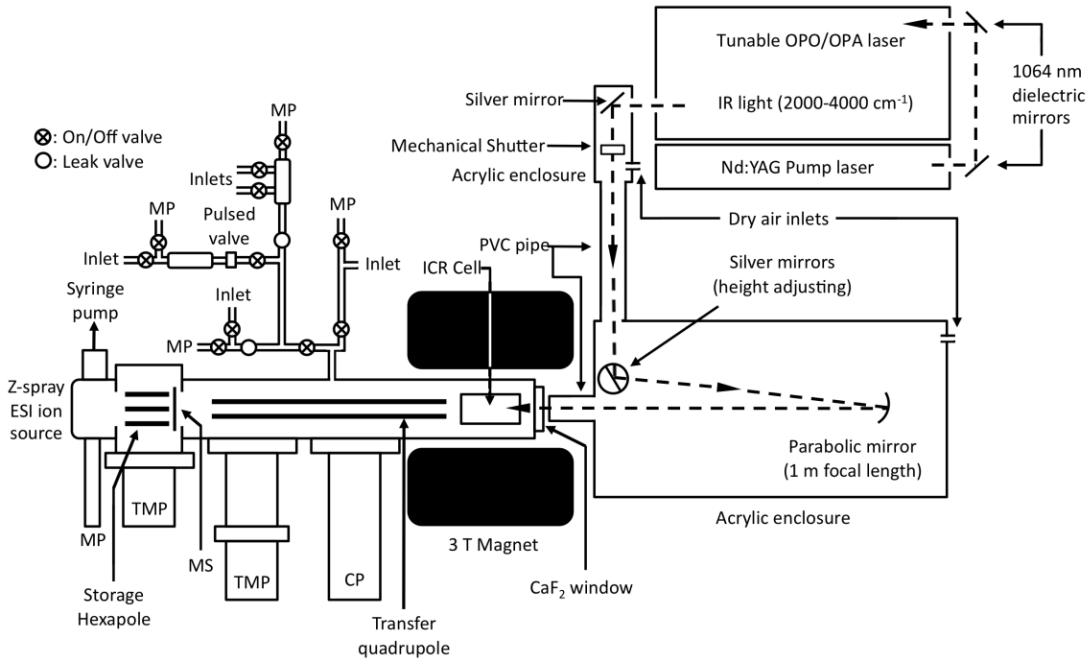

Figure 2.1. Schematic of the IRMPD/FTMS apparatus where the following abbreviations were used: CP = cryopump, MP = mechanical pump, MS = mechanical shutter, and TMP = turbomolecular pump.

In carrying out these IR measurements, it was essential to remove atmospheric moisture from the beam path since water strongly absorbs IR radiation between 3500 – 4000 cm^{-1}. This was accomplished by placing the optical elements external to the OPO/OPA laser along with the mechanical shutter in two different acrylic boxes and connecting them with 2" diameter PVC pipe so that the system up to the CaF_2 window could be purged with large flows of dry air. The resulting relative humidity was continually monitored and was maintained at ≤ 5%; the reading on a Fisher model 06-664-37 hygrometer was 0.1% but this device has an absolute uncertainty of 5.5% in this range. This was accomplished by passing the air through a 20' long by 3/8" diameter copper coil filled with activated molecular sieves and cooled down to -78 ˚C. After each use, the trap was regenerated over night by heating it under vacuum.

Electrospray ionization was employed to generate $GlyH^{+}\cdots Gly$, $Arg\cdots Li^{+}$, and the $(M + 1)^{+}$ ion of *p*-aminobenzoic acid. The first two ions fragmented readily and were examined to verify that literature data could be reproduced.[7-9] Subsequently, the photofragmentation of protonated *p*-aminobenzoic acid was explored. In this case it proved necessary to carry out extensive cooling of the ion to reliably observe fragmentation. This was accomplished by pulsing argon gas up to a constant pressure of ~10^{-6} Torr for 5 – 10 s, and then allowing a 15 s delay for the system to equilibrate and the pressure to drop below 2 x 10^{-8} Torr before irradiating the ions. Isolation of the parent ion using an arbitrary waveform before photofragmenting it was found to have no effect on the resulting spectrum other than to improve the signal-to-noise ratio, so the reported spectra were taken after isolation of the precursor ion.

Data collection was automated by interfacing the FTMS and Laser Vision computers so that the laser wavelength could be selected, the shutter could be opened and closed at selected times, and the resulting photofragmentation mass spectrum could be labeled and stored in a file such that the whole process could be repeated over a user specified step–size and wavelength range.[9] In this way, spectra were obtained by plotting the fragmentation (%) of the irradiated ion versus wavelength. The resulting data could be normalized for the irradiation time (t) and the laser power (P) at a given wavelength using eq. 2.1, where n was determined to be 2.9 at 10 Hz from a log-log plot of the photofragmentation rate vs the laser power (see below). A similar equation with n = 1 has been given previously,[10] but it is only appropriate for single photon processes. In this work no corrections to the intensities were made since $t_{irradiation}$ = 20 s at each wavelength, the changes in power at the different absorption band positions were small, and a number of additional factors can affect the observed intensities.[11]

$$\text{Fragmentation (\%)} = (100 \times (\Sigma I_{\text{fragment ions}})/(\Sigma I_{\text{fragment ions}} + I_{p\text{AB}}))/(t_{\text{irradiation}} \times P^{n}) \quad (2.1)$$

Hydrogen-deuterium exchange experiments were carried out on the $(M + 1)^+$ ion with EtOD at ~5 x 10^{-8} Torr after exposing the gas inlet system and the ICR cell to ~7 x 10^{-7} Torr of the deuterated reagent overnight (15 h) so as to equilibrate any exchangeable sites on the walls of the instrument. The resulting isotopic envelope was subsequently irradiated.

Carbon NMR data were obtained with a Varian Unity 300 MHz spectrometer at a ^{13}C field strength of 75.4 MHz. The hydrogen chloride salt of *p*-aminobenzoic acid was prepared for this experiment by dissolving *p*AB in CH_3CN and adding concentrated HCl to this solution. The desired salt formed as a precipitate, and was filtered and dried under vacuum using a mechanical pump.

Computational Methods.

B3LYP[12] and M06-2X[13] geometry optimizations were carried out using the cc-pVDZ and cc-pVTZ basis sets,[14] and vibrational frequencies were then computed for all of the resulting structures. Single-point energies on the cc-pVDZ geometries were also calculated using the cc-p-VTZ basis set. All of these computations were carried out at the Minnesota Supercomputer Institute for Advanced Computational Research using Gaussian 09.[15] The resulting energies reported herein correspond to enthalpies and have been corrected to 298 K. Unscaled vibrational frequencies were used for this purpose, but small vibrations which contribute more than ½(RT) to the temperature correction were replaced by 0.3 kcal mol^{-1}.

Results and Discussion

An aqueous methanol solution of *p*-aminobenzoic acid afforded an abundant $(M + 1)^+$ ion signal at *m/z* 138 upon spraying the sample into our FTMS. This ion was

isolated and collisionally cooled with a pulse of argon gas up to a steady state pressure of ~10^{-6} Torr for 5-10 s. After waiting 15 s for the pressure to drop below 2 x 10^{-8} Torr and the system to equilibrate, the $(M + 1)^+$ ion was irradiated for 20 s with IR light from 2800 – 4000 cm^{-1} in 10 cm^{-1} sized steps; this was narrowed to 4–5 cm^{-1} in regions where fragmentation was observed. The resulting spectrum (Figure 2.2) has three absorption bands at 3455, 3565, and 3605 cm^{-1}, and in each case photofragmentation resulted in the loss of CO_2 (*m/z* 94) and H_2O (*m/z* 120) in an ~65 : 35 ratio. The largest feature occurs at 3565 cm^{-1} and upon increasing the irradiation time to 60 s more than 96% of the parent ion was fragmented (Figure 2.3). As expected for a resonant photon process, the extent of fragmentation increases linearly with irradiation time. That is, a plot of ln (100 - [100 x I_{pAB}]/[$\Sigma I_{fragments}$ + I_{pAB}]) vs the number of laser shots (time) is linear over approximately four half-lifes (Figure 2.3, inset). The slope of this line provides the first-order photofragmentation rate constant, and in accord with results of McLafferty et al.,[7] it is dependent on the repetition rate of the laser. In principle one could obtain the IR radiative cooling lifetime by measuring the photofragmentation rates at different laser frequencies, but lowering the frequency of the Nd:YAG flash lamp or Q-switch led to changes in the power which makes it difficult to carry out such a determination.

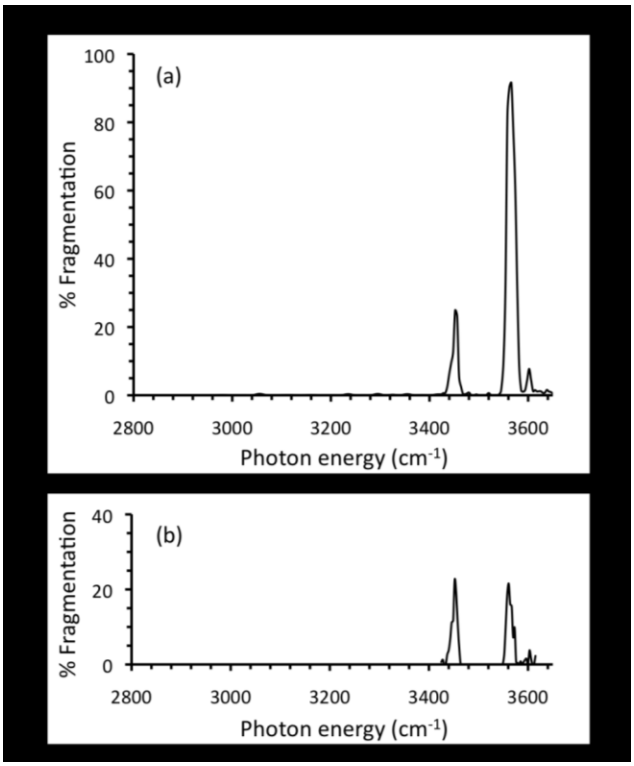

Figure 2.2. IRMPD spectra of protonated *p*-aminobenzoic acid generated by ESI from CH_3OH/H_2O (a) and after 2 H/D exchanges with EtOD (b).

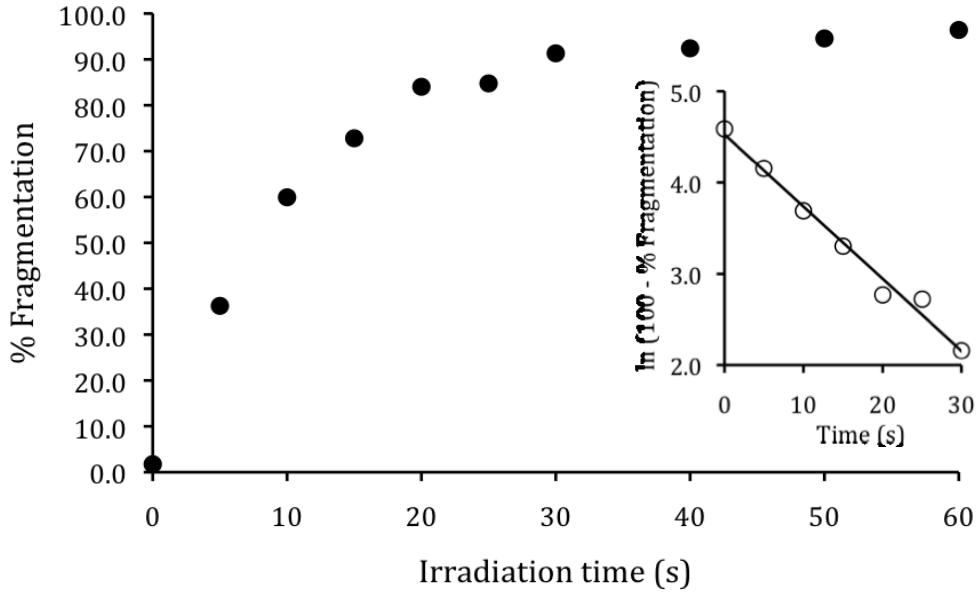

Figure 2.3. Photofragmentation at 3565 cm^{-1} of protonated *p*-aminobenzoic acid generated by ESI from CH_3OH/H_2O plotted as a function of time. The inset is a plot of ln (100 x I_{pAB} /[$SI_{fragment\ ion}$ + I_{pAB}]) vs time for 4 half-lifes.

The smallest observed band in the IRMPD spectrum is at 3605 cm^{-1}, and due to some initial difficulties with moisture in the house nitrogen supply, we found that this feature diminishes with increasing humidity along the ~2.5 m path that the IR light travels before entering into the high-vacuum chamber of the FTMS. When the relative humidity was ≥ 25% this band disappeared altogether as it falls on top of a water absorption which greatly reduces the IR power at this wavelength. Consequently, all of the spectra reported herein were obtained at a relative humidity of ≤ 5% using high flows (18 L min^{-1}) of dried air that had been passed through a 20' long trap cold trap (-78 °C) filled with activated molecular sieves.

The effect of laser power on the extent of fragmentation upon irradiation at 3565 cm^{-1} was also examined. A plot of ln (100 - fragmentation [%]) vs the laser energy is linear as previously noted,[7] but the slope of a linear log–log plot has been used to determine the number of photons needed to induce photofragmentation.[16] For this, we plotted ln ($[I_{pAB}/(\Sigma I_{fragment\ ions} + I_{pAB})/t_{irradiation}]$), where $t_{irradiation}$ = 20 s, against the logarithm of the laser pulse energy (Figure 2.4). The slope of the resulting line from a least-squares fit of the data is 2.9 which suggests that at least 3 photons are needed to fragment protonated *p*AB. This value corresponds to a lower limit for the number of photons (and the energy) required to break apart the ground-state ion because the trapped ions may possess some additional internal energy, and at a repetition rate of 10 Hz not all of the IR energy is dissipated between the laser shots. In accord with this, our calculations (see below) indicate that 41.2 kcal mol^{-1} or ~4 photons are needed to cleave the ground-state ion.

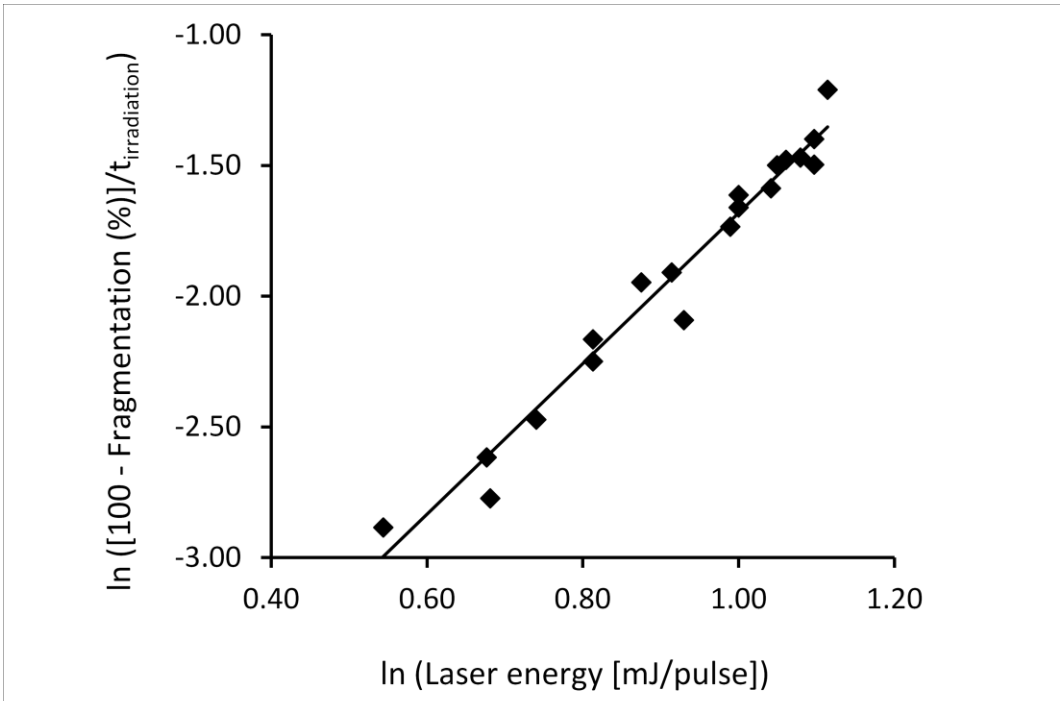

Figure 2.4. The effect of laser energy on fragmentation of protonated *p*-aminobenzoic acid generated by ESI from a CH_3OH/H_2O solution upon irradiation at 3565 cm^{-1}. This ln ([100 – fragmentation (%)]/$t_{irradiation}$] vs ln (laser energy [mJ/pulse]) plot, where $t_{irradiation}$ = 20 s, gives a least-squares line of y = 2.88x – 4.56, r^2 = 0.98. The slope (m = 2.88) reflects the number of photons needed to fragment the $(M + 1)^+$ ion.

Our IRMPD data suggests that the structure of the conjugate acid of *p*AB is the *O*-protonated ion because the $(M + 1)^+$ ions of carboxylic acids are well-known to lose H_2O upon fragmentation.[17] To verify this assignment, hydrogen-deuterium (H/D) exchange was carried out on the parent ion with EtOD. Two hydrogen atoms were replaced by two deuterium atoms in accord with previous reports on carboxy-protonated ions.[18] Photofragmentation of the isotopic envelope containing 11% d_0, 41% d_1, and 48% d_2-ions gave no indication of H/D scrambling upon irradiation and led to a spectrum in which the bands at 3565 and 3605 cm^{-1} were greatly reduced or eliminated (Figure 2.2b). Individual spectra of the d_1- and d_2-ions were also obtained from the data by using just the fragmentation channel corresponding to the loss of CO_2 since different mass ions are produced from the two isotopomers (i.e. the d_1- and d_2-ions afford *m/z* 95

and 96 ions, respectively). The resulting spectra are provided in the supporting information (Figure S1) and show that the d_1-ion gives greatly reduced bands at 3565 and 3605 cm^{-1}, whereas both of these absorptions are missing in the d_2 spectrum. Since it is the two O–H hydrogens in the *O*-protonated ion which undergo exchange, these results indicate that the bands at 3565 and 3605 cm^{-1} correspond to O–H stretches while the absorption at 3455 cm^{-1} is presumably due to an N–H stretch. All of these assignments are fully supported by computations (see below), and are in accord with our previous report that the *O*-protonated ion (i.e., the gas-phase structure) is produced upon spraying *p*AB from an aqueous methanol solution. Therefore, an isomerization of the ionization site is taking place at some point during the electrospray and desolvation process.

Can the *N*-protonated ion also be produced by ESI? To address this question, *p*AB was sprayed from an aqueous CH_3CN solution and the IRMPD spectrum of the resulting $(M + 1)^+$ ion was recorded. It was found to be identical to the spectrum obtained from CH_3OH/H_2O (Figure S2), but fragmentation was significantly less efficient. When the depletion of the $(M + 1)^+$ ion was examined as a function of time, it was observed to level off to a constant value of 70% (Figure 2.5). This reveals that a second isomer is present, which presumably is the *N*-protonated ion. Extended irradiation times up to 5 minutes in length did not lead to further fragmentation indicating that our laser system does not have enough power to break apart the *N*-protonated ion. Its formation, however, indicates that the ion composition changes with the electrospray solvent as we previously communicated.[4] In this work, however, a 70/30 mixture of *O*-and *N*-protonated ions was observed whereas only the former species was previously noted. This difference may be due to an acid-catalyzed isomerization of the *N*-protonated ion to its more stable *O*-protonated

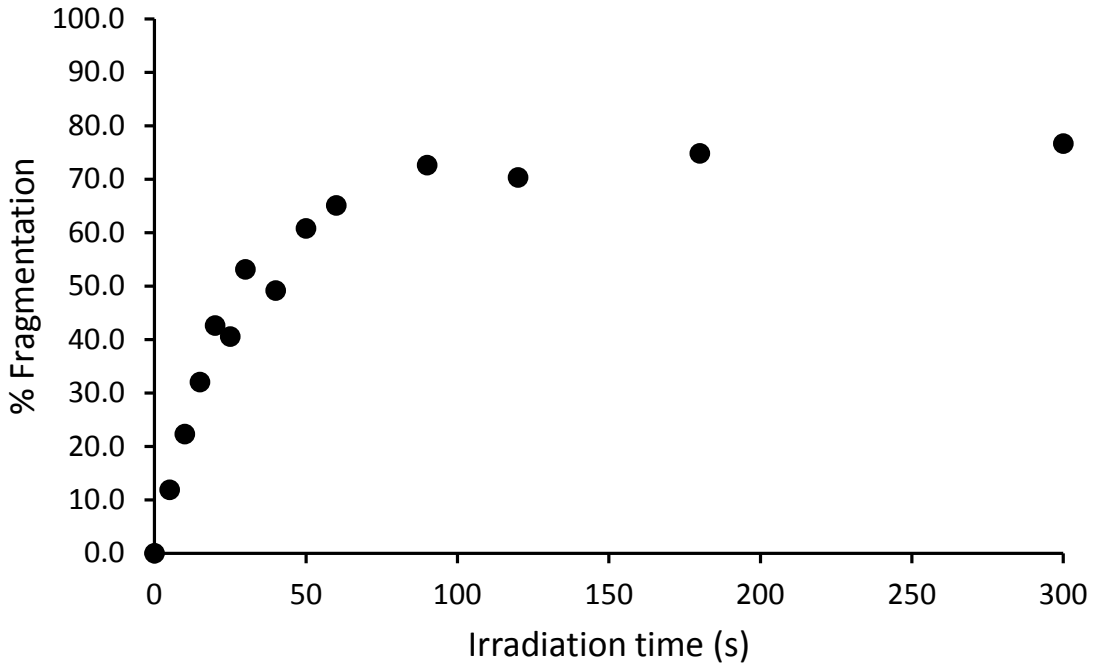

Figure 2.5. Photofragmentation at 3565 cm^{-1} of protonated *p*-aminobenzoic acid generated by ESI from CH_3CN/H_2O plotted as a function of time

isomer as a result of small amounts of inadvertent acids in our instrument such as in the argon gas used to trap and collisionally cool the electrosprayed ions. This possibility is greater than in the previous experiments because a higher pressure of argon for a much longer period of time was employed. Alternatively, in our previous H/D exchange study the reactivity was not examined as a function of the pressure of the deuterium exchange reagent. Since the *O*-protonated ion reacts 25 times faster than the *N*-protonated isomer, the former species may have been selectively removed from a mixture before the d_0-reactant ion was isolated and the reaction progress was monitored.

These results indicate that two different ionization sites for the $(M + 1)^+$ ion of *p*AB are formed when the ESI solvent is changed from CH_3OH/H_2O to CH_3CN/H_2O. In water, it is well known that the protonation of *p*AB occurs at nitrogen to afford the ammonium ion,[19] and it is reasonable to assume that the same structure is produced in a

1:1 (v/v) CH_3CN/H_2O mixture (i.e., a solution comprised of 50% water by volume). To test this assumption, the ^{13}C NMR spectra of *p*AB and its hydrogen chloride salt were recorded in 1:1 (v/v) CD_3CN/H_2O solutions. The carbonyl carbon resonance was found to shift upfield in the salt in accord with a previous report in D_2O,[20] and in contrast to the known downfield shift of a carboxyl group upon its protonation.[21] The changes in the ring carbon shifts also mimic those in water indicating that the ammonium ion is the preferred structure in both solutions. As a result, the ionization site of *p*AB was retained to a significant extent (30%) when CH_3CN/H_2O was used as the ESI solvent, but it changed when a CH_3OH/H_2O solution was used.

B3LYP and G3 calculations were previously used to investigate the stability of the conjugate acid of *p*AB.[4] *O*-Protonation was found to be thermodynamically preferred over *N*-protonation by 4.1 (G3) and 9.5 (B3LYP/cc-pVTZ) kcal mol^{-1} (Table 2.1). This energy difference

Method	**PA($PhNH_2$)**	**PA($PhCO_2H$)**	**Relative Energies**	
			p-$H_2NC_6H_4CO_2H_2^+$	*p*-$HO_2CC_6H_4NH_3^+$ [b]
B3LYP/cc-pVDZ	209.5	202.4	0.0	9.0 (1.4)
B3LYP/cc-pVTZ// B3LYP/cc-pVDZ	210.3	201.6	0.0	9.5 (3.5)
B3LYP/cc-pVTZ	210.4	201.5	0.0	9.5 (3.8)
G3	210.8	197.1	0.0	4.1 (3.1)
M06-2X/cc-pVDZ	211.3	199.0	0.0	7.5 (5.0)
M06-2X/cc-pVTZ// M06-2X/cc-pVDZ	209.9	198.1	0.0	8.5 (5.3)
M06-2X/cc-pVTZ	209.2	198.1	0.0	7.9 (4.3)
Expt	210.9 ± 2.0	196.2 ± 2.0		

Table 2.1. Calculated B3LYP, G3, and M06-2X Proton Affinities for Aniline and Benzoic Acid and the Energy Difference Between *N*- versus *O*-Protonated *p*-Aminobenzoic Acid. All values are in kcal mol^{-1}. The B3LYP, G3, and experimental values come from reference 22. [b] Parenthetical values have been corrected using the isodesmic reaction given in eq. 2.2.

drops to 3.1 (G3) and 3.8 (B3LYP/cc-pVTZ) kcal mol^{-1} if the errors in the computed proton affinities of aniline and benzoic acid are corrected for via the isodesmic reaction given in eq. 2.2.[22] The large change in the latter result is primarily due to a 5.3 kcal mol^{-1} error in the computed proton affinity for benzoic acid. In this work, the newer M06-2X functional developed by Truhlar and coworkers was also employed.[13] *O*-Protonation is predicted again to be the favored pathway, and our best calculation (M06-2X/cc-pVTZ) leads to a 7.9 kcal mol^{-1} difference which decreases to 4.3 kcal mol^{-1} when one corrects for the computed proton affinities of aniline and benzoic acid. All of these computational results paint a consistent picture in which the carbonyl oxygen in *p*AB is the most basic site by ~3 – 5 kcal mol^{-1}. This is also in accord with H/D exchange and CID experiments.[4]

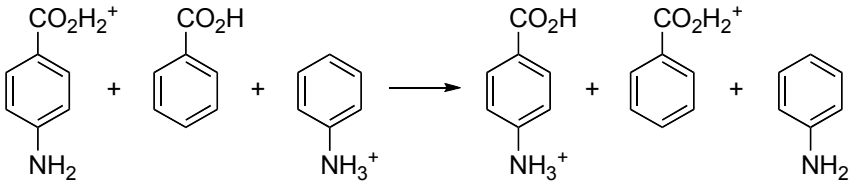

(2.2)

PA (*O*-*p*AB ĞN-*p*AB) = ΔHůrxn (calc) - 14.7 ± 2.8 kcal $mol^{Ğ1}$

IR spectra were computed using the B3LYP and M06-2X functionals with several basis sets. All of the results are provided in Table S1 in the supporting information, but since the predictions are qualitatively the same, only the B3LYP/cc-pVDZ spectra are given in Figure 6 because they are the most economical and they are in the best agreement with experiment. As can be seen, the calculated frequencies for the *O*- and *N*-protonated ions are quite different from each other which makes it relatively straightforward to differentiate these species. The predicted spectrum for the former ion is in excellent accord with the experimental results and all of the scaled frequencies (0.966) are within 8 cm^{-1} of the observed positions.

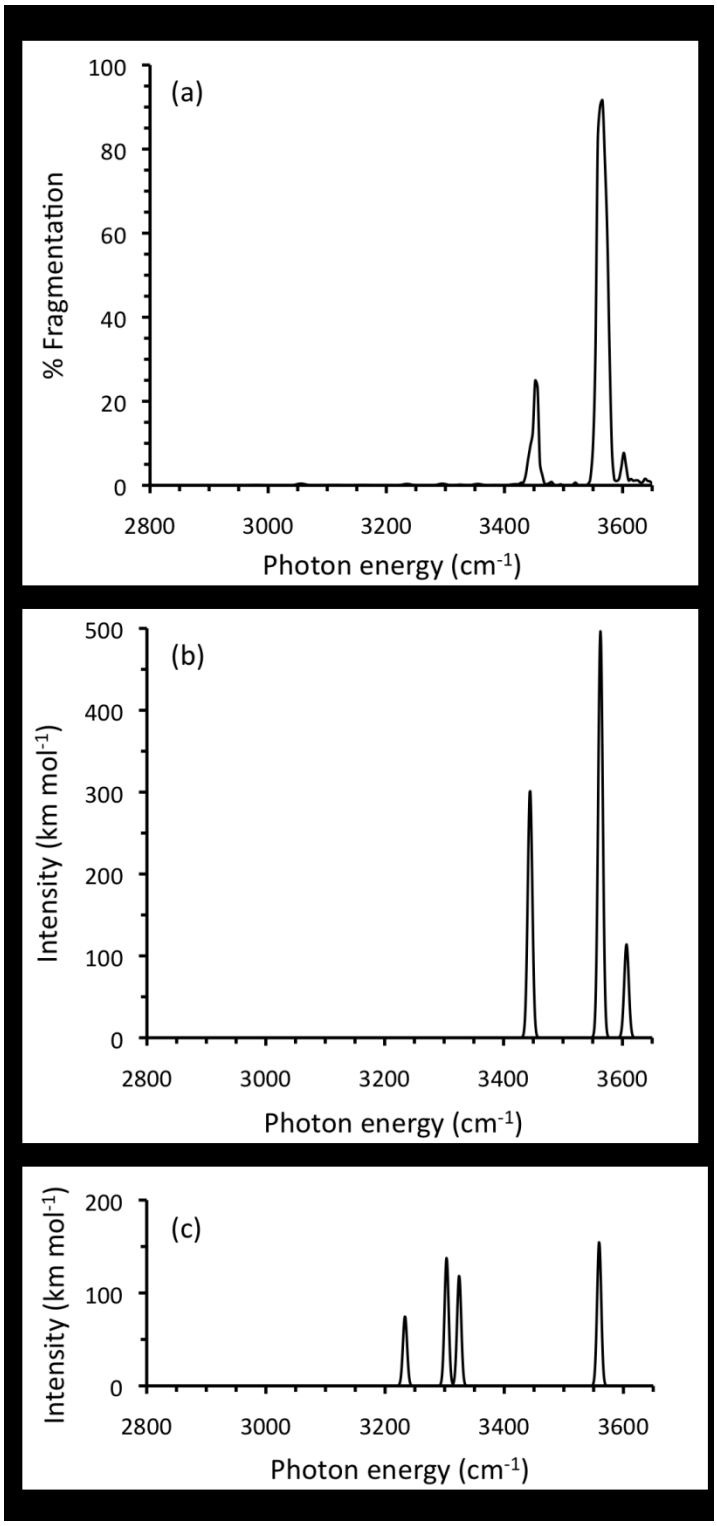

Figure 2.6. Comparisons of the experimental IRMPD spectrum of protonated *p*-aminobenzoic acid generated by ESI from a CH_3OH/H_2O solution (top) to the calculated B3LYP/cc-pVDZ spectra of *O*- (middle) and *N*-protonated *p*AB (bottom); Gaussian peak shapes with a width of 10 cm^{-1} at the base were used for the computed spectra.

In contrast, the *N*-protonated ion is predicted to have three similarly intense bands below 3350 cm^{-1}, but no such features are observed in the experimental spectrum. Therefore, the computational results indicate that the observed spectrum is of the *O*-protonated ion, and this supports the experimental assignment. Our calculations also indicate that the computed bands at 3447 and 3609 cm^{-1} are due to the symmetric N–H and anti H–O–C–O O–H stretches, respectively, whereas the absorption at 3656 cm^{-1} is the result of two overlapping bands corresponding to the antisymmetric N–H and syn H–O–C–O O–H stretches. This too is in agreement with experiment since the absorptions at 3566 and 3609 cm^{-1} disappear upon H/D exchange; the absence of the overlapping N–H stretch is not surprising since the computed intensity is ~65% of that for the weakest feature observed in the spectrum (i.e., the band at 3605 cm^{-1}).

Fragmentation pathways were computed to probe the dissociation barriers and explore why the *N*-protonated ion does not break apart upon irradiation. The loss of H_2O from the *O*-protonated ion to afford *p*-aminobenzoyl cation (*p*-$NH_2C_6H_4CO^+$) is calculated to be endothermic by 20.8 and 26.8 kcal mol^{-1} at the B3LYP/cc-pVTZ//B3LYP/cc-pVDZ and M06-2X/cc-pVTZ// B3LYP/cc-pVDZ levels of theory, respectively. Several mechanisms were explored for this process and the most favorable one (Scheme 2.1) turned out to be the simplest. Direction isomerization of the most stable *O*-protonated structure via a 1,3-proton shift leads to the hydrated benzoyl cation (i.e., protonated *p*AB at the hydroxyl group)[23] which can easily lose H_2O apparently without a significant reverse activation barrier. The first step is rate-determining and has a predicted activation barrier of 44.1 (B3LYP) and 45.7 (M06-2X) kcal mol^{-1}.[24] This corresponds to an ~4 photon process (i.e., 4 x 3600 cm^{-1} = 41.2 kcal mol^{-1}) which is in accord with the experimental power study indicating that ≥ 3 photons are needed.

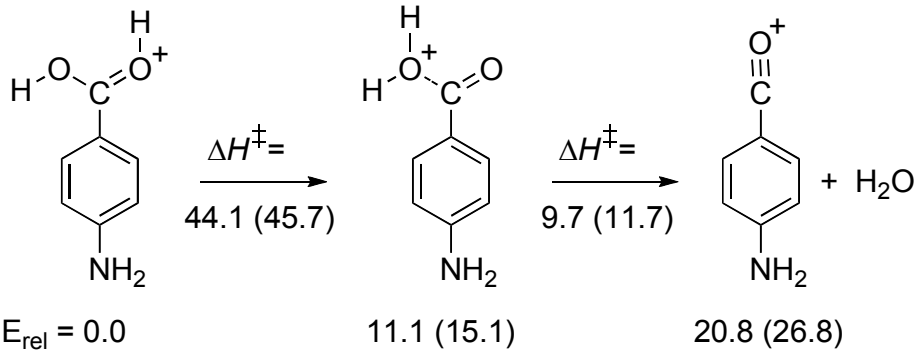

Scheme 2.1. Proposed Fragmentation Pathway for the Loss of H_2O From *O*-Protonated *p*-Aminobenzoic Acid. All values are in kcal mol^{-1}. B3LYP/cc-pVTZ single-point energies corrected to 298 K using the B3LYP/cc-pVDZ vibrational frequencies are provided first and M06-2X/cc-pVTZ//B3LYP/ cc-pVDZ values follow and are given in parentheses.

A few pathways for the expulsion of CO_2 from the *O*-protonated ion were explored too. The most favorable route that we located involves 4 steps as illustrated in Scheme 2.2. Proton transfer from the *O*-protonated ion to the ortho position of the aromatic ring is the most difficult step and has a calculated barrier of 43.2 kcal mol^{-1}.[25] A subsequent 1,2-hydride shift to the carbon bearing the carboxyl group leads to a much more stable ring-protonated structure, and this two-step process is predicted to be more facile than the direct one-step pathway which has an activation energy of 48.5 kcal mol^{-1}. Rotation of the C–OH bond in the resulting *ipso*-protonated *p*AB ion leads to the anti form of the carboxyl group which can then transfer the hydrogen to the aromatic ring concomitantly with the loss of CO_2 to afford ortho-protonated aniline.[26] This process is computed to be thermoneutral overall and is ~24 kcal mol^{-1} more favorable than for the loss of H_2O. The activation energies for both processes are very similar, but the loss of CO_2 is computed to be slightly favored (i.e., $\Delta H^{\ddagger}$ = 43.2 ($-CO_2$) vs 44.1 ($-H_2O$) kcal mol^{-1}).[27] In accord with this calculation, the cleavage of CO_2 was found to occur to a

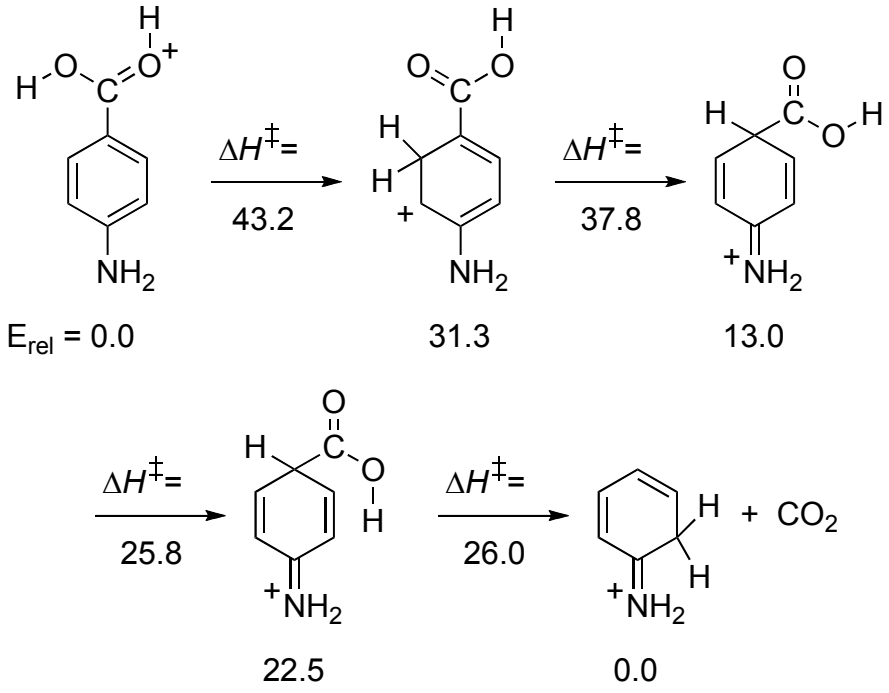

Scheme 2.2. Proposed Fragmentation Pathway for the Loss of CO_2 From *O*-Protonated *p*-Aminobenzoic Acid. All values are in kcal mol^{-1} and correspond to B3LYP/cc-pVTZ//B3LYP/cc-pVDZ energies at 298 K.

greater extent than the fragmentation of H_2O at each wavelength (i.e., ~65% to 35% ratios were observed). This pathway also provides a mechanism for isotopic scrambling of the deuterium atoms in $H_2NC_6H_4CO_2D_2^+$ (produced by H/D exchange) with the aromatic hydrogens in the ortho position. It is not surprising; however, that there is no evidence for H/D exchange since once the *O*-protonated ion transfers a deuteron to the aromatic ring, fragmentation of CO_2 is more facile than reverting back to the carboxy-protonated ion.

Cleavage of the *N*-protonated ion was calculated to be significantly more difficult than for the *O*-protonated isomer. The loss of NH_3 from the former species is computed to be endothermic by 81.9 kcal mol^{-1} at the B3LYP/cc-p-VTZ//B3LYP/cc-p-VDZ level (eq. 2.3). Proton shifts from the ammonium ion to the ipso or ortho positions of the aromatic ring have predicted barriers of 65.3 and 66.8 kcal mol^{-1}, respectively at the

same level of theory (eq. 2.4). A decarboxylation transition structure was also located but the barrier was even a little larger (i.e., 69.7 kcal mol^{-1}). These results indicate that the fragmentation of the *N*-protonated ion is energetically more demanding than for the *O*-protonated isomer by ~20 kcal mol^{-1} and thus at least 6 photons would be needed to cleave the ground-state ion. Our OPO/OPA laser system does not have the necessary power to carry out such a process.

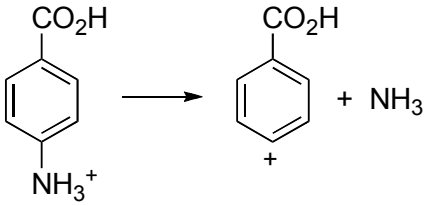

(2.3)

$\Delta H\hat{u}_{rxn}$ = 81.9 kcal mol$^{\check{G}1}$

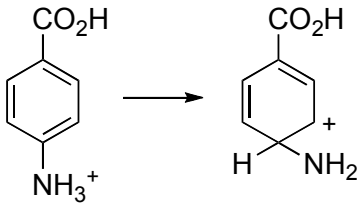

(2.4a)

ΔH = 65.3 kcal mol$^{\check{G}1}$

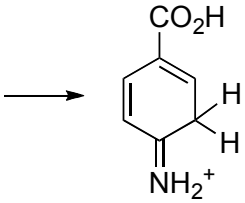

(2.4b)

ΔH = 66.8 kcal mol$^{\check{G}1}$

A previous IRMPD study on *p*-hydroxybenzoic acid (*p*-$HOC_6H_4CO_2H$) by Oomens et al. also found that the ionization site can be altered by changing the ESI solvent from CH_3OH/H_2O to CH_3CN/H_2O or CH_3SOCH_3.[5] They assumed that the deprotonation site is different in these solutions and, consequently, concluded that ESI maintains the liquid-phase structure. Given that the aprotic acetonitrile solution contained 10% water, it

seemed unlikely to us that the hydroxyl group of the phenol is the most acidic site in *p*-hyroxybenzoic acid. A review of the literature revealed that the pK_a of *p*-hydroxybenzoic acid (*p*-$HOC_6H_4CO_2H$) in DMSO (11.8) fits on a Hammett acidity plot for substituted benzoic acids,[28] thereby indicating that the carboxy group is the most acidic position, and that the ionization site does not change upon going from H_2O to DMSO. In addition, the DMSO pK_a of *p*-methoxybenzoic acid (*p*-$CH_3OC_6H_4CO_2H$, 11.5) is 2.8 pK_a units lower than that for methyl *p*-hydroxybenzoate (*p*-$HOC_6H_4CO_2CH_3$, 14.3).[29] This too indicates that in DMSO the carboxy group is the most acidic position in *p*-hydroxybenzoic acid. As a result, the assumption by Oomens et al. that the deprotonation site of *p*-hydroxybenzoic acid changes upon going from a protic (aqueous methanol) to a nonprotic (acetonitrile or dimethyl sulfoxide) solvent is unwarranted, and their results are in accord with our own.[3] That is, ESI does not necessarily produce the ionic structure present in solution, and the solvent can play an important role in determining where the ionization site is located.

Conclusions

ESI of an aqueous methanol solution of *p*AB affords an $(M + 1)^+$ ion which undergoes photofragmentation of carbon dioxide and water in an ~65 to 35 ratio to afford an action spectrum between 2800 – 4000 cm^{-1} consisting of three bands at 3455, 3565, and 3605 cm^{-1}. Irradiation of the largest feature at 3565 cm^{-1} as a function of time revealed that kinetically there is evidence for only one species, and it requires the absorption of at least three photons to break apart. Based upon the well-known behavior of protonated carboxylic acids to lose water upon energetic collisions, the incorporation of two deuterium atoms into the $(M + 1)^+$ ion upon reaction with EtOD, and the loss of HDO and/or D_2O upon photofragmentation of the d_1- and d_2-containing ions,

respectively, enabled us to assign the carboxy-protonated structure to this ion. We were also able to assign the lowest frequency band to a N–H stretch and the higher frequency features to O–H stretches. Calculations support these assignments in that the computed IR spectrum for the *O*-protonated ion reproduces the experimental data whereas the spectrum for the *N*-protonated ion does not match the observed results. The band assignments are also in accord with those deduced from the experimental results. In addition, theory indicates that carbon dioxide should be lost a little more readily (0.9 kcal mol^{-1}) than water and that four photons are needed to fragment the ion in its ground state. Both of these predictions are also consistent with our observations. The conjugate acids of *p*AB do not readily interconvert nor do they have similar IR band positions, consequently, our observed spectrum of the carboxy-protonated ion indicates that this is the structure of the ion that is produced in the ICR cell. That is, an isomerization takes place during the electrospray and desolvation process leading to a gas-phase ion that has a different ionization site than in methanol/water.

When an aqueous acetonitrile solution was used as the ESI solvent then a significant amount of the ammonium ion (30%) was produced in the gas phase. This was determined by kinetics (i.e., monitoring the extent of photofragmentation with time) since we were unable to fragment the *N*-protonated ion even with extended irradiation times up to 5 min. This is not surprising since our computations indicate that more than 60 kcal mol^{-1} are needed to cleave this covalently-bound ion, and this is currently beyond the capabilities of OPO/OPA laser systems. In any case, these findings reveal that the structure of the $(M + 1)^+$ ion of *p*AB is sensitive to the solvent from which it is sprayed. This conclusion is in accord with several reports using different structurally diagnostic tools, but the specific structures which are formed may be dependent on the electrospray conditions and the design of the source.

References

1. Walsh, C. *Enzymatic Reaction Mechanisms*; W. H. Freeman: San Francisco, 1979.
2. (a) Bordwell, F. G.; Bartmess, J. E.; Drucker, G. E.; Margolin, Z.; Matthews, W. S. *J. Am. Chem. Soc.* **1975**, *97*, 3226-3227.
   (b) Kebarle, P.; McMahon, T. B. *J. Am. Chem. Soc.* **1977**, *99*, 2222-2230.
   (c) Kebarle, P.; Davidson, W. R.; French, M.; Cumming, J. B.; McMahon, T. B. *Faraday Trans*. **1977**, *64*, 220-229.
   (d) Deward, M. J. S. *Enzyme* **1986**, *36*, 8-20.
3. (a) Tian, Z.; Kass, S. R. *J. Am. Chem. Soc*. **2008**, *130*, 10842-10843.
   (b) Tian, Z.; Wang, X. B.; Wang, L. S.; Kass, S. R. *J. Am. Chem. Soc*. **2009**, *131*, 1174-1181.
4. Tian, Z.; Kass, S. R. *Angew. Chemie, Int. Ed. Engl*. **2009**, *48*, 1321-1323.
5. Steill, J. D.; Oomens, J. *J. Am. Chem. Soc.* **2009**, *131*, 13570-13571.
6. Meyer, M. M.; Chan, B.; Radom, L. Kass, S. R. *Angew. Chemie. Int. Ed. Eng*. **2010**, *49*, 5161-5164.
7. Oh, H.-B.; Lin, C.; Hwang, H. Y.; Zhai, H.; Breuker, K.; Zabrouskov, V.; Carpenter, B. K.;
   McLafferty, F. W. *J. Am. Chem. Soc*. **2005**, *127*, 4076-4083.
8. Bush, M. F.; O'Brien, J. T.; Prell, J. S.; Saykally, R. J.; Williams, E. R. *J. Am. Chem. Soc*. **2007**, *129*, 1612-1622.
9. Meyer, M. M. Ph.D. Thesis, University of Minnesota, Minneapolis, MN, 2010.
10. Bush, M. F.; Saykally, R. J.; Williams, E. R. *ChemPhysChem* **2007**, *8*, 2245-2253.
11. Oomens, J.; Sartakov, B. G.; Meijer, G.; Helden, G. v. *Int. J. Mass Spectrom.* **2006**, *254*, 1-19.
12. (a) Becke, A. D. *J. Chem. Phys.* **1993**, *98*, 5648-5652.
    (b) Lee, C. T.; Yang, W. T.; Parr, R. G. *Phys. Rev. B* **1988**, *37*, 785-789.
13. (a) Zhao, Y.; Truhlar, D. G. *J. Phys. Chem. A* **2008**, *112*, 1095-1099.
    (b) Zhao, Y.; Truhlar, D. G. *Theor. Chem. Acc.* **2008**, *120*, 215-241.
    (c) Zhao, Y.; Truhlar, D. G. *Acc. Chem. Res.* **2008**, *41*, 157-167.
14. Dunning, Jr., T. H. *J. Chem. Phys.* **1989**, *90*, 1007-1023.
15. Frisch, M. J.*, et al. Gaussian 09*, Gaussian, Inc., Wallingford, CT, 2009.
16. (a) Thorne, L. R.; Beauchamp, J. L. In *Gas Phase Ion Chemistry*; Bowers, M. T., Ed.; Academic Press: New York, 1984; Vol. 3, pp 41-97.
    (b) Greene, J. R.; Francisco, J. S.; Huang, J.; Xu, D.; Jackson, W. M. *J. Chem. Phys.* **2004**, *121*, 5868-5873.
17. (a) Middlemiss, N. E.; Harrison, A. G. *Can. J. Chem.* **1979**, *57*, 2827-2833.
    (b) Uggerud, E. *Top. Curr. Chem*. **2003**, *225*, 3-36.
18. Ranashinghe, A.; Cooks, R. G.; Sethi, S. Org. Mass Spectrom. **1992**, *27*, 77-88.
19. Zhang, X. X.; Oscarson, J. L.; Izatt, R. M.; Schuck, P. C.; Li, D. *J. Phys. Chem*. *B* **2000**, *104*, 8598-8605.
20. Laufer, D. A.; Gelb, R. I.; Schwartz, L. M. *J. Org. Chem*. **1984**, *49*, 691-696.
21. (a) Olah, G. A.; White, A. M. J. Am. Chem. Soc. **1967**, *89*, 7072-7075.
    (b) Maciel G. E.; Traficante, D. D. J. Phys. Chem. **1965**, *69*, 1030-1033.
22. Hunter, E. P. L.; Lias, S. G. "Proton Affinity Evaluation" and "Ionization Energy Evaluation" in *NIST Chemistry WebBook, NIST Standard Reference Database Number 69* (Eds.: Linstrom, P. J.; Mallard, W. G.), June 2005, National Institute

of Standards and Technology, Gaithersburg MD, 20899 (http://webbook.nist.gov).
23. Scaled (0.966) B3LYP/cc-pVDZ vibrational frequencies (cm^{-1}) and intensities (km mol^{-1}, given in parentheses) for the higher energy hydroxy-protonated *p*AB isomer follow: 2176 (1299), 3113 (63), 3443 (269), 3562 (75), 3621 (58), and 3709 (84). Three small bands (≤ 2 km mol^{-1}) have been omitted.
24. The computed free energy barriers are 44.4 and 45.9 kcal mol^{-1}, respectively.
25. The computed free energy barrier is 43.7 mol^{-1}.
26. Ring protonation of aniline is competitive with *N*-protonation in the gas phase. See: (a) Pasker, F. M.; Solca, N.; Dopfer, O. *J. Phys. Chem. A* **2006**, *110*, 12793-12804, (b) Flammang, R.; Dechamps, N.; Pascal, L.; Van Haverbeke, Y.; Gerbaux, P.; Nam, P. C.; Nguyen, M. T. *Lett Org Chem*. **2004**, *1*, 23-30, and (c) Russo, N.; Toscano, M.; Grand, A.; Mineva, T. *J. Phys. Chem. A* **2000**, *104*, 4017-4021. This is not the case for *p*AB as indicated by our computations (ref. 4) and H/D exchange data which are inconsistent with ring protonation at the CH carbons.
27. The corresponding free energies are 43.7 and 44.4 kcal mol^{-1}, respectively.
28. Ritchie, C. D.; Uschold, R. E. *J. Am. Chem. Soc*. **1968**, *90*, 2821-2834.
29. (a) Arnett, E. M.; Moe, K. D. *J. Am. Chem. Soc*. **1991**, *113*, 7288-7293. (b) Arnett, E. M.; Moriarity, T. C.; Small, L. E.; Rudolph, J. P.; Quirk, R. P. *J. Am. Chem. Soc*. **1973**, *95*, 1492-1495.[1]

[1] Support from the National Science Foundation, the Minnesota Supercomputer Institute for Advanced Computational Research, and the NSF-REU program in chemistry at the University of Minnesota are gratefully acknowledged. We also thank Dr. Zheng Yang and Profs. Blank, Leopold, and Massari for helpful advice and assistance regarding optics and laser systems, Prof. Johnson for hosting a visit by Dr. Meyer to his laboratory and providing many useful pointers, and Dr. Dean Guyer for his assistance and a wealth of information. Supporting Information Available: B3LYP/aug-cc-pVDZ geometries in the form of xyz coordinates and energies are given for the computed structures as are Table S1, Figures S1 and S2, and the complete citation to reference 15 (16 pages). This material is available free of charge via the internet at **http://pubs.acs.org**.

Chapter 3

Probing the Effects of a Series of Anions on the Infrared Action Spectroscopy of a Hydrogen Bonded Cluster

Introduction

Hydrogen bonding catalysts are important species that are widely used in organic synthesis.[1] These catalysts can lower reaction barriers by two different pathways. That is, they can activate an electrophile via one or more hydrogen bonds or they can abstract an anion to afford a highly electrophilic carbocation intermediate.[2] In both cases, multiple contacts (hydrogen bonds) may enhance the effectiveness of the catalyst. One such species capable of serving as a three hydrogen bond donor that is being studied in the Kass lab is triphenol **1**. To model the transition state of this catalyst, infrared multiphoton dissociation (IRMPD) spectroscopy was used to investigate the structure of a 1:1 catalyst:anion complex. Infrared spectroscopy is particularly valuable in this regard since free hydroxyl groups and those participating in a hydrogen bond have distinctly different O-H stretching frequencies. In particular, a strong interaction between the triphenol **1** and an anion involving three hydrogen bonds should be evident by the lack of a free O-H stretch. Alternatively, a cluster structure with one or two hydrogen bonds should be apparent by the presence of one or more free hydroxyl O-H stretching bands.

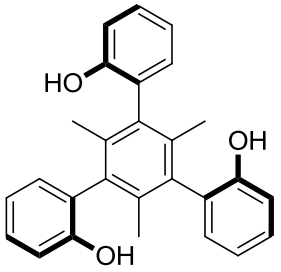

1 syn

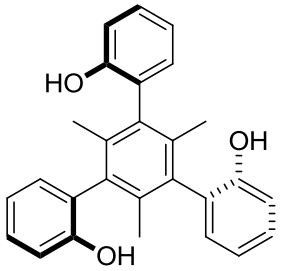

1 anti

Chloride and alkoxide anion complexes of **1** were studied as transition state analogs for anion abstraction and hydrogen bond catalysis. Clusters of this sort can also be used as models for oxyanion holes and enzyme catalyzed processes.[3] To probe these processes, chloride, phenyl thiolate, 2,2,2-trifluoroethoxide, acetate and nitrite anion complexes with **1** were studied.

To further explore the effect of multiple hydrogen bonds in a substrate : anion complex, the chloride clusters of **2** and **3** were also studied. The lowest energy conformer of diphenol **2** clustered with chloride anion (**2 • Cl**$^-$) is predicted to have two hydrogen bonds with the chloride anion; likewise the triphenol clustered with chloride anion (**3 • Cl**$^-$) is predicted to have three hydrogen bonds with the chloride anion. While the total clustering energy of **3 • Cl**$^-$ is predicted to be larger than **2 • Cl**$^-$, the hydrogen bond energy on a per hydrogen bond basis should be smaller for the former complex. Due to the weaker third hydrogen bond in **3 • Cl**$^-$ its IR absorption frequency for the O-H stretch should be larger than for **2 • Cl**$^-$. This change in IR absorption frequency can be monitored by IRMPD and can give insight into the individual hydrogen bond strengths of gas phase ions.

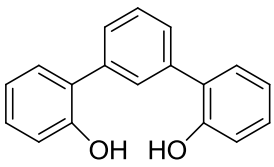

2

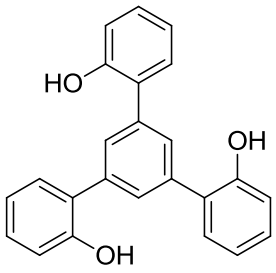

3

Experimental Section

A Fourier transform mass spectrometer (FTMS) coupled to a tunable infrared laser that has been previously described was used in these studies.[4] Triphenol **1**, diphenol **2**, and triphenol **3** were prepared by Eugene Beletskiy in the Kass lab. Electrospray solutions were prepared by dissolving **1**, **2**, or **3** in a 3:1 methanol:water solution at approx. 2 mM concentration. Ammonium chloride, thiophenol, 2,2,2-trifluoroethanol, ammonium acetate, or ammonium nitrite were added to the solution in approx. a 1:1 ratio with triphenol **1**. Ions were generated in a Waters Z-spray electrospray ionization (ESI) source by a direct infusion of the solution at 10 μL/min. A voltage of +4500V was applied to the ESI needle while the sample cone was held at -45V. An extractor cone at -5V guided the ions into an RF storage hexapole (75V RF, -0.8V DC) where ions were accumulated for 3 seconds by holding the end cap at -12V. The ions were then expelled from the hexapole (0V RF, -3V DC, +50V end cap), and a mechanical shutter was opened to allow them into the quadrapole ion guide (120V RF, +25V DC, 1.325 MHz) and on into the ion cyclotron resonance (ICR) cell. To facilitate this process, the trapping plate facing the quadrapole was grounded for 3 ms, and then raised back to -15V. A pulse of argon gas was also introduced into the ICR cell during the ion transfer to help trap the ions in the cell as well as to collisionally cool them. After the ions had been trapped for 1.5 seconds the trapping potentials on the end plates were lowered to -1.5V.

Cluster ions were isolated via a stored waveform inverse Fourier transform (SWIFT) excitation before being subjected to IR irradiation. They were then irradiated for 5-10 s at a 10 Hz pulse rate at a given wavelength of IR light which was scanned from 2700 – 4000 cm^{-1} in either 5 cm^{-1} increments or 10 cm^{-1} increments. Each spectrum

datum point is comprised of a single sequence, that is, new ions are generated, transferred, isolated, cooled, and irradiated for each data point. The energy of the IR light was 5 mJ/pulse at 2700 cm^{-1} and increases roughly linearly to 26 mJ/pulse at 4000 cm^{-1}. After irradiation the total ion abundance was observed and the amount of fragmentation in terms of percentage (Eq. 3.1) was plotted vs. IR wavelength.

$$\text{Fragmentation (\%)} = (100 \times (\Sigma I_{\text{fragment ions}})/(\Sigma I_{\text{fragment ions}} + I_{\text{parent ions}})) \quad (3.1)$$

IR action spectra data points were smoothed using a simple moving average according to equation 2. This was done to more easily differentiate true spectral features from natural variations primarily resulting from fluctuations in the Nd:YAG shot to shot laser power. IR data were not corrected for the change in photon energy due to wavelength or the change in laser power output over the scanned range.

$$y_{avg} = \frac{y_{x-1} + y_x + y_{x+1}}{3} \quad (3.2)$$

The cluster of syn-triphenol **1** with chloride anion (**1 syn • Cl^-**) was subjected to fragmentation vs. time studies by generating, transferring, and isolating ions as described above. These ions were irradiated with IR light at 3065 cm^{-1} at a frequency of 10 Hz for between 0.5 seconds and 150 seconds. The amount of fragmentation was calculated by equation 1 and plotted vs. irradiation time in seconds. Up to 94% of the ions fragmented upon irradiation for 2.5 minutes.

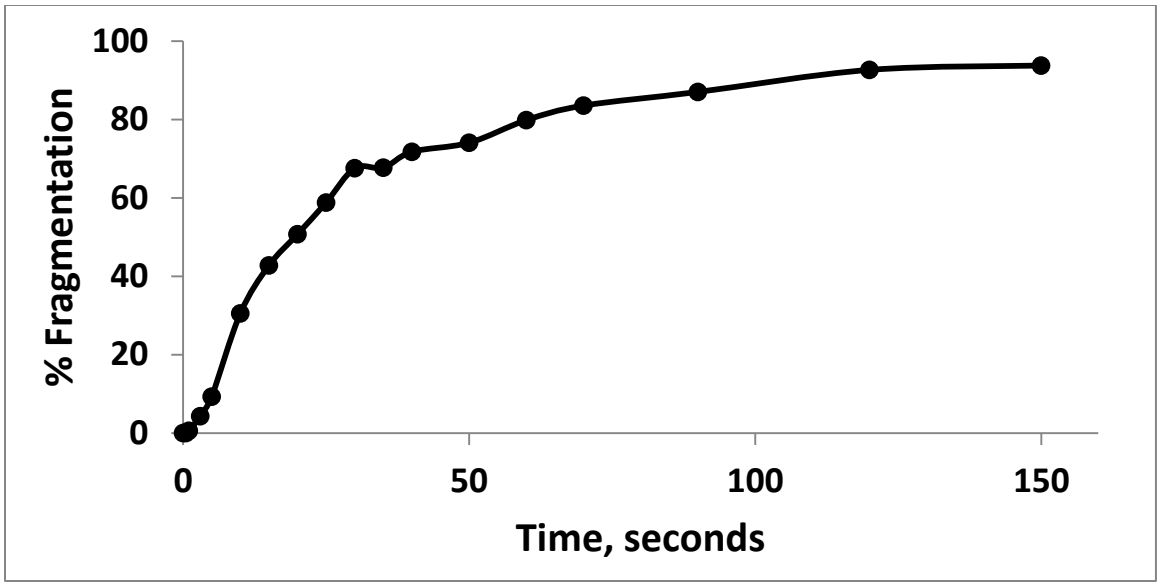

Figure 3.1. Fragmentation (%) vs. time (s) for the photofragmentation of the syn-triphenol **1 • Cl**$^-$ cluster at 3069 cm^{-1}.

Results and Discussion

*Diphenol **2***

The infrared action spectrum of diphenol **2** clustered with chloride anion was recorded from 2700 – 4000 cm^{-1} (Figure 3.2). A doublet is observed with peaks at 3055 cm^{-1} and 3080 cm^{-1}. A broad low-intensity feature is seen from 2750 cm^{-1} to the onset of the doublet at 3025 cm^{-1}. Photofragmentation at all wavelengths yielded the conjugate base of diphenol **2** (eq. 3.3) as the sole ion product.

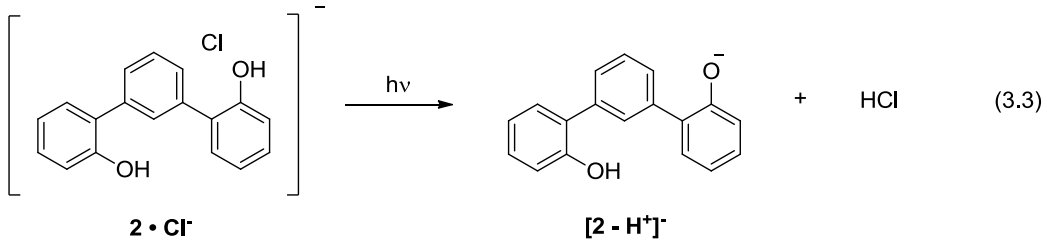

The strong doublet at 3055 and 3080 cm^{-1} is a common feature in all of the spectra that were obtained, and consequently can be assigned to aryl C-H stretching modes. The low intensity absorption below 3000 cm^{-1} presumably are combination bands of the hydroxyl O-H and aryl C-H stretches. Lastly, the absence of an absorption at ~3600 cm^{-1} indicates that the chloride anion interacts with both hydroxyl groups showing that there are two hydrogen bonds in **2 • Cl**$^-$.

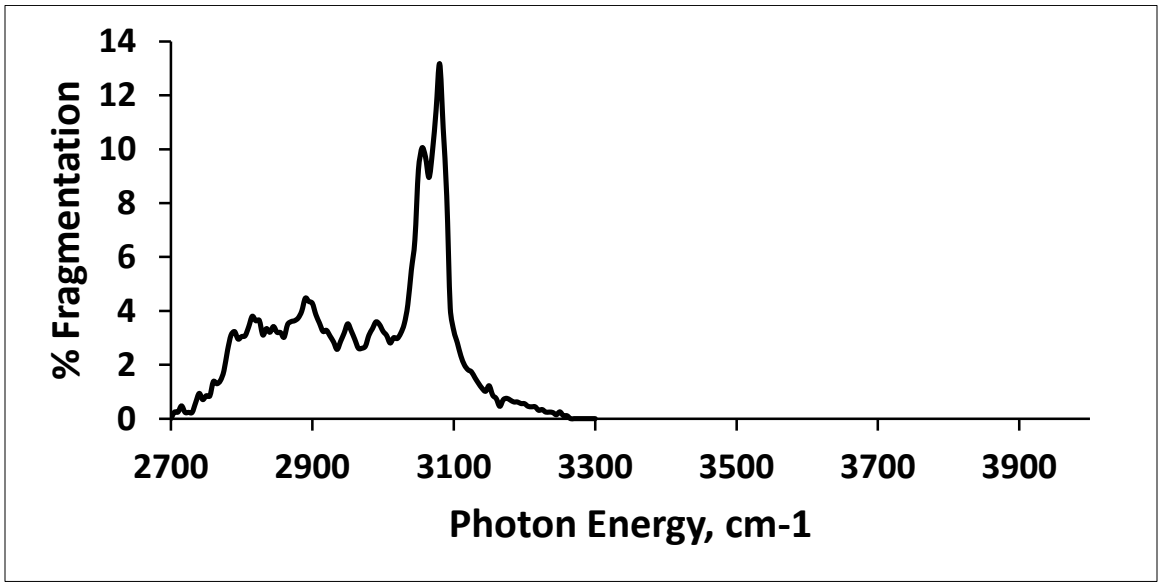

Figure 3.2. Infrared action spectrum of the diphenol **2** cluster with chloride anion (i.e. **2 • Cl**$^-$).

*Triphenol **3***

The infrared action spectrum of triphenol **3** clustered with chloride anion was recorded between 2700 – 3300 cm^{-1} and between 3450 – 3650 cm^{-1} (figure 3.3). A doublet is observed with peaks at 3065 cm^{-1} and 3080 cm^{-1} and a moderate intensity

band is observed at 3025 cm^{-1}. Low intensity absorptions are observed between 2850 cm^{-1} and 2970 cm^{-1} including a small peak at 2940 cm^{-1}. No absorption is observed between 3450 – 3650 cm^{-1}. At all of these wavelengths photofragmentation yielded the conjugate base of triphenol **3** (eq. 3.4) as the sole ion product.

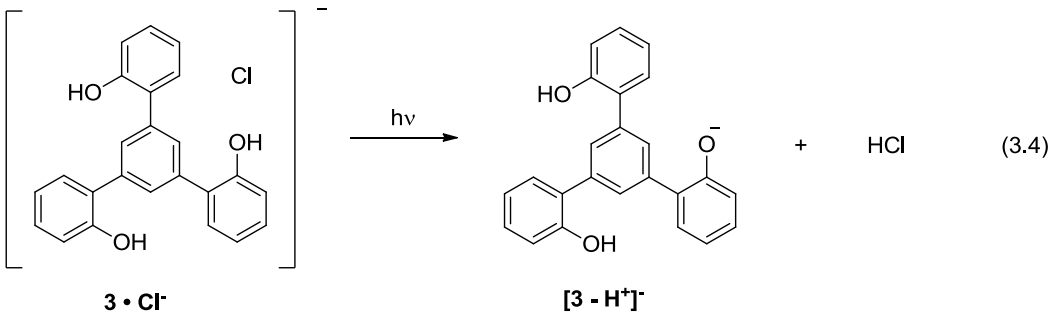

The most intense feature, the doublet at 3065 cm^{-1} and 3080 cm^{-1}, is similar to the absorption feature observed in the diphenol cluster (**2 • Cl**$^-$) which presumably is due to aryl C-H stretching modes. No absorption band is observed for a free hydroxyl group in the spectrum of **3 • Cl**$^-$.

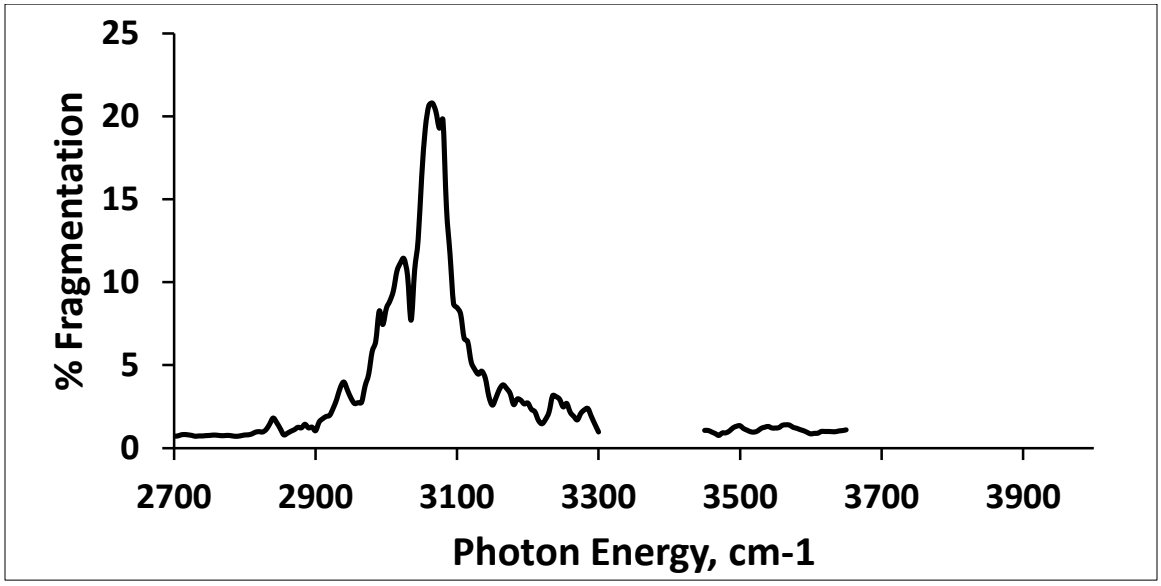

Figure 3.3. Infrared action spectrum of the triphenol **3** cluster with chloride anion (**3 • Cl**$^-$).

When interpreting these infrared action spectra, one must consider the possibility of IR induced isomerization. During the IRMPD process the vibrationally excited ion must convert vibrational energy into thermal energy in a process call intramolecular vibrational relaxation (IVR) in order to return to the ground vibrational state to absorb subsequent photons. The thermal energy gained by the ion is thus available for isomerization to occur. This isomerization can lead to an enhancement of a spectral feature by populating higher energy isomers or conformers that absorb the wavelength of IR light more readily than the ground state ion, thus artificially increasing the fragmentation yield. Conversely, photoinduced isomerization may also lead to a reduction, or complete elimination, of a spectral feature by populating higher energy isomers or conformers that do not absorb IR light at the wavelength being studied. These ions will not fragment because they are no longer absorbing IR light and thus no IRMPD yield will be observed.

Triphenol – Chloride

The infrared action spectrum of the syn-triphenol **1** clustered with chloride anion (**1 syn • Cl**$^-$) was recorded from 2600 – 4000 cm-^{1} (figure 3.4). A strong band was observed having peak maxima at 3054 and 3069 cm^{-1} and a few weaker features appear to be present to the red. At all wavelengths, photofragmentation resulted in the formation of the conjugate base of the triphenol (observed) and HCl (inferred, eq. 3.5).

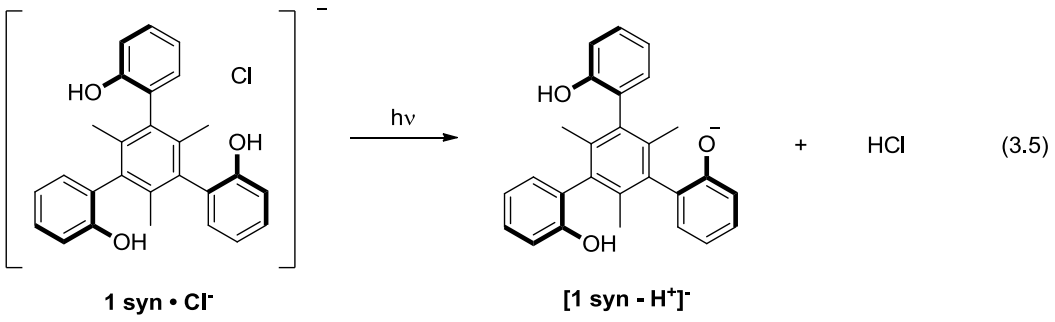

The strong band is undoubtedly due to aryl C-H stretching modes. The weaker red shifted bands presumably are due to aliphatic C–H stretches or combination modes of C-H and O-H stretches. Since no free O-H band is observed between 3500 cm^{-1} and 3700 cm^{-1}, this suggests that all three hydroxyl groups are interacting with the chloride anion.

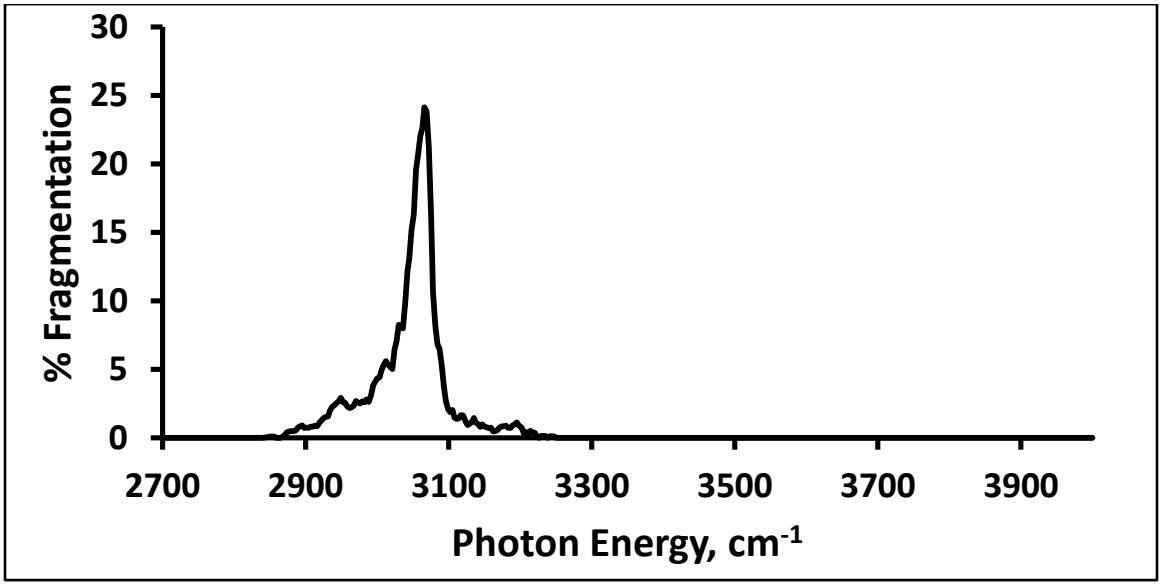

Figure 3.4. Infrared action spectrum of the syn-triphenol **1** cluster with chloride anion (**1 syn • Cl^-**).

To test our assignment, the IR action spectrum of the chloride anion cluster with anti-triphenol **1** (**1 anti • Cl^-**) was obtained (Figure 3.5). A strong band was observed at 3076 cm^{-1} along with a broad complex absorption band from 2700 – 3000 cm^{-1}. Additionally, a sharp band was observed at 3548 cm^{-1}. Photofragmentation yielded **[1 anti – H^+]$^-$** (observed) and HCl (inferred, equation 3.6).

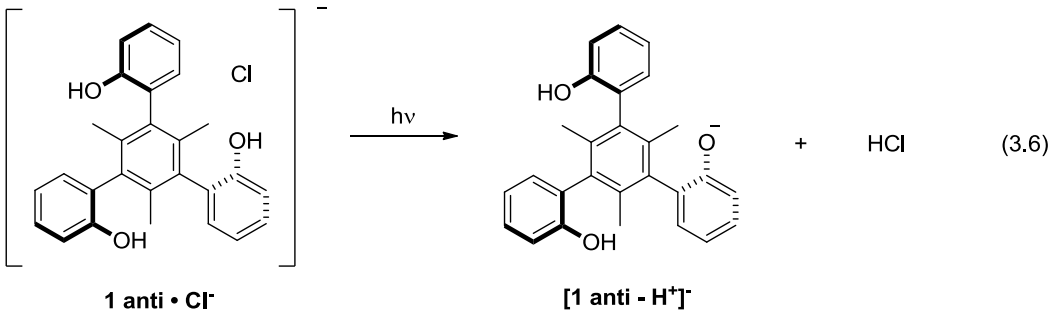

The sharp band at 3548 cm^{-1} is unmistakably due to a free hydroxyl group. The strong absorption band at 3076 cm^{-1} corresponds to the aryl C-H stretching modes. The relatively flat top of this peak shows evidence for two unresolved features, corresponding to the more apparent doublets observed in the other spectra. The broad complex absorption between 2700 and 3000 cm^{-1} can be assigned to O-H/C-H combination bands. This spectrum suggests that the two syn hydroxyl groups interact with Cl^- while the anti O-H group is uncoordinated, i.e. free.

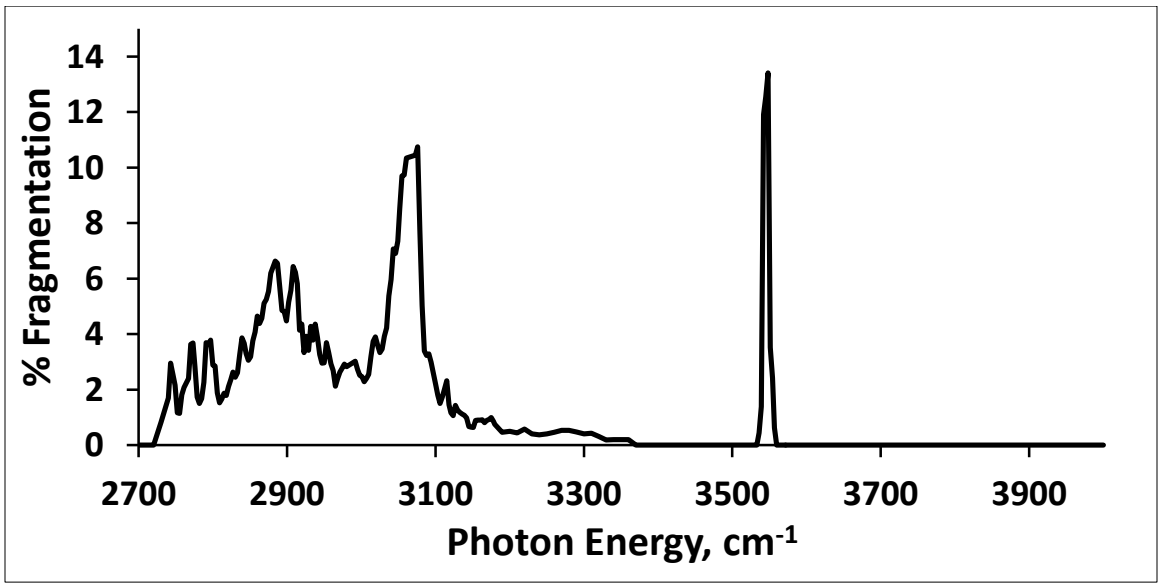

Figure 3.5. Infrared action spectrum of the anti-triphenol **1** cluster with chloride anion (**1 anti • Cl^-**).

Syn-triphenol : alkoxide

To explore the importance of the size and shape of the anion in hydrogen bonding clusters, the IR action spectrum of syn-triphenol **1** clustered with trifluoroethoxide was obtained (figure 3.6). A strong doublet was observed at 3050 cm^{-1} and 3080 cm^{-1} along with several weaker features to both the red and blue of this doublet. Also observed was a band of moderate intensity at 3540 cm^{-1}. Photofragmentation products at all wavelengths were **[1 syn – H^+]$^-$** (observed) and 2,2,2-trifluoroethanol (inferred, equation 3.7).

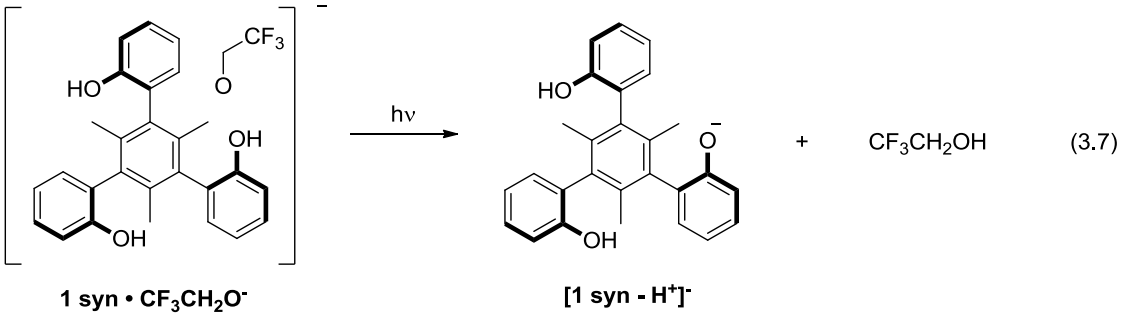

The strong doublet at 3050 cm^{-1} and 3080 cm^{-1} is the characteristic aryl C-H absorption whereas the feature at 3545 cm^{-1} is indicative of a free O-H stretch. The weaker modes between 2800 cm^{-1} and 3200 cm^{-1} can be assigned as C-H and O-H combination bands. These results indicate that the cluster ion cannot simply have a structure in which $CF_3CH_2O^-$ forms three hydrogen bonds to the triol. This is different than for **1 syn • Cl^-** and maybe due to the greater basicity of trifluoroethoxide anion or the smaller size of oxygen compared to chlorine.

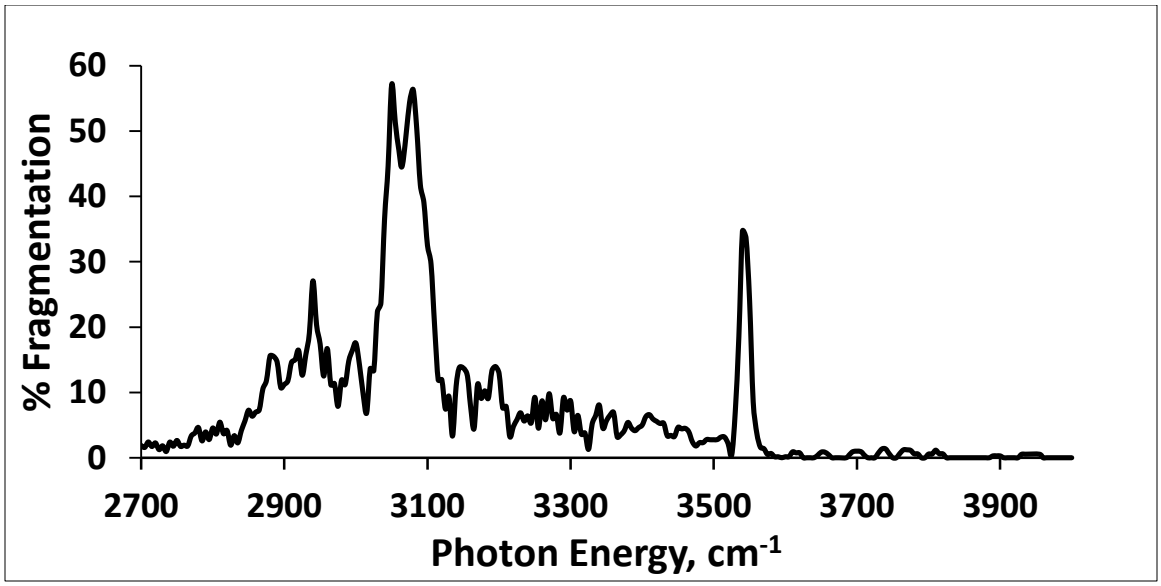

Figure 3.6. Infrared action spectrum of the syn-triphenol **1** cluster with 2,2,2-trifluoroethoxide (i.e. **1 syn • $CF_3CH_2O^-$**)

Syn-triphenol : thiolate

The IR action spectrum of syn-triphenol **1** clustered with thiophenoxide was obtained (Figure 3.7). A strong doublet was observed at 3055 cm^{-1} and 3070 cm^{-1} and a broad, less intense, band centered at 2950 cm^{-1} was seen. Several very low intensity bands were also recorded at 3715, 3760, and 3795 cm^{-1}. Photofragmentation led to **[1 syn – H^+]$^-$** (observed) and thiophenol (inferred, equation 3.8) at all wavelengths.

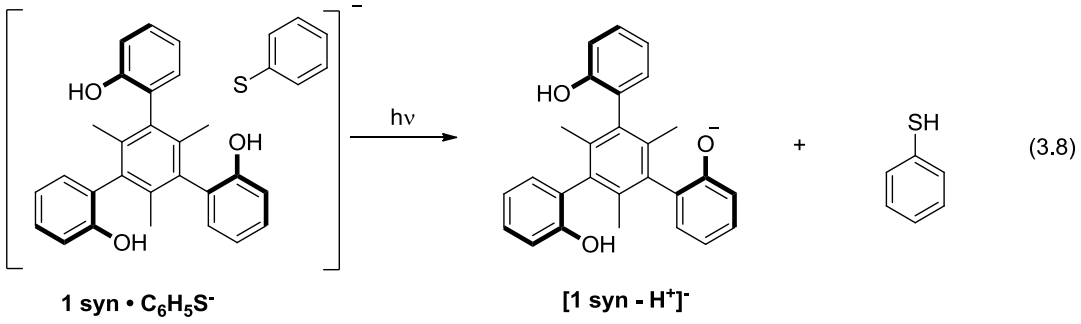

The strong doublet at 3055 cm^{-1} and 3070 cm^{-1} is, again, due to C-H stretching modes. The weaker absorptions between 2800 cm^{-1} and 3000 cm^{-1} can be assigned to C-H and O-H combination bands. As for the absence of a free OH band this suggests that the structure of the **1 syn • $C_6H_5S^-$** cluster anion has three-hydrogen bonds. This is in agreement with the **1 syn • Cl^-** cluster but contrary to the **1 syn • $CF_3CH_2O^-$** anion. This suggests that the size of the anionic atom maybe important since the Van der Waals radii of Cl, S, and O are 1.75, 1.8, and 1.52 Å, respectively.[5] Alternatively, these results maybe a reflection of the proton affinities of these anions since $PA(Cl^-) = 333.6 < PA(PhS^-) = 340.4 < PA(CF_3CH_2O^-) = 361.7$ kcal mol^{-1}.[6]

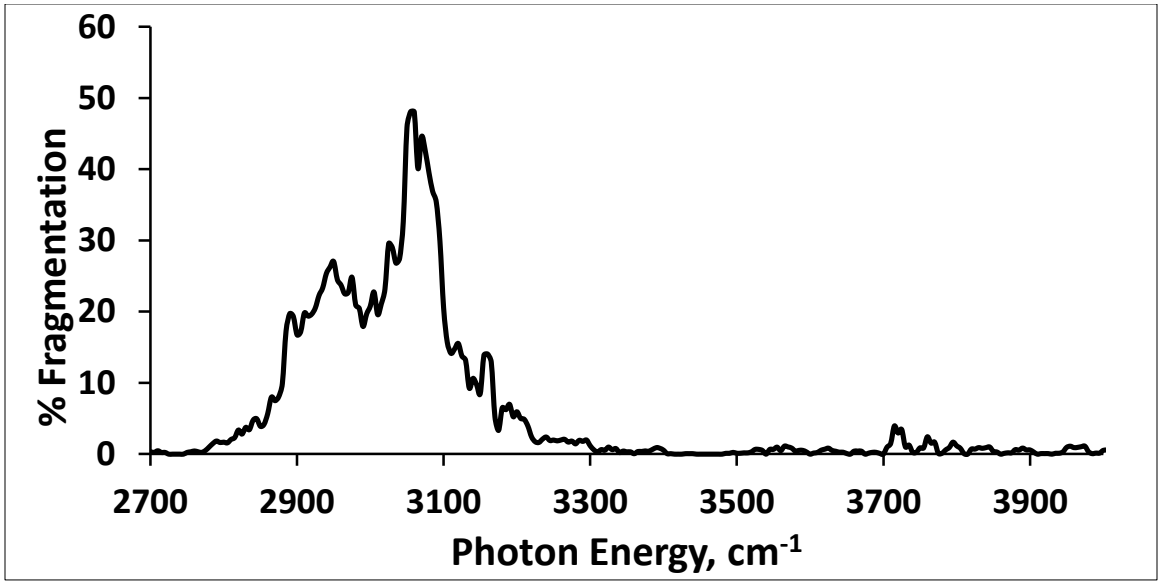

Figure 3.7. Infrared action spectrum of the syn-triphenol **1** cluster with thiophenoxide (i.e. **1 syn • $C_6H_5S^-$**)

Syn-triphenol : acetate, Syn-triphenol : nitrite

The last complexes studied were the clusters of syn-triphenol **1** with the delocalized acetate and nitrite anions. The IR action spectra of the syn-triphenol **1**

clusters shown in figure 3.8 contain an absorption band at ~3550 cm^{-1}. The two spectra also show a low intensity absorption band at 2940 cm^{-1} and the requisite C-H absorption at 3060 cm^{-1}. Photofragmentation products at all wavelengths were **[1 syn – H^+]$^-$** (observed) and acetic acid or nitrous acid, respectively (inferred, equation 3.9).

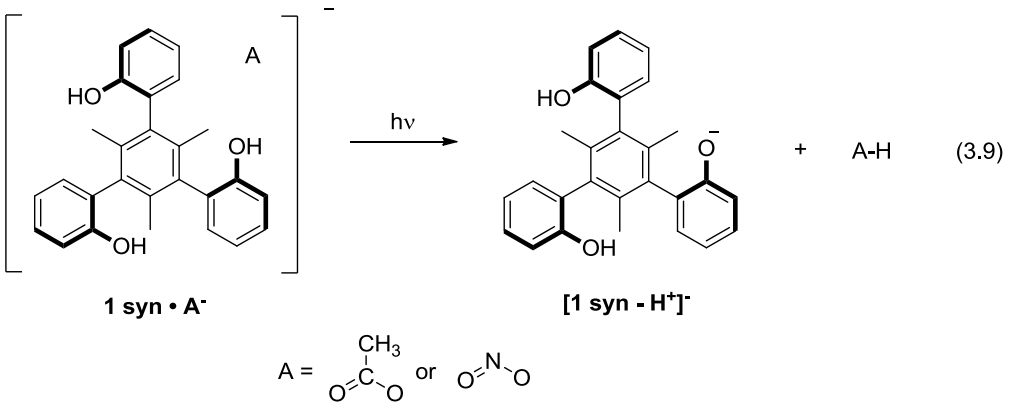

Due to the IR action spectra being acquired in 10 cm^{-1} increments instead of 5 cm^{-1} increments, as in all previous spectra, some spectral resolution was lost. Because of this, the characteristic C-H doublet is not resolved, but is assumed to be present in the absorption band at 3060 cm^{-1}. Both spectra show evidence of a C-H and O-H combination band at 2940 cm^{-1} which is consistent with previous spectra. Most importantly both spectra also show evidence of a free hydroxyl group at 3540 cm^{-1}. This suggests that the cluster ions **1 syn • $CH_3CO_2^-$** and **1 syn • NO_2^-** do not form a simple three hydrogen bonded structure.

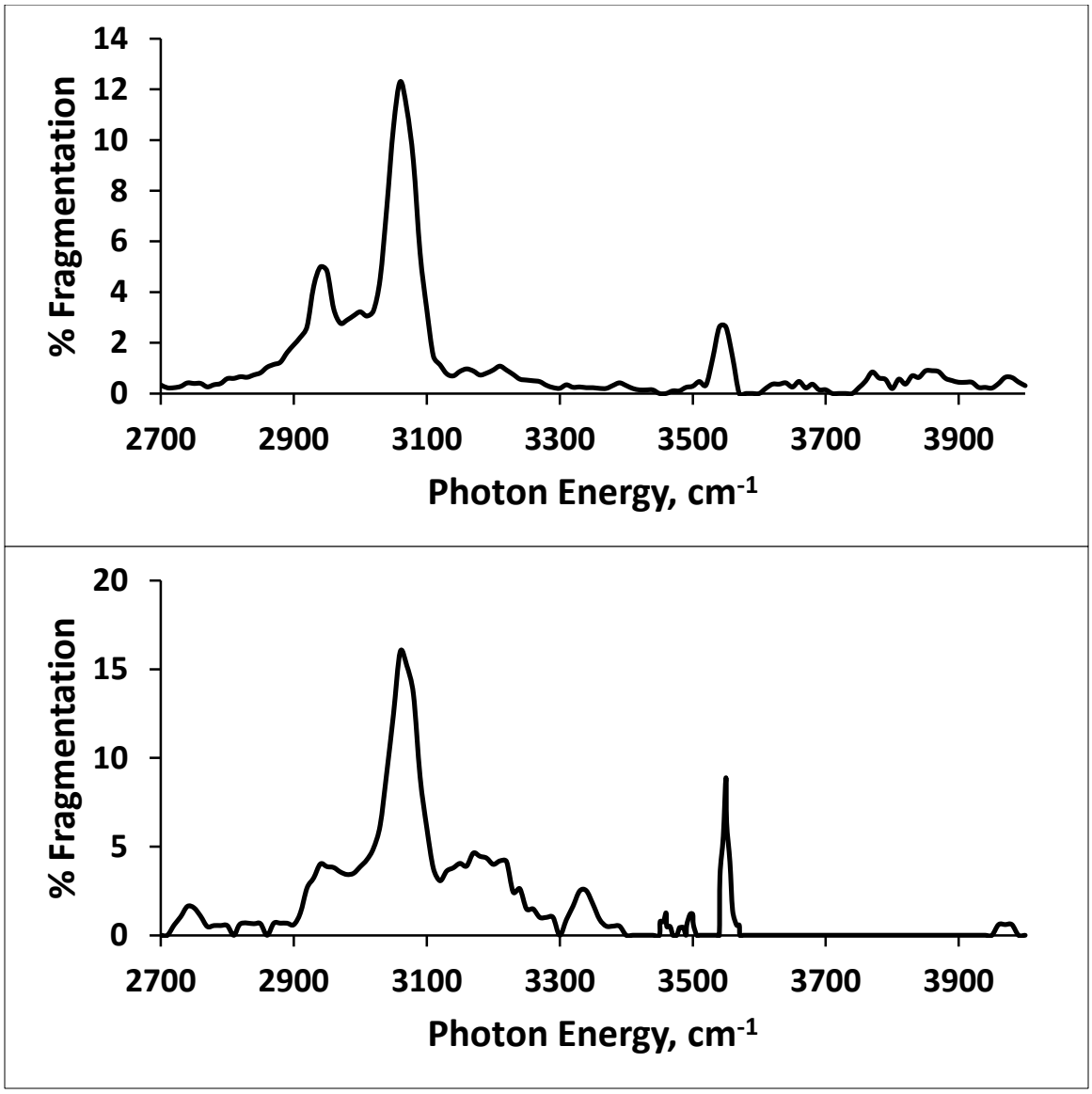

Figure 3.8. Infrared action spectrum of the syn-triphenol **1** cluster with (a) acetate (i.e. **1 syn** • $CH_3CO_2^-$) and (b) nitrite (i.e. **1 syn** • NO_2^-)

Computed Spectra

In all experimental spectra, no absorption of a hydroxyl hydrogen bond to chloride anion was observed in the expected range (i.e. 3150-3200 cm^{-1}). Furthermore, no significant difference was observed in absorption frequencies of the cluster ions even when vastly different anions are substituted for chloride. To investigate this, the infrared spectrum of the triphenol **1** • Cl^- clusters were computed using B3LYP/aug-cc-pVDZ calculations. The computed spectra for the lowest energy conformers were then compared to the experimentally obtained IR action spectra (figure 3.9). The *syn*-**1** • Cl^- structure contains three hydrogen bonds between hydroxyl groups and the chloride anion. The *anti*-**1** • Cl^- structure contains two hydrogen bonds between hydroxyl groups and the chloride, and one free hydroxyl group.

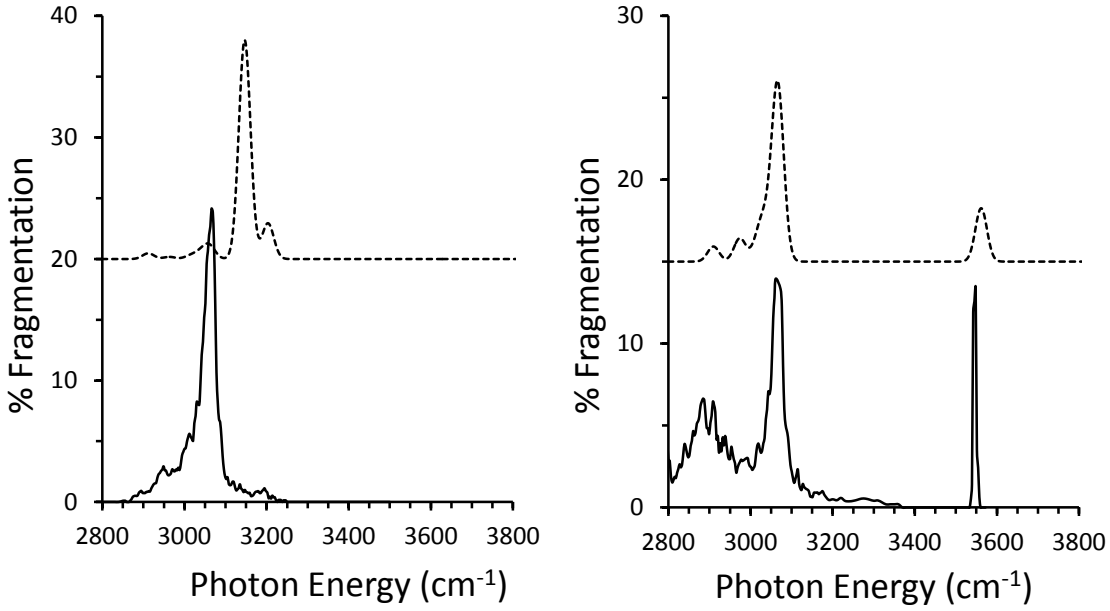

Figure 3.9. Comparison of IR action spectra of *syn*-**1** • Cl^- (left) and *anti*-**1** • Cl^- (right) from 2800 – 3800 cm^{-1}. B3LYP/aug-cc-pVDZ computations with a scaling factor of 0.96 are shown as dotted lines.

While the *anti*-**1** • Cl^- spectra agree, the experimental spectrum for the *syn*-**1** • Cl^- cluster is lacking the prominent hydroxide absorption computed at ~3150 cm^{-1}. When comparing these spectra it should be noted that the experimental data do not correspond to absorption infrared spectra but rather are action spectra. That is, in order to observe absorption at a particular wavelength, the ion must absorb the infrared light and undergo fragmentation. It is likely that the *syn*-**1** • Cl^- cluster photodissociates in a step-wise fashion rather than breaking all three hydrogen bonds simultaneously. Therefore, in order to observe fragmentation, all of the intermediates along the way must absorb infrared light at the same wavelength. If an isomerization takes place and the new species does not absorb infrared photons at the given wavelength, then it will not go on to fragment and no band will be observed in the action spectrum.

We therefore propose that *syn*-**1** • Cl^- with three hydrogen bonds converts to a structure with one hydrogen bond upon absorption of an infrared photon or two, and then this conformer goes on to fragment if and only if it absorbs at the same wavelength. To compute the resulting overlap spectrum, the individual infrared spectra were calculated and the weaker absorption intensity of either species was adopted at each wavelength. The resulting spectrum is given in figure 3.10 and is in good agreement with the experimental spectrum for the *syn*-**1** • Cl^- cluster.

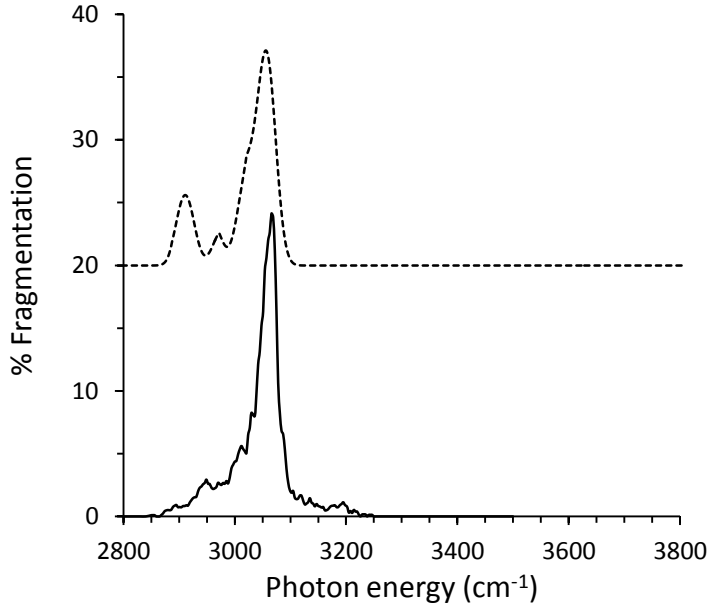

Figure 3.10. Comparison of the IR action spectra of *syn*-**1** • Cl^- (solid line) with the computed overlap spectrum of *syn*-$\mathbf{1}_{3HB}$ and *syn*-$\mathbf{1}_{1HB}$ clusters (dotted line); a scaling factor of 0.96 was used.

The effect of requiring all intermediate ions along the fragmentation pathway to absorb the same frequencies of infrared light results in the elimination of any infrared features unique to any one of the ions from the observed spectrum. In all of the syn-triphenol **1** clusters studied herein the absorption frequency of the prominent hydrogen bonded hydroxyl groups changed as the ion proceeded through the fragmentation pathway. Because of this, the hydrogen bonded hydroxyl groups were not observed in these infrared action spectra.

Conclusions

The effect of hydrogen bonding between triphenol **1** and a variety of anions was probed via IRMPD. Table 3.1 contains absorption peaks for each cluster studied and arranges them by characteristic features: absorptions below 3000 cm^{-1} are due to methyl C–H stretches, absorptions between 3000-3100 cm^{-1} are due to aryl C–H stretches, and absorptions above 3500 cm^{-1} are the result of free OH groups.

Regardless of the species studied, all of the clusters show significant absorption in the C–H region. The anion clustered to a particular polyol should have little interaction with the aliphatic and aromatic hydrogen atoms, so it is not surprising that this absorption feature varies little among the IRMPD spectra. As demonstrated by the computational studies, the expected absorption bands due to hydrogen bonded hydroxyl groups is absent in all spectra due to the change in conformation upon irradiation.

All of the clusters studied also show absorption below 3000 cm^{-1}, although the absorption characteristics vary significantly between different clusters. Since these compounds were designed to form intramolecular hydrogen bonds, it is comforting to see this experimental evidence. The change in absorption characteristics is a subject for future study, but may be due to changes in symmetry of the cluster, which can greatly affect infrared absorption.

By far the most significant feature of these IRMPD spectra is the absorption (or lack thereof) at greater than 3500 cm^{-1}. This absorption is due to the stretching mode of a non-interacting (i.e. free) hydroxyl group. When chloride is used as the anion only anti-triphenol **1** shows evidence of a free hydroxyl substituent. This implies that the more symmetric diol **2**, freely rotating triol **3**, and syn-triphenol **1** all form gas phase structures where all of the hydroxyl groups participate in hydrogen bonds. Conversely, anti-

triphenol **1** cannot form three hydrogen bonds due to the high rotation barrier imposed by the three methyl groups and a free O–H stretch is observed in its cluster.

By studying the IRMPD spectra of triphenol **1** with other anions we were able to gain some insight into the selectivity of the binding of triphenol **1**. Chloride and thiophenoxide are able to accommodate all three hydrogen bonds as shown by the lack of absorption by a free hydroxyl group. Conversely, acetate, nitrite, and an alkoxide (2,2,2-trifluoroethoxide) either undergo a proton transfer in the cluster ion or they can accomodate two hydrogen bonds since the characteristic absorption of a free OH group is observed. One can conclude from these data that since oxygen is smaller than both chlorine and sulfur that the geometry required to accommodate all three hydrogen bonds is too strained and structures with two hydrogen bonds are preferred with smaller atom receptors.

Cluster	**Methyl C-H region**	**Aryl C-H region**	**Free OH**
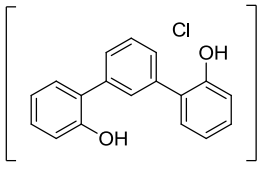 **2 • Cl⁻**	2875 cm^{-1} (broad)	3050 cm^{-1} 3080 cm^{-1}	Not observed
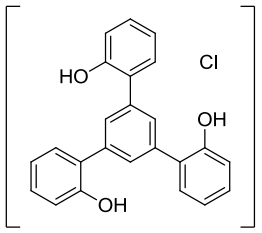 **3 • Cl⁻**	2940 cm^{-1}	3025 cm^{-1} 3065 cm^{-1}	Not observed

Cluster	Hydrogen bonded OH	C-H region	Free OH
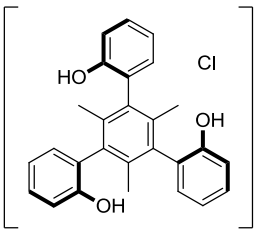 **1 syn • Cl^-**	2946 cm^{-1}	3054 cm^{-1} 3069 cm^{-1}	Not observed
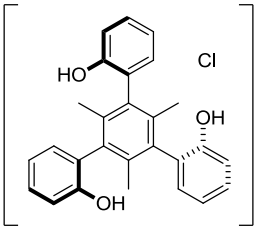 **1 anti • Cl^-**	2887 cm^{-1} (broad)	3073 cm^{-1}	3548 cm^{-1}
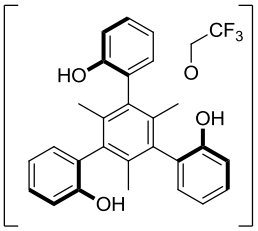 **1 syn • $CF_3CH_2O^-$**	2940 cm^{-1}	3080 cm^{-1} 3050 cm^{-1}	3540 cm^{-1}
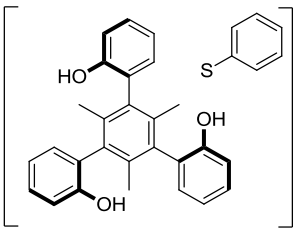 **1 syn • $C_6H_5S^-$**	2950 cm^{-1}	3055 cm^{-1} 3070 cm^{-1}	Not observed
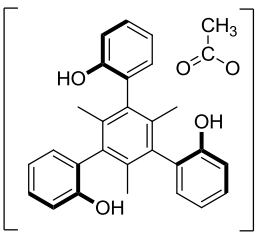 **1 syn • CH_3COO^-**	2940	3060	3540 cm^{-1}

Cluster	Hydrogen bonded OH	C-H region	Free OH
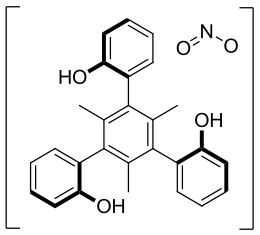 1 syn • NO_2^-	2940 cm^{-1}	3070 cm^{-1}	3550 cm^{-1}

Table 3.1. Infrared Absorption Peaks for all Clusters Studied Arranged by Functional Group.

Triphenol **3** has many potential applications. Due to its ability to bind to different anions, it can be used as an analog for many biological interactions, such as those seen in anion channels and other ion transporters.[7] It has potential for use as an organic catalyst via an anion abstraction mechanism and as a hydrogen bond donor; encouraging results have been obtained in this regard. Finally, compounds related to **syn 1** are being explored as potential chemoselective sensors.[8]

References

1. (a) Schreiner, P. R.; Wittkopp, A. *Org. Lett.* **2002**, *4*, 217-220.
   (b) Schreiner, P. R. *Chem. Soc. Rev*. **2003**, *32*, 289-296.
   (c) Takemoto, Y. *Org. Biomol. Chem*. **2005**, *3*, 4299-4306.
   (d) Taylor, M. S.; Jacobsen, E. N. *Angew. Chem. Int. Ed.* **2006**, *45*, 1520-1543.
   (e) Stephen, J. C. *Chem. Eur. J.* **2006**, *12*, 5418–5427.
   (f) Doyle, A. G.; Jacobsen, E. N. *Chem. Rev.* **2007**, 107, 5713-5743.
   (g) Rawal, V. H.; Thadani, A. N. *Asymmetric Synthesis – The Essentials*, 2nd Edition; Christmann, M., Brase, S., Eds., Wiley-VCH: Weinheim, **2008**, pp. 144-148.
   (h) Pihko, P. M. Ed., *Hydrogen Bonding in Organic Synthesis*, Wiley-VCH: Weinheim, **2009**.
   (i) Zhang, Z.; Schreiner, P. R. *Chem. Soc. Rev.* **2009**, *38*, 1187-1198.
   (j) Knowles, R. R.; Jacobsen, E. N. *Proc. Natl. Acad. Sci. USA* **2010**, *107*, 20678-20685.
2. Reisman, S. E.; Doyle, A. G.; Jacobsen, E. N. *J. Am. Chem. Soc.* **2008**, *130*, 7198-7199.
3. (a) Martinez, C.; Nicolas, A.; van Tilbeurgh, H.; Egloff, M. P.; Cudrey, C.; Verger, R.; Cambillau, C. *Biochem.* **1994**, 33, 83-89.
   (b) Harel, M.; Quinn, D. M.; Nair, H. K.; Silman, I.; Sussman, J. L. *J. Am. Chem. Soc*. **1996**, *118*, 2340-2346.
   (c) Machajewski, T. D.; Wong, C.H. *Angew. Chem. Int. Ed*. **2000**, *39*, 1352-1374.
   (d) Zhang, Y.; Kua, J.; McCammon, J. A. *J. Am. Chem. Soc*. **2002**, *124*, 10572-10577.
   (e) Zhu, X.; Larsen, N. A.; Basran, A.; Bruce, N. C.; Wilson, I. A. *J. Biol. Chem.* **2003**, *278*, 2008-2014.
   (f) Lo, Y. C.; Lin, S. C.; Shaw, J. F.; Liaw, Y. C. *J. Mol. Biol*. **2003**, *330*, 539–551.
   (g) Nachon, F.; Asojo, O. A.; Borgstahl, G. E. O.; Masson, P.; Lockridge, O. *Biochemistry* **2005**, *44,* 1154-1162.
   (h) Simóna, L.; Muñiza, F. M.; Sáeza, S.; Raposob, C.; Morána, J. R. *ARKIVOC* **2007**, 47-64.
   (i) Chen, X.; Fang, L.; Liu, J.; Zhan, C. G. *Biochemistry* **2012**, *51*, 1297−1305.
4 Schmidt, J.; Meyer, M.M.; Spector, I.; Kass, S.R. *J. Phys. Chem. A.* **2011,** *115*, 7625-7632.
5 Bondi, A. *J. Phys. Chem.* **1964**, 68, 441-451.
6 (a) Fujio, M.; McIver, R.T., Jr.; Taft, R.W., *J. Am. Chem. Soc.* **1981**, 103, 4017.
   (b) Taft, R.W.; Bordwell, F.G., *Acc. Chem. Res*. **1988**, 21, 463.
   (c) Robin, M.B.; Kuebler, N.A., *J. Electron Spectrosc. Relat. Phenom*. **1973**, 1, 13.
7 (a) Raghavan, A.; Sheiko, T.; Graham, B. H.; Craigen, W. J. *Biochimica et Biophysica Acta, Biomembranes.* **2012**, *1818*, 1477-1485.
   (b) Haynes, C. J. E.; Gale, P. A. *Chem. Commun*. **2011**, *47,* 8203-8209.
   (c) Gale, P. A. *Acc. Chem. Res*. **2011**, *44*, 216-226.
   (d) Brotherhood, P. R.; Davis, A. P. Chem. Soc. Rev. **2010**, 39, 3633-3647.
   (e) Davis, J. T.; Okunola, O.; Quesada, R. Chem. Soc. Rev. **2010**, 39, 3843-3862.
   (f) Gale, P. A. Coord. Chem. Rev. **2006**, 250, 2939-2951.
8 Buhlmann, P.; Chen, L. D. Supramolecular Chemistry: From Molecules to Nanomaterials, Steed, A. W., Gale, P. A., Eds., Wiley: New York, **2012**, Vol. 5, pp 2539-2580.

Chapter 4

Infrared spectroscopy of a hydrogen bonded network.

Introduction

Hydrogen bonding is ubiquitous in nature and required for life as we know it to exist. All biological macromolecules, such as DNA and proteins, rely on hydrogen bonding to maintain their three dimensional structure and intermolecular interactions. Enzymes have been shown to utilize hydrogen bonding to recognize,[1] transport,[2] sequester,[3] and catalyze the reactions of anions.[4]

Of particular interest are the hydrogen bonds involved in enzyme-substrate interactions in which the enzyme utilizes multiple hydrogen bonds to stabilize a reaction intermediate, thus catalyzing a chemical reaction. Some of these stabilizations have been calculated to be over 20 kcal mol^{-1}.[5] Since the strongest hydrogen bond measured in solution has a strength of less than 10 kcal mol^{-1},[6] Cleland, Gerlt and Gassman, Kreevoy, and Frey have proposed the existence of a separate class of hydrogen bonds, called low barrier hydrogen bonds (LBHBs). These LBHBs can achieve hydrogen bonding strengths greater than those measured in solution due to their shorter than typical hydrogen bond lengths.

An alternative explanation for the unusually strong stabilizations seen in enzymes is the use of an intramolecular hydrogen bonding network. Unlike the LBHB proposal which consists of only a few strong hydrogen bonds, a hydrogen bond network might

consist of many otherwise ordinary hydrogen bonds. The total stabilization achieved by this network, however, can overcome the 20 kcal mol^{-1} stabilization seen in enzymes. For example, the gas phase acidities of several aliphatic alcohols containing intramolecular hydrogen bonds have been measured.[7] The tertiary tetraol **1** was found to have an acidity (ΔG°_{acid}) of 334.4 ± 1.7 kcal mol^{-1} which is about 35 kcal mol^{-1} more acidic than *tert*-butanol (ΔG°_{acid} = 369.2 ± 0.7 kcal mol^{-1}). This significant increase in acidity is directly related to the stabilization of the conjugate base by the intramolecular hydrogen bonding as shown below. Tetraol **1**, however, only utilizes three intramolecular hydrogen bonds to mimic an inner solvation shell. A second set of hydrogen bonds can be incorporated into the molecule to introduce a second solvation shell, as seen in heptaol **2**. The gas phase acidity of heptaol **2** has been measured to 313.5 ± 5.0 kcal mol^{-1}, which is roughly as acidic as HBr (ΔG°_{acid} = 318.3 ± 0.1 kcal mol^{-1})[8] and 21 kcal mol^{-1} more acidic than tetraol **1**.[9] This increase in acidity over tetraol **1** can largely be attributed to the addition of the second solvation shell of hydrogen bonds.

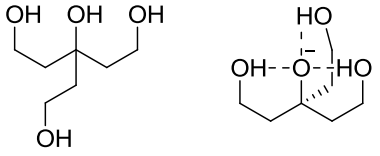

1

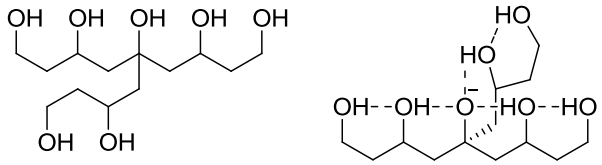

2

While gas phase acidities can give insight into the total stabilization of an ion, determining the strengths of individual hydrogen bonds (and the actual molecular structures) is more difficult. Infrared spectroscopy, however, can be used to probe structure and individual bond strengths by measuring the absorption frequencies of the hydrogen bonds. Infrared multiphoton dissociation (IRMPD) spectroscopy has been used previously by the Kass lab and others to record the infrared spectrum of gas phase

ions. In this work, IRMPD was used to investigate the geometry and the relative difference in hydrogen bonding strengths of different hydrogen bonds in a chloride anion cluster with heptaol **2**.

Experimental Section

A Fourier transform mass spectrometer (FTMS) coupled to a tunable infrared laser that has been previously described was used in these studies. Heptaol **2** was prepared by Alireza Shokri in the Kass lab. Electrospray solutions were prepared by dissolving **2** in a 3:1 methanol:water solution at approx. 2 mM concentration. For deutero studies heptaol **2** was dissolved in a 3:1 CD_3OD:D_2O solution at approx. 2 mM concentration. Ammonium chloride was then added to the solution in approx. a 1:1 ratio with heptaol **2**. Ions were generated in a Waters Z-spray electrospray ionization (ESI) source by a direct infusion of the solution at 10 μL/min. A voltage of +4500V was applied to the ESI needle while the sample cone was held at +5V. An extractor cone at -5V guided the ions into an RF storage hexapole (75V RF, -3V DC) where ions were accumulated for 10 seconds by using a -30V end cap potential.

After the accumulation time, the hexapole was set to expel ions (0V RF, -5V DC, +1V end cap) and a mechanical shutter was opened to allow transfer of ions into the quadrapole ion guide (220V RF, +10V DC, 1.325 MHz) which moved them along into the Penning trap, or ion cyclotron resonance (ICR) cell. To allow for ions to enter the cell, the trapping plate facing the quadrapole was grounded for 2.616 ms, then a trapping potential of -15V was re-applied. A pulse of argon gas was introduced into the quadrupole region during ion transfer to both help trap the ions in the cell as well as to

collisionally cool them. Ions were trapped with a -15V potential on either end of the cell for 1.5 seconds, after which the trapping potentials were lowered to -1.5V.

Cluster ions were isolated by ejecting unwanted ions with short duration, high voltage, rf bursts, or "chirps". Ions were irradiated for 10 s at a 10 Hz pulse rate at a given wavelength of IR light which was scanned from 2800 – 3800 cm^{-1} in 5 cm^{-1} increments. Each spectrum datum point is comprised of a single sequence, that is, new ions are generated, transferred, isolated, cooled, and irradiated at each wavelength. The energy of the IR light was 5 mJ/pulse at 2700 cm^{-1} and this increases roughly linearly to 26 mJ/pulse at 4000 cm^{-1}. After irradiation, the total ion abundance was observed and the amount of fragmentation in terms of percentage (Eq. 4.1) was plotted vs. IR wavelength.

$$\text{Fragmentation (\%)} = (100 \times (\Sigma I_{\text{fragment ions}})/(\Sigma I_{\text{fragment ions}} + I_{\text{parent ion}})) \quad (4.1)$$

IR action spectra data points were smoothed using a simple moving average according to equation 2. This was done to more easily differentiate true spectral features from natural variations primarily resulting from fluctuations in the Nd:YAG shot to shot laser power. IR data were not corrected for the change in photon energy due to wavelength or the change in laser power output over the scanned range.

$$y_{avg} = \frac{y_{x-1} + y_x + y_{x+1}}{3} \quad (4.2)$$

The cluster of heptaol **1** with chloride anion (**2** • $\mathbf{Cl^-}$) was subjected to fragmentation vs. time studies by generating, transferring, and isolating ions as described above. These ions were irradiated with IR light at 3400 cm^{-1} at a frequency of 10 Hz for between 0.5 seconds and 150 seconds. The amount of fragmentation was calculated by equation 1 and plotted vs. irradiation time in seconds.

Results and Discussion

Infrared Spectroscopy

The infrared action spectrum of heptaol **2** clustered with chloride anions (**2** • Cl^-) was recorded from 2800 – 3800 cm^{-1} (figure 4.1). A sharp absorption band was observed at 2945 cm^{-1} followed by three overlapping features centered at 3245, 3400, 3540 cm^{-1}. Photofragmentation of the (**2** • Cl^-) cluster at all wavelengths yields the conjugate base of heptaol **2** as the ionic product and HCl as the unobserved neutral product, as shown in equation 4.3.

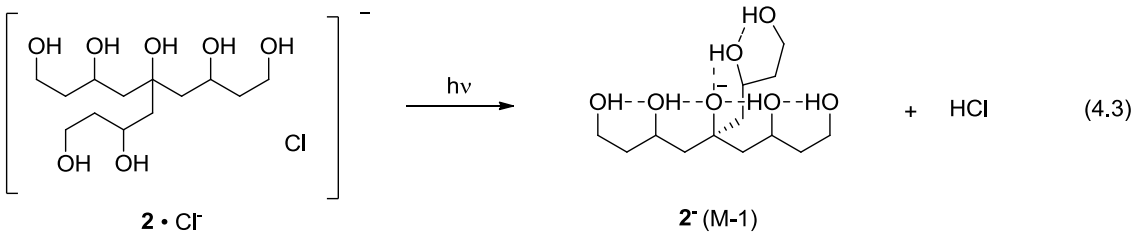

2 • Cl^- **2**$^-$ (M-1)

The band observed at 2945 cm^{-1} can be attributed to C-H stretching, but the remaining bands have absorption frequencies too high for aliphatic C-H stretches. This implies that the remaining three features are due to O-H stretching.

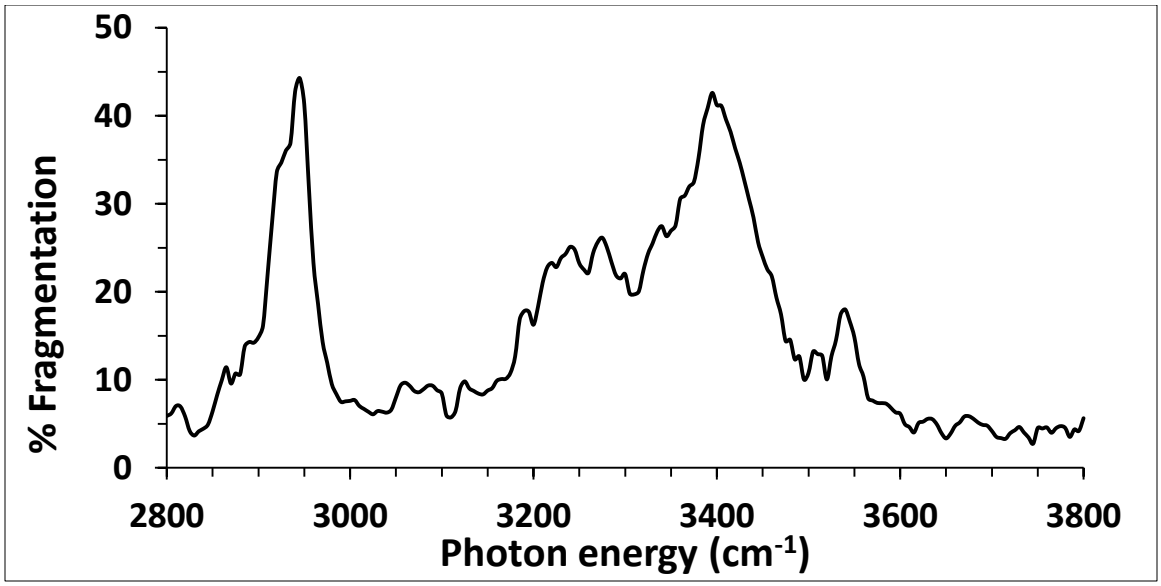

Figure 4.1. Infrared action spectrum of heptaol **2** clustered with chloride anion (**2** • Cl^-).

To confirm the band assignment, the infrared action spectrum of d_7-heptaol **2** clustered with chloride ($\mathbf{2_{d7}}$ • Cl^-) was obtained from 2800 to 3700 cm^{-1} (figure 4.2). A sharp doublet was observed with peaks at 2940 and 2944 cm^{-1}. As with the (**2** • Cl^-) cluster, photofragmentation yields the conjugate base of heptaol **2** as the ionic product and DCl as the neutral product (equation 4.2).

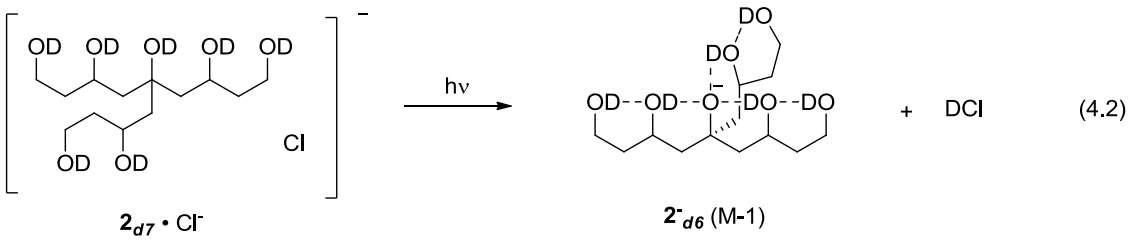

$\mathbf{2}_{d7}$ • Cl^- $\mathbf{2}^-_{d6}$ (M-1)

Since the O-D bond absorbs IR light at a much lower frequency than the O-H bond (i.e., $\nu_{OH}/\sqrt{2}$), the only observable features must be due to C-H stretching. Conversely, since no absorption above 3000 cm^{-1} was observed for the ($\mathbf{2}_{d7}$ • Cl^-) cluster all of the absorptions above this value for **2** • Cl^- must be due to O-H stretching.

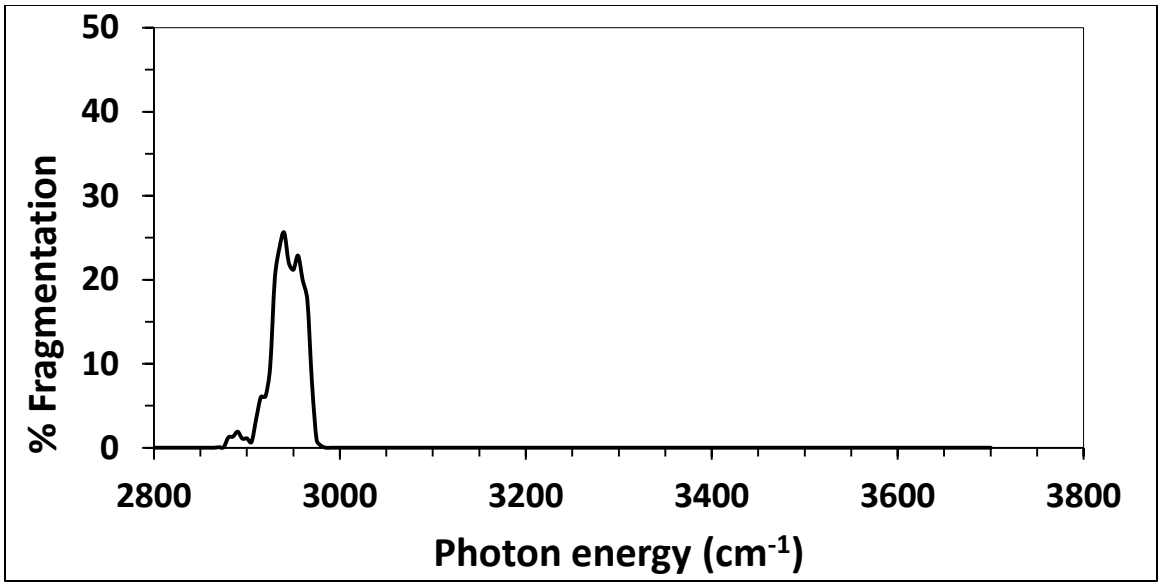

Figure 4.2. Infrared action spectrum of heptaol $\mathbf{2}_{d7}$ clustered with chloride anion ($\mathbf{2}_{d7} \bullet Cl^-$).

The frequency of the stretching of a chemical bond is directly related to the bond strength. Due to the existence of three different IR spectral features that can all be attributed to O-H stretching, we can conclude that there are distinctly different O-H bonds with varying strengths. In other words, the IRMPD action spectrum suggests that heptaol **2** adopts more than one solvation shell around the chloride anion.

Computational comparisons

To gain further insight into the structure of the heptaol **2** – chloride cluster the experimental IR action spectrum can be compared to the B3LYP/aug-cc-pVDZ calculated spectrum for the same ion. Shown in figure 3 are the predicted frequencies for the lowest energy conformer using a scaling factor of 0.964 at all wavelengths.

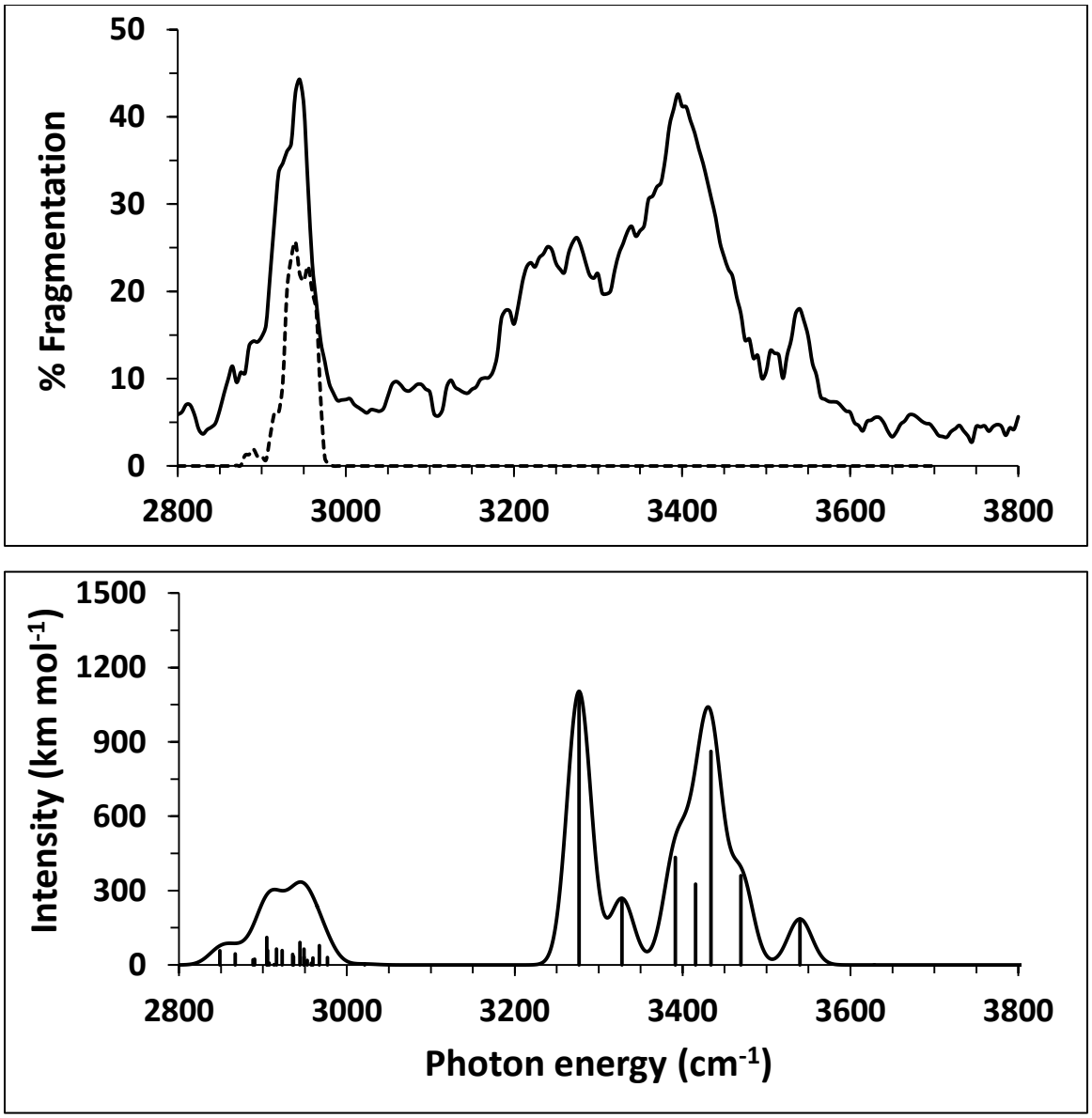

Figure 4.3. Top: Infrared action spectra of heptaol **2** clustered with chloride anion (**2** • Cl^-, solid line) and heptaol $\mathbf{2}_{\mathbf{d7}}$ clustered with chloride anion ($\mathbf{2}_{\mathbf{d7}}$ • Cl^-, dotted line). Bottom: Computational spectrum (B3LYP/aug-cc-pVDZ). The simulated spectrum was generated by assigning and summing Gaussian peaks with a width of 35 cm^{-1} at half height for each predicted frequency.

All bands predicted below 3000 cm^{-1} are due to C-H stretches which is in accordance with the heptaol $\mathbf{2}_{\mathbf{d7}}$ • Cl^- results. The strong band predicted at 3265 cm^{-1} is due to the stretching of two secondary hydroxyl groups hydrogen bonded to the chloride

anion (OH • • Cl^-). These hydrogen bonds are the strongest ones since they are interacting directly with the anion and have the lowest O-H stretching frequency. This band is a good match for the experimental absorption observed at 3245 cm^{-1}. The second largest predicted band has a frequency of 3434 cm^{-1} and is due primarily to secondary hydroxyls hydrogen bonded to other hydroxyl groups (OH • • OH). These hydrogen bonds are weaker since they are interacting with neutral moieties rather than the charged chloride anion, and thus have intermediate stretching frequencies. This predicted band is a good match for the observed absorbance at 3400 cm^{-1}. Finally, the last distinct predicted band has a frequency of 3540 cm^{-1} and is due to the primary hydroxyl group which is not directly interacting with the chloride ion. This neutral OH..OH hydrogen bond is the weakest one in the molecule and has the highest vibrational frequency. It is also a good match for the experimentally observed band at 3540 cm^{-1}.

Conclusions

The infrared action spectrum of a heptaol-chloride cluster was obtained. At least three hydroxyl groups with distinct absorbance frequencies were observed as well as a C-H absorption. Furthermore, the experimental IR action spectrum is in excellent accord with computational predictions.

The existence of at least three distinct hydroxide groups is evidence of multiple hydrogen bonds of different types in the heptaol-chloride cluster ion; the different interaction energies affect the resulting IR absorption frequencies. Stronger hydrogen bonds weaken the covalent O-H bond and consequently appear at lower frequencies. The highest frequency feature corresponds to a weak neutral–neutral OH..OH hydrogen

bond far from the charged center whereas the other bands are the result of stronger interactions.

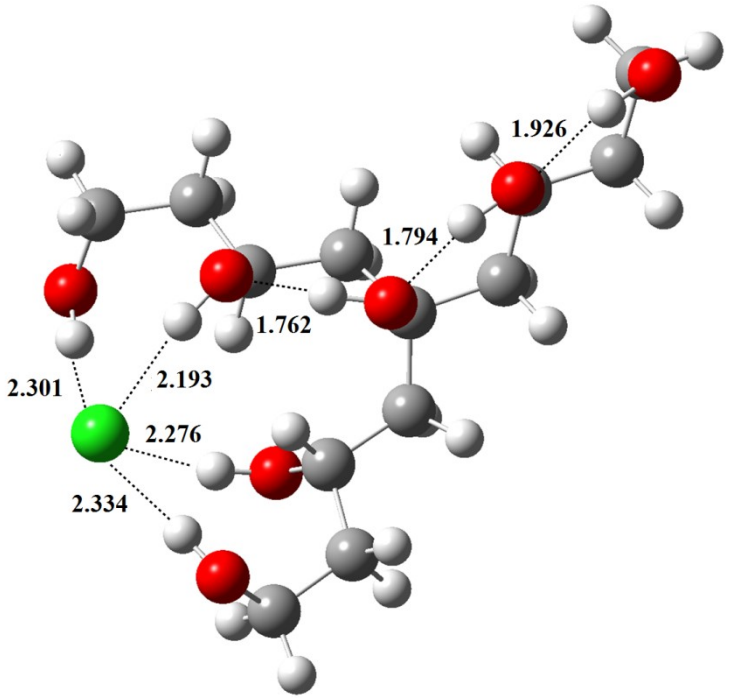

Fig. 4.4. Lowest energy B3LYP/aug-cc-pVDZ structure for the addition complex of **2** and Cl^{-}.

Considering the structure of the heptaol-chloride cluster ion, we propose the two distinct hydrogen bonds observed via IR action spectroscopy relate to an inner and outer solvation shell, as shown in figure 4.4, which corresponds to the computationally predicted IR spectrum above. The four hydroxyl groups directly interacting with the chloride anion, observed at ~3250 cm^{-1}, have the strongest hydrogen bond, and therefore the weakest O-H bond strength. These hydroxyls make up the first solvation shell. The next two hydrogen bonds, observed at ~3400 cm^{-1}, make up the second and third solvation shells. Finally, the remaining, and weakest, hydrogen bonded hydroxyl

accounts for the absorption observed at 3540 cm $^{-1}$ and comprises the fourth solvation shell.

References

1. (a) Kavallieratos, K., de Gala, S.R., Austin, D.J., Crabtree, R.H., *J. Am Chem. Soc.* **1997,** *119*, 2325-2326.
   (b) Kavallieratos, K., Bertao, C.M., Crabtree, R.H., *J. Org Chem*. **1999,** *64*, 1675-1683.
   (c) Chmielewski, M.J., Jurczak, J., *Chem. Eur. J*. **2005,** *11*, 6080–6094.
   (d) Kang, S.O., Begum, R.A., Bowman-James, K., *Angew. Chem., Int. Ed*. **2006**, *45,* 7882–7894.
   (e) Esteban-Gomez, D., Fabbrizzi, L., Licchelli, M., *J. Org. Chem.* **2005**, *70* 5717–5720.
   (f) Lee, K.H., Hong, H.I., *Tetrahedron Lett.* **2000**, *41* 6083–6087.
   (g) Garcia-Garrido, S.E., Caltagirone, C., Light, M.E., Gale, P.A., *Chem. Commun*. **2007**, 1450–1452.
   (h) Sessler, J.L., Camiolo, S., Gale, P.A., *Coord. Chem. Rev*. **2003**, *240,* 17–55.
2. (a) Dutzler, R., Campbell, E.B., Cadene, M., Chait, B.T., MacKinnon, R., *Nature* **2002**, *415,* 287-294.
   (b) Dutzler, R., Campbell, E.B., MacKinnon, R., *Science,* **2003,** *300,* 108-112.
   (c) Accardi, A., Miller, C., *Nature,* **2004**, *427,* 803-807.
   (d) Miller, C., *Nature,* **2006**, *440,* 484-489 (2006).
3. Pflugrath, J.W., Quiocho, F.A., *Nature,* **1985**, *314,* 257-260.
4. Simon, L., Goodman, J.M., *J. Org. Chem.,* **2010,** *75,* 1831-1840.
5. (a) Jencks, W. P. *Adv. Enzymol. Relat. Areas Mol. Biol.* **1975**, 43, 219– 410.
   (b) Jencks, W. P. *Acc. Chem. Res.* **1976**, 9, 425– 432.
6. Guthrie, J. P. *Chem. Biol.* **1996**, 3, 163– 170.
7. Tian, Z., Fattahi, A., Lis, L., Kass, S.R., *J. Am. Chem. Soc.*, **2009**, *131*, 16984-16988.
8. Blondel, C.; Cacciani, P.; Delsart, C.; Trainham, R., *Phys. Rev. A*, **1989**, 40, 3698.

Chapter 5

Zwitterion vs Neutral Structures of Amino Acids Stabilized by a Negatively Charged Site: Infrared Photo-dissociation and Computations of Proline–Chloride Anion

Introduction

All 20 protein forming α-amino acids adopt neutral structures (i.e., $H_2NCH(R)CO_2H$) in the gas phase but exist as zwitterions (i.e., $^{+}H_3NCH(R)CO_2^{-}$) in aqueous solutions over a wide pH range.[1] This structural difference has prompted extensive experimental and computational studies on the sequential hydration of amino acids, particularly for glycine (R = H), the simplest of these compounds.[2,3] Calculations indicate that the zwitterionic form of glycine does not exist in that it is not a minimum on the potential energy surface,[4] but in a landmark study Jensen and Gordon found that only two water molecules are needed to make the zwitterion a local minimum energy structure.[2b] In a subsequent mass spectrometric and photoelectron spectroscopy investigation on Gly • $(H_2O)_n^{-}$ clusters, Bowen et al. deduced that five water molecules is the lower limit for the switching point when zwitterionic glycine becomes more stable than its neutral form.[3a] This conclusion is supported by recent computations from three research groups using different methodologies that indicate 7, 8, or 9 is the minimum number of waters needed to stabilize the zwitterion below the energy of the neutral structure.[2c-e]

While the hydration of amino acids is an important topic, peptides and proteins typically are charged species. Ion transport across cell membranes and from one cellular region to another are also critical biochemical processes.[5] As a result, the structures of

amino acid–ion complexes have garnered attention too, and there are numerous reports of positively charged clusters in the literature.[6] Anionic species are much less studied, even though proteins and enzymes commonly are negatively charged.[7] Small charged cluster ions can also serve as transition state or reactive intermediate models for hydrogen-deuterium exchange processes, which are widely used reactions for determining the three-dimensional structures of proteins.[8] Simple electrostatic arguments for both negatively and positively charged complexes indicate that the zwitterionic structures are preferentially stabilized relative to their neutral counterparts by the presence of an ion. This does not mean that the zwitterionic clusters are necessarily more stable than the neutral ones because the latter forms of the free α-amino acids are the lower energy structures in the gas phase. In any case, cations are attracted to electron rich regions whereas anions coordinate to electrophilic sites and commonly form N–H •• X^- and O–H •• X^- hydrogen bonds. The structural features of small negatively and positively charged complexes, consequently, should be quite different from each other.

Infrared photodissociation (IRPD) spectroscopy has been widely used as a structural tool for the determination of many cationic amino acid and peptide complexes.[9] Recently, the first IRPD spectra of anionic amino acid clusters were reported for halide complexes with arginine (Arg), histidine (His) and glutamic acid (Glu).[10] Of the 20 protein forming α-amino acids, these three are among the strongest acids and bases.[11,12] One might expect this to promote zwitterion formation, but only the Arg spectra are of such a species. We have been interested in zwitterions and amino acid – anion clusters for a long time,[13] and report herein our work on the chloride complex of proline (Pro). This α-amino acid was chosen, in part, because it is known to stabilize proteins and play an important role in determining their structures.[14] It also accumulates in plants and animals

in response to osmotic and low temperature stress,[15] and is the only cyclic protein-forming α-amino acid with its *N*-terminus incorporated into a ring (i.e., a secondary amine). As a result, it is less flexible than other amino acids and this reduces conformational issues, and facilitates carrying out computations on proline–containing species. One might also anticipate that the zwitterionic structure of Pro • Cl^- is disfavored because proline is also one of the weakest α-amino acids (i.e., ΔH_{acid}(Pro) = 342.0 ± 2.2 vs ΔH_{acid}(Gly) = 342.7 ± 2.2 kcal mol^{-1} (weakest) and ΔH_{acid}(Asp) = 321.5 ± 3.3 kcal mol^{-1} (strongest))[11] and its proton affinity (225.1 kcal mol^{-1}) is closer in magnitude to the weakest base (PA(Gly) = 211.9 kcal mol^{-1}) than to the strongest one (PA(Arg) = 250.1 kcal mol^{-1}).[12]

Experimental Section

A Fourier transform mass spectrometer (FTMS) coupled to a tunable infrared laser that has been previously described was employed in these studies.[16] L-Proline and DL-proline-d_7 were used as received from Sigma-Aldrich and Cambridge Isotopes Laboratories, respectively. Electrospray solutions with concentrations of ~2 mM were prepared by dissolving proline or its d_7-isotopomer and one equivalent of ammonium chloride in a 3:1 (v/v) mixture of methanol and water. The d_2-isotopomer was also generated by dissolving unlabeled proline in a 3:1 mixture of methanol-d_4 and deuterium oxide.

Electrospray ionization (ESI) was used to form ions by direct infusion of the appropriate solution at a flow rate of 10 μl min^{-1} into a Waters Z-spray source. The ESI needle, sample, and extractor cones were held at voltages of 4000, -25, and -4 V, respectively, to guide the negative ions into a RF storage hexapole (80 V RF, -0.8 V DC)

where they were accumulated for 2 s by applying a -12 V potential to the end cap. The anions were subsequently extracted from the hexapole (0 V RF, -3 V DC, and 50 V end cap), and a mechanical shutter was opened to enable them to pass into a quadrupole ion guide (35 V RF, 25 V DC) operating at 1.325 MHz. These negatively charged ions were captured in the FTMS by grounding the trapping plates for 2.5 ms before lowering their potential to -15 V and introducing a gas pulse of argon. Both end plates were held at -15 V for 1.5 s before being ramped up to -2 V; the outer and inner rings were held constant through out at -1 V and ground potential, respectively.

Cluster ions were isolated by ejecting unwanted ions with short duration rf bursts or chirps.[17] The isolated anions subsequently were irradiated with IR light for 5 s at 10 Hz from 2580 – 3500 cm^{-1} in 5 cm^{-1} increments. Each datum point is comprised of a single sequence that consists of ion generation, transfer, isolation, cooling and irradiation. The energy of the IR light was ~0.8 mJ $pulse^{-1}$ at 2500 cm^{-1}, 5 mJ $pulse^{-1}$ at 2700 cm^{-1} and at higher wavelengths it increases roughly linearly to 26 mJ $pulse^{-1}$ at 4000 cm^{-1}. Spectra are presented by plotting the smoothed fragmentation percentage using a simple moving average vs the IR wavelength. No power corrections were made to the data except for an anomalous increase in our system between 3070 – 3090 cm^{-1}. In addition, the unlabeled cluster ion was irradiated at a single wavelength (2965 cm^{-1}) for between 0.5 and 20 s at 10 Hz and the amount of fragmentation was determined at each time point.

Monte Carlo conformational searches using the MMFF force field were carried on MacIntosh computers with Spartan.[18] The most favorable conformations and additional ones based upon chemical intuition were reoptimized with B3LYP[19] and the aug-cc-pVDZ basis set[20] at the Minnesota Supercomputer Institute for Advanced Computational Research using Gaussian 09.[21] Vibrational frequencies were calculated for each species and unscaled values were used to compute zero-point energies, thermal corrections to

the enthalpies, and entropies. Single-point energies were calculated for the most stable conformers with the M06-2X functional[22] and the MP2[23] and CCSD(T)[24] levels of theory with the maug-cc-pVT(+d)Z,[25] aug-cc-pVTZ, and 6-31+G(d,p) basis sets, respectively. Estimates of the CCSD(T)/aug-cc-pVTZ energies were also obtained as indicated in equation 5.1.

$$E(\text{CCSD(T)/aug-cc-pVTZ}) \approx E(\text{CCSD(T)/6-31+G(d,p)}) + E(\text{MP2/aug-cc-pVTZ}) - E(\text{MP2/6-31+G(d,p)}) \quad (5.1)$$

Geometry optimizations of the lowest energy conformations were also carried out using the meta-hybrid generalized gradient approximation M06-2X functional and coupled cluster theory (CCSD) with the maug-cc-pVT(+d)Z and 6-31+G(d,p) basis sets, respectively. In the former case, CCSD(T)/aug-cc-pVTZ energies were predicted as illustrated in eq. 1. Similarly, CCSD(T)/maug-cc-pVTZ single-point energies were predicted for the CCSD structures in an analogous manner (i.e., eq 5.1), but the maug-cc-pVT(+d)Z basis set was used instead of the aug-cc-pVTZ basis set for the MP2 calculation.

Computed infrared spectra were obtained by converting each predicted vibrational frequency ν (cm^{-1}) into a Gaussian peak using equation 5.2, where *I* is the intensity at a given wavelength x, *a* is the computed intensity in km mol^{-1}, and *c* (50 cm^{-1}) is the full width at half height maximum. Overlapping peaks had their intensities added together and scaling factors of 0.93 (NH and OH) and 0.98 (CH) were used.[26]

$$I(x) = \sum_{\nu=2700}^{3500} ae^{\frac{-(x-\nu)^2}{0.3607c^2}} \quad (5.2)$$

Results and Discussion

Electrospray ionization of an aqueous methanolic solution containing equal amounts of proline and ammonium chloride readily afforded the Pro • Cl^- cluster anion in our Fourier transform mass spectrometer (FTMS). To characterize this complex, its infrared photodissociation spectrum was obtained from 2580 to 3500 cm^{-1} using an optical parametric oscillator (OPO) / optical parametric amplifier (OPA) laser system. Irradiation of Pro • Cl^- led to its cleavage at select wavelengths and the exclusive formation of Cl^-. The recorded spectrum (Figure 5.1) has two prominent absorption bands at 2895 and 2965 cm^{-1}. A low intensity but distinct and reproducible feature at 3255 cm^{-1} is also observed. It is difficult to assign these three absorptions based solely upon experimental data, so isotopically labeled species were also investigated.

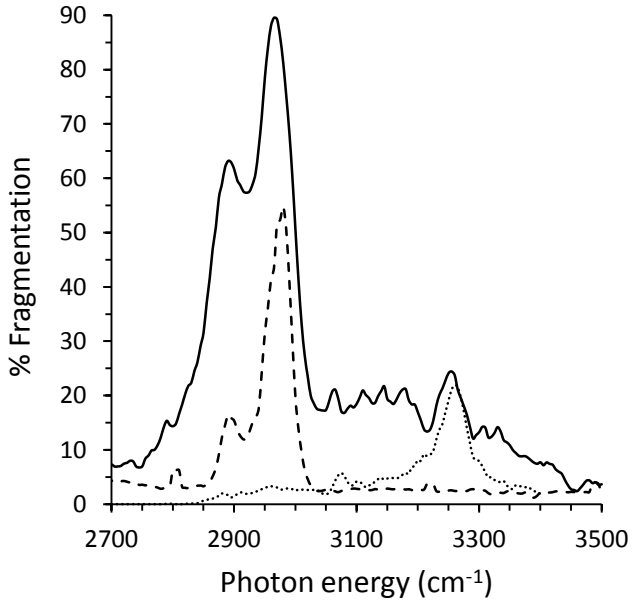

Figure 5.1. IRPD spectrum of Pro • Cl^- (solid line), Pro-d_2 • Cl^- (dashed line), and Pro-d_7 • Cl^- (dotted line).

Proline was dissolved in CD_3OD/D_2O to exchange the labile hydrogens for deuterium, and this led to formation of the proline-d_2 • Cl^- complex. Its IRPD spectrum was recorded (Figure 1) and two bands at 2885 and 2970 were observed. Both of these modes are present in the unlabeled spectrum, so they can be assigned to C–H stretching motions. They are also within 6-8 cm^{-1} of the reported IR positions for the CH bands of proline in the gas phase (i.e. 2891 and 2973 cm^{-1}), and their relative intensities are similar as well.[27] Since proline adopts a neutral structure in the gas phase, and its zwitterionic form in D_2O has a somewhat different CH absorption region,[28] this suggests that proline adopts a neutral structure in the Pro • Cl^- cluster. As for the weak mode at 3255 cm^{-1} in the unlabeled spectrum, it can be assigned to a N–H or O–H stretch because there are no absorbances above 3050 cm^{-1} in the spectrum for the d_2-labeled species.

Overlapping N–H and/or O–H stretching modes could be buried underneath the strong C–H absorptions in the Pro • Cl^- spectrum. To address this possibility, proline-d_7 (where all of the hydrogens attached to carbon were replaced by deuterium) was used to make the chloride complex. Its IRPD spectrum has no observed features below 3050 cm^{-1} (Figure 5.1), consequently, overlapping bands in the C–H stretching region can be ruled out. This also enables us to assign the absorbance at 3255 cm^{-1} to a N–H stretch since one would expect the more acidic carboxyl group in neutral proline to preferentially bind chloride anion and be red-shifted to a much lower frequency. In addition, the small intensity of this band is consistent with the absence of the N–H stretch in the experimental spectrum of gaseous proline due to the weak nature of this mode. A red shift of ~125 cm^{-1} can be estimated for the N–H stretch in the cluster ion given

predictions of 3364 and 3399 cm^{-1} for the NH band of proline.[27,29] This modest reduction in frequency is indicative of a weak hydrogen bond as predicted for the neutral structure N1 but not N2 or the zwitterionic species ZW illustrated in Figure 5.2.

Computations were carried out on Pro • Cl^- to further explore its structure and fit the experimental IRPD spectrum. B3LYP, M06-2X, and CCSD geometry optimizations were performed on a number of conformations (see the Supporting Information) with the aug-cc-pVDZ, maug-cc- pVT(+d)Z, and 6-31+G(d,p) basis sets, respectively. The most favorable neutral (**N1–N4**) and zwitterionic (**ZW1** and **ZW2**) structures are illustrated in Figure 3 and their relative energies are listed in Table I; ΔG values are given, and while the relative energies of the conformers change somewhat if enthalpies are used (< 1 kcal mol^{-1}), the most stable form of the cluster (neutral vs zwitterion) is the same. B3LYP predicts the lowest energy structure is zwitterionic and that it is preferred over the most stable neutral form by 1.12 kcal mol^{-1}.

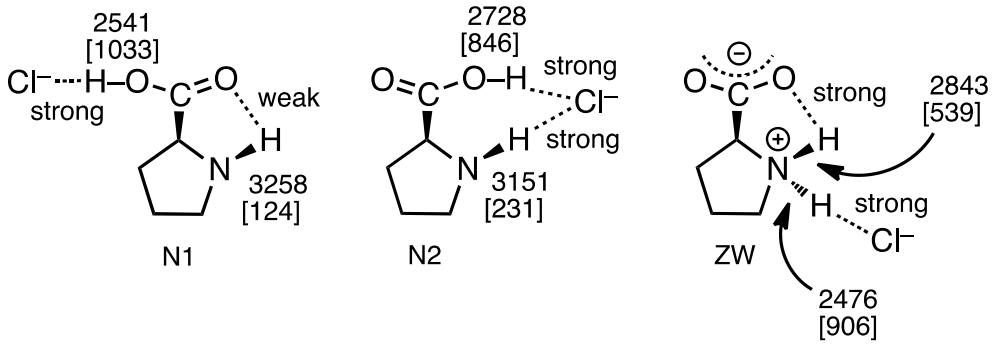

Figure 5.2. Proposed Pro • Cl^- structure N1 as opposed to N2 or ZW based upon the observed IRPD spectra and computations. Vibrational frequencies are in cm^{-1} and come from B3LYP/aug-cc-pVDZ calculations. The values in brackets are the predicted red shifts for the NH and OH stretches relative to proline.

This is reversed with the M06-2X functional and the neutral species is found to be more stable by 1.98 or 1.18 kcal mol^{-1} depending upon whether B3LYP or M06-2X geometries and vibrational frequencies are used. To address this situation further, CCSD(T) energies with a large basis set (aug-cc-pVTZ) were estimated using both the B3LYP and M06-2X optimized structures. In both cases the results agree with the B3LYP prediction, but the energy preference for **ZW1** is reduced to 0.10 and 0.67 kcal mol^{-1}, respectively. CCSD(T)/maug-cc-pVT(+d)Z energies were also computed for the CCSD optimized geometries but these results are in accord with the M06-2X findings. That is, the neutral form of proline in Pro • Cl^- is favored by 0.05 or 0.64 kcal mol^{-1} depending upon whether M06-2X or B3LYP thermal corrections and entropies are used. All of these results taken together indicate that the neutral and zwitterionic forms of proline in the anion cluster are very similar in energy, and that a number of conformations for both structures should be populated at room temperature

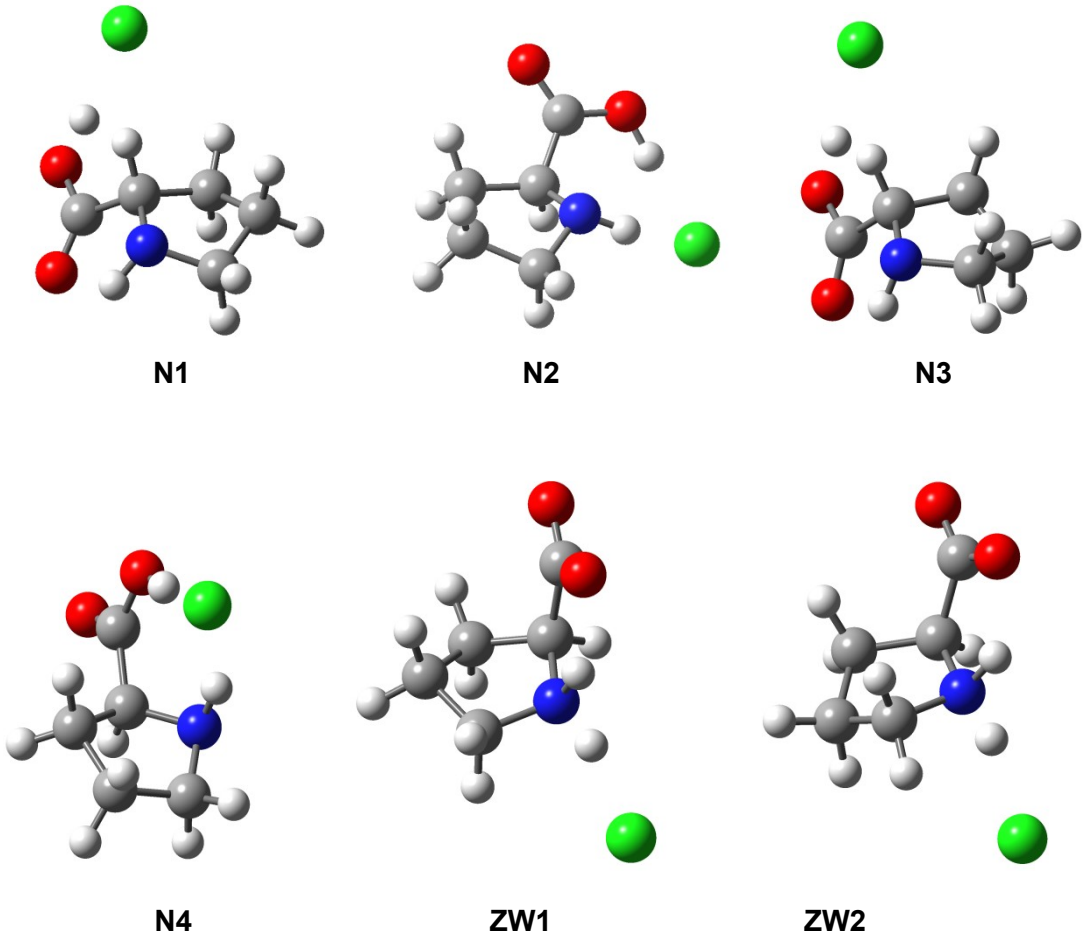

Figure 5.3. The most favorable neutral and zwitterionic B3LYP/aug-cc-pVDZ structures located for Pro • Cl^-.

Table 5.1. Computed B3LYP, M06-2X, and CCSD(T) Relative Free Energies at 298 K.[a]

method	relative energy (ΔG°_{298})							
	N1	N2	N3	N4	N5	N6	ZW1	ZW2
B3LYP/aug-cc-pVDZ	*1.12*	1.34	1.25	2.13	2.27	1.97	***0.00***	0.42
M06-2X/maug-cc-pVT(+d)Z[b]	***0.00***	0.41	0.08	2.38	0.73	2.26	*1.98*	2.50
CCSD(T)/aug-cc-pVTZ[b,c]	0.35	*0.10*	0.25		0.16		***0.00***	0.60
M06-2X/maug-cc-pVT(+d)Z	***0.00***	0.44	0.07	1.97	0.89	1.61	*1.18*	1.84
CCSD(T)/aug-cc-pVTZ[c,d]	0.90	*0.67*	0.93		1.11		***0.00***	0.74
CCSD(T)/maug-cc-pVT(+d)Z[c,e]	0.28 (0.21)	***0.00*** (***0.00***)	***0.00*** (0.23)[f]		0.26 (0.71)		*0.64 (0.05)*	

[a]All values are in kcal mol^{-1}. [b]Single-point energies computed with the B3LYP/aug-cc-pVDZ geometries. [c]CCSD(T)/aug-cc-pVTZ estimated energies were computed via an additivity scheme as illustrated in eq. 5.1. [d]Single-point energies computed with the M06-2X/maug-cc-pVT(+d)Z geometries. [e]Single-point energies were computed using CCSD/6-31+G(d,p) geometries and either B3LYP or M06-2X (in parentheses) vibrational frequencies and entropies. [f]In this case the additivity scheme was tested and found to be within 0.23 kcal mol^{-1} of the directly obtained CCSD(T)/maug-cc-pVT(+d)Z result.

(i.e., **N1**-**N3**, **N5**, **ZW1**, and **ZW2**). These computations, however, do not reliably indicate the most stable type of structure.

Predicted IR spectra were obtained with both the B3LYP and M06-2X functionals, but the results are similar so only the former method is presented in Fig. 5.4. As can be seen, there is excellent accord between the computed spectrum for **N1** and the experimental results with

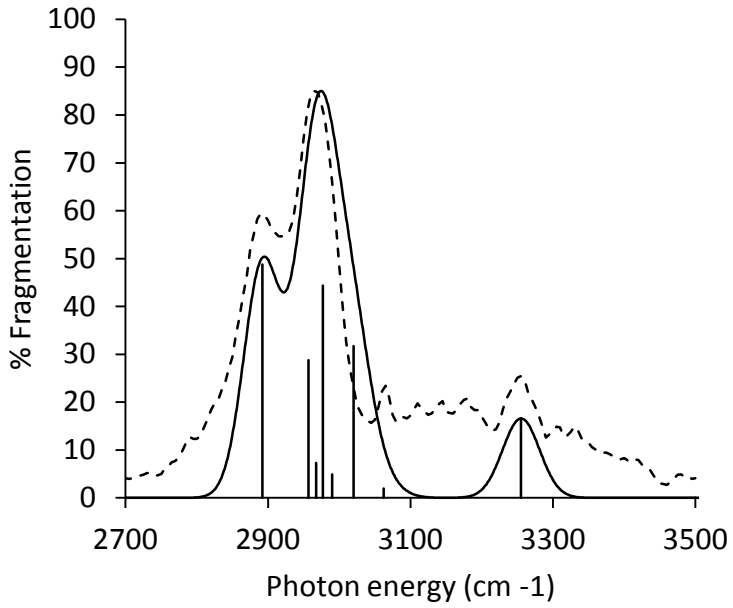

Figure 5.4. Computed B3LYP/aug-cc-pVDZ IR spectra of N1 (vertical bars and solid lines) along with the experimental IRPD data (dashed line). The intensity of the computed spectrum has been normalized to fit the experimental intensity at 2973 cm^{-1}.

the calculated bands at 2892, 2973, and 3258 cm^{-1} all being within 8 cm^{-1} of the observed frequencies. A similarly good fit also can be obtained using **N3** (see supporting information, Fig. S1), and in both cases the vibrational assignments are in accord with the deductions based upon the isotope-labeled results. That is, the calculated bands at 2892 and 2973 cm^{-1} corresponds to C-H stretching modes, and the absorption at 3258 cm^{-1} arises from the N-H stretch. In contrast, the O–H stretching modes in **N1** and **N3** are predicted to be red-shifted to 2540 and 2515 cm^{-1}, respectively, due to the strong OH •• Cl^- interaction. These frequencies are out of the useful operating region of our laser system and were not observed. Both **ZW1** and **ZW2** are predicted to have strong NH stretches at 2876 and 2843 cm^{-1}, respectively (Figure 5.5),[30] so they can be ruled out as the major species giving rise to the observed IRPD spectra. One concern,

however, is that several different computational approaches indicate that these zwitterionic structures should be populated, and may represent the most stable form of the cluster ion. If this is the case, than the observed IRPD spectra of Pro • Cl^- would not reflect the most stable structure of the complex.

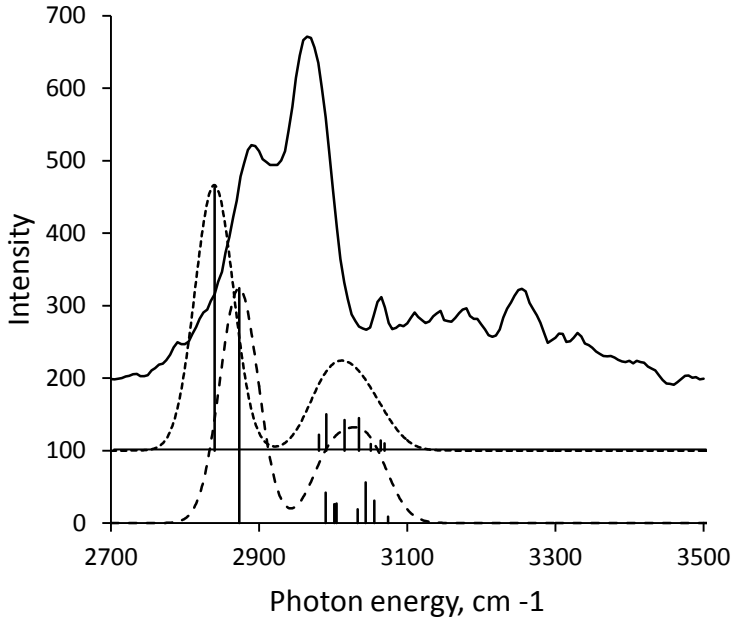

Figure 5.5. Comparison of experimental IRPD data (solid line) with computed B3LYP/aug-cc-pVDZ IR spectra of ZW1 (dashed line) and ZW2 (dotted line).

To investigate this issue, additional computations and experiments were carried out. Since the zwitterionic forms of the protein-forming α-amino acids are less stable than their neutral counterparts in the gas phase,[1] it is plausible that photofragmentation of charge-separated species is disfavored (i.e., slower) in at least some instances. Both potential energy surfaces (PESs) for the loss of chloride anion from **N1** and **ZW1** were examined to assess this possibility. This was accomplished by carrying out B3LYP/aug-cc-pVDZ partial optimizations of the proline–chloride anion cluster in which the NH •• Cl^- distance was stretched from its equilibrium value and kept constant over a wide range of

values while the rest of the molecule was minimized. When starting with the zwitterionic form, it did not convert to the neutral structure even when the NH •• Cl^- distance was stretched to 104.3 Å, and the dissociation energy was found to be larger than for **N1**. The 8.4 kcal mol^{-1} difference largely reflects the zwitterion–neutral energy difference for proline, which we estimate to be 15.8 kcal mol^{-1}.[31] This value was obtained by removing the chloride anion from the zwitterionic Pro • Cl^- cluster structures that resulted from mapping out the PES when NH •• Cl^- was 24.3 and 54.3 Å, and carrying out single-point energy calculations on these geometries and comparing the results to the canonical (neutral) form of proline. This procedure was carried out because full optimizations on zwitterionic structures led to their conversion to neutral conformers. The resulting zwitterion – neutral energy difference is similar to values reported for glycine.[2] These results suggest that the cleavage of the zwitterionic cluster anion is less efficient (i.e. slower) than when it has a neutral structure.

To test the computational prediction about photofragmentation rates of the Pro • Cl^- cluster ion, it was irradiated at 2965 cm^{-1} as a function of time (Figure 5.6). Irradiation up to 20 s led to 92% fragmentation with no indication of a nonlabile species. If both neutral and zwitterionic forms of proline are present in the cluster anions, then they both must be photoactive at 2965 cm^{-1}. A semi logarithmic plot of the fragmentation percentage versus time should be linear and this is the case for fragmentation up to 79%, but the last few points deviate from the correlation. That is, the amount of fragmentation is too small and this may be the result of poor overlap between the laser light and some of the trapped ions in the FTMS cell. Alternatively, it may indicate the presence of a kinetically distinct structure. If the latter situation is assumed to be the case, and this is reasonable given the work of Williams et al.[32] and that linear behavior up to 92% has been observed with our instrument,[16] then a linear fit of the last five time

points enables the earlier data to be corrected for the presence of two reacting populations.

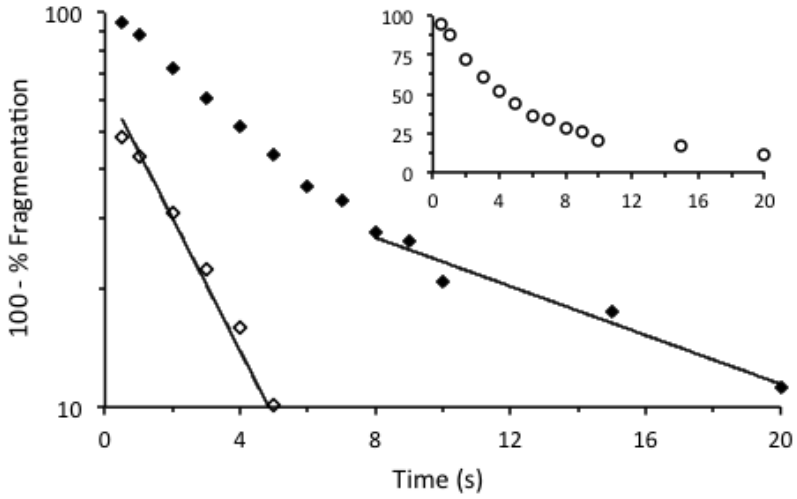

Figure 5.6. Fragmentation (%) vs. time (s) for the photoirradiation of Pro • Cl^- at 2965 cm^{-1} (inset) and a semi logarithmic plot of this data. Least squares fits of the last 5 data points (filled diamonds) and corrected values for the initial 6 points (open diamonds) afford the following respective equations: $y = 47.6e^{-0.0713x}$, $r^2 = 0.960$ and $y = 60.6e^{-0.346x}$, $r^2 = 0.995$.

This leads to a more abundant (i.e., 56% vs 44%) and more labile species (~5 times) which is assigned to the cluster ion with the canonical form of proline. The less abundant and less readily fragmented fraction is assigned to the zwitterionic structure for the anion complex. This scenario is consistent with several theoretical methods, all of which predict that the neutral and zwitterionic forms of the cluster ion are very similar energetically to each other. The failure to observe the zwitterion bands can be attributed to its slower fragmentation rate and photoisomerization to the neutral form of the cluster. Photokinetics, as originally suggested by Williams et al.,[32] consequently, is a powerful

means for obtaining structural evidence even for species that do not give rise to distinct absorptions in observed IRPD spectra.

Conclusions

IRPD spectra of Pro • Cl^- and its d_2 and d_7 isotopically labeled forms were obtained. Three bands are observed for the all protio-containing ion, and the two dominant features at 2895 and 2965 cm^{-1} can be assigned to C–H stretching motions based entirely upon the experimental results. The band positions also indicate that proline is in its neutral or canonical form in the cluster anion. As for the weak mode at 3255 cm^{-1}, it can be attributed to an N–H stretch as opposed to an O–H absorption due to its weak intensity, modest red shift, and the anticipated preferential binding of the more acidic carboxyl group to the chloride anion. Computations are fully in accord with these assignments, and indicate that both the canonical and salt-bridge structures of proline are nearly isoenergetic in the cluster ion. The absence of features in the IRPD spectra that can be attributed to the zwitterionic form of the cluster is consistent with potential energy surface calculations that indicate its fragmentation is more difficult than for the neutral form of the complex. Photokinetic data, however, suggests that both the neutral and zwitterionic form of the cluster are produced in nearly equal amounts (56 vs. 44%, respectively), but the latter ions break apart more slowly.

References

1. Bush, M. F.; O'Brien, J. T.; Prell, J. S.; Saykally, R. J.; Williams, E. R. *J. Am. Chem. Soc.* 2007, *129*, 1612-1622.
2. (a) Paterson, Y.; Nemethy, G.; Scheraga, H. A. *Ann. N. Y. Acad. Sci.* 1981, *367*, 132-150.
   (b) Jensen, J. H.; Gordon, M. S. *J. Am. Chem. Soc.* 1995, *117*, 8159-8170.
   (c) Aikens, C. M.; Gordon, M. S. *J. Am. Chem. Soc*. 2006, *128*, 12835–12850.
   (d) Bachrach, S. M. *J. Phys. Chem. A* 2008, *112*, 3722-3730.
   (e) Kayi, H.; Kaiser, R. I.; Head, J. D. *Phys. Chem. Chem. Phys.* 2012, *14*, 4942-4958.
3. (a) Xu, S.; Nilles, J. M.; Bowen, Jr., K. H. *J. Chem. Phys.* 2003, *119*, 10696-10701.
   (b) Diken, E. G.; Hammer, N. I.; Johnson, M. A. *J. Chem. Phys.* 2004, *120*, 9899-9902.
   (c) Pappas, C. G.; Tzakos, A. G.; Gerothanassis, I. P. *J. Amino Acids* 2012, *2012*, 1-11.
4. (a) Tse, Y. C.; Newton, M. D.; Vishveshwara, S.; Pople, J. A. *J. Am. Chem. Soc.* 1978, *100*, 4329-4331.
   (b) Ding, Y.; Krogh-Jesperson, K. *Chem. Phys. Lett.* 1992, *199*, 261-266.
   (c) Yu, D.; Armstrong, D. A.; Rauk, A. *Can. J. Chem.* 1992, *70*, 1762-1772.
5. (a) Hoffmann, E. K. *Biochem. Biophys. Acta* 1986, *864,* 1-31.
   (b) Sessler, J. L.; Gale, P. A.; Cho, W. S. In Anion Receptor Chemistry (*Monographs in Supramolecular Chemistry*), Stoddart, J. F. Ed.; RSC: Cambridge, 2006; pp 1-413.
   (c) Raghavan, A.; Sheik, T.; Graham, B. H.; Craigen, W. J. *Biochim. Biophys. Acta, Biomembranes* 2012, *1818*, 1477-1485.
6. (a) Burt, M. B.; Fridgen, T. D. *Eur. J. Mass Spectrom.* 2012, *18*, 235-250.
   (b) Wyttenbach, T.; Bowers, M. T. *Chem. Phys. Lett.* 2009, *480*, 1-16.
   (c) Turecek, F. *Mass Spectrom. Rev.* 2007, *26*, 563-582.
   (d) Williams, E. R.; Jurchen, J. C.; Garcia, D. E.; Lemoff, A. S.; Bush, M. F. *Adv. Mass Spectrom.* 2004, *16*, 79-94.
   (e) Rodgers, M. T.; Armentrout, P. B. *Acc. Chem. Res*. 2004, *37*, 989-998.
7. (a) Milner, E. M.; Nix, M. G.; Dessent, C. E. *J. Phys. Chem. A* 2012, *116*, 801-809.
   (b) Merenbloom, S. I.; Flick, T. G.; Daly, M. P.; Williams, E. R. *J. Am. Soc. Mass Spectrom.* 2011, *22*, 1978-1990.
   (c) Chomicz, L.; Rak, J.; Paneth, P.; Sevilla, M.; Ko, Y. J.; Wang, H.; Bowen, K. H. *J. Chem. Phys*. 2011, *135*, 114301/1-114301/7.
   (d) Li, X.; Wang, H.; Bowen, K. H.; Martinez, A.; Salpin, J.-Y.; Schermann, J.-P. *J. Chem. Phys*. 2010, *133*, 084303/1-084303/6.
   (e) Ferreira da Silva, F.; Denifl, S.; Maerk, T. D.; Ellis, A. M.; Scheier, P. *J. Chem. Phys*. 2010, *133*, 214306/1-214306/6.
   (f) Yang, G.; Zu, Y.; Liu, C.; Fu, Y.; Zhou, L. *J. Phys. Chem. B* 2008, *112*, 7104-7110.
   (g) Kass, S. R. *J. Am. Chem. Soc.* 2005, *127*, 13098-13099.
   (h) Aflatooni, K.; Hitt, B.; Gallup, G. A.; Burrow, P. D. *J. Chem. Phys.* 2001, *115*, 6489-6494.
8. (a) Englander, S. W. *J. Am. Soc. Mass Spectrom*. 2006, *17*, 1481-1489.
   (b) Maier, C. S.; Deinzer, M. L. *Methods Enzymol*. 2005, *402*, 312-360.
   (c) Busenlehner, L. S.; Armstrong, R. N. *Arch. Biochem. Biophys*. 2005, *433*, 34-46.
   (d) Taylor, S. S.; Yang, J.; Wu, J.; Haste, N. M.; Radzio-Andzelm, E.; Anand, G. *Biochimica Biophysica Acta, Proteins Proteomics* 2004, *1697*, 259-269.

(e) Grandori, R. *Curr. Org. Chem*. 2003, *7*, 1589-1603.
(f) Engen, J. R.; Smith, D. L. *Anal. Chem*. 2001, *73*, 256A-265A.
9. (a) Corral, I.; Lamsabhi, A. M.; Mo, O.; Yanez, M. *Int. J. Quant. Chem*. 2012, *112*, 2126-2134.
(b) Citir, M.; Hinton, C. S.; Oomens, J.; Steill, J. D.; Armentrout, P. B. *J. Phys. Chem. A* 2012, *116*, 1532-1541.
(c) Hofstetter, T. E.; Howder, C.; Berden, G.; Oomens, J.; Armentrout, P. B. *J. Phys. Chem. B* 2011, *115*, 12648-12661.
(d) Burt, M. B.; Decker, S. G. A.; Atkins, C. G.; Rowsell, M.; Peremans, A.; Fridgen, T. D. *J. Phys. Chem. B* 2011, *115*, 11506-11518.
(e) Drayss, M. K.; Armentrout, P. B.; Oomens, J.; Schäfer, M. *Int. J. Mass Spectrom.* 2010, *297*, 18-27.
(f) Prell, J. S.; Correra, T. C.; Chang, T. M.; Biles, J. A.; Williams, E. R. *J. Am. Chem. Soc.* 2010, *132*, 14733-14735.
(g) Prell, J. S.; O'Brien, J. T.; Williams, E. R. *J. Am. Soc. Mass Spectrom*. 2010, *21*, 800-809.
(h) Prell, J. S.; Chang, T. M.; O'Brien, J. T.; Williams, E. R. *J. Am. Chem. Soc.* 2010, *132*, 7811-7819.
(i) Carl, D. R.; Cooper, T. E.; Oomens, J.; Steill, J. D.; Armentrout, P. B. *Phys. Chem. Chem. Phys.* 2010, *12*, 3384-3398.
(j) Zhu, H.; Blom, M.; Compagnon, I.; Rijs, A. M.; Roy, S.; von Helden, G.; Schmidt, B. *Phys. Chem. Chem. Phys.* 2010, *12*, 3415-3425.
(k) Citir, M.; Stennett, E. M. S.; Oomens, J.; Steill, J. D.; Rodgers, M. T.; Armentrout, P. B. *Int. J. Mass Spectrom.* 2010, *297*, 9-17.
(l) Polfer, N. C.; Oomens, J. *Mass Spectrom. Rev.* 2009, *28*, 468-494.
(m) Drayss, M. K.; Blunk, D.; Oomens, J.; Gao, B.; Wyttenbach, T.; Bowers, M. T.; Schäfer, M. *J. Phys. Chem. A* 2009, *113*, 9543-9550.
(n) Bush, M. F.; Oomens, J.; Saykally, R. J.; Williams, E. R. *J. Am. Chem. Soc.* 2008, *130*, 6463-6471.
(o) Drayss, M. K.; Blunk, D.; Oomens, J.; Schäfer, M. *J. Phys. Chem. A* 2008, *112*, 11972-11974.
(p) Bush, M. F.; Oomens, J.; Saykally, R. J.; Williams, E. R. *J. Phys. Chem. A* 2008, *112*, 8578-8584.
(q) Armentrout, P. B.; Rodgers, M. T.; Oomens, J.; Steill, J. D. *J. Phys. Chem. A* 2008, *112*, 2248-2257.
(r) Dunbar, R. C.; Polfer, N. C.; Oomens, J. *J. Am. Chem. Soc.* 2007, *129*, 14562-14563.
(s) Kamariotis, A.; Boyarkin, O. V.; Mercier, S. R.; Beck, R. D.; Bush, M. F.; Williams, E. R.; Rizzo, T. R. *J. Am. Chem. Soc.* 2006, *128*, 905-916.
(t) Oh, H.-B.; Lin, C.; Hwang, H. Y.; Zhai, H.; Breuker, K.; Zabrouskov, V.; Carpenter, B. K.; McLafferty, F. W. *J. Am. Chem. Soc*. 2005, *127*, 4076-4083.
(u) Lemoff, A. S.; Bush, M. F.; Williams, E. R. *J. Phys. Chem. A* 2005, *109*, 1903-1910.
(v) Kapota, C.; Lemaire, J.; Maitre, P.; Ohanessian, G. *J. Am. Chem. Soc.* 2004, *126*, 1836-1842.
10. O'Brien, J. T.; Prell, J. S.; Berden, G.; Oomens, J.; Williams, E. R. *Int. J. Mass Spectrom.* 2010, *297*, 116-123.
11. (a) Jones, C. M.; Bernier, M.; Carson, E.; Colyer, K. E.; Metz, R.; Pawlow, A.; Wischow, E. D.; Webb, I.; Andriole, E. J.; Poutsma, J. C. *Int. J. Mass Spectrom.* 2007, *267*, 54-62.

(b) O'Hair, R. A. J.; Bowie, J. H.; Gronert, S. *Int. J. Mass Spectrom. Ion Proc.* 1992, *117*, 23-36.
(c) Stover, M. L.; Jackson, V. E.; Matus, M. H.; Adams, M. A.; Cassady, C. J.; Dixon, D. A. *J. Phys. Chem. B* 2012, *116,* 2905-2916.
12. (a) Gronert, S.; Simpson, D. C.; Conner, K. M. *J. Am. Soc. Mass Spectrom.* 2009, *20*, 2116-2123.
(b) Uddin, K. M.; Warburton, P. L.; Poirier, R. A. *J. Phys. Chem. B* 2012, *116*, 3220-3234.
13. (a) Wang, X. B.; Broadus, K. M.; Wang, L. S.; Kass, S. R. *J. Am. Chem. Soc.* 2000, *122*, 8305-8306.
(b) Broadus, K. M.; Kass, S. R. *J. Am. Chem. Soc*. 2000, *122*, 9014-9018.
(c) Reed, D. R., Ph.D. Thesis, University of Minnesota, 2001; pp 71–87.
14. (a) Richardson, J. S.; Richardson, D. C. *Sci*ence 1988, *240*, 1648-1652.
(b) MacArthur, M.; Thornton, J. M. *J. Mol. Biol*. 1991, *218*, 397-412.
15. (a) Stewart, G. R.; Lee, J. A. *Planta* 1974, *120*, 279-289.
(b) Schobert, B. *J. Theor. Biol.* 1977, *68*, 17-26.
(c) Chu, T. M.; Jusaitis, M.; Aspinall, D.; Paleg, L. G. *Physiol. Plant.* 1978, *43*, 254-260.
(d) Levy, D. *Physiol. Plant.* 1983, *57*, 169-173.
16. Schmidt, J.; Meyer, M. M.; Spector, I.; Kass, S. R. *J. Phys. Chem. A* 2011, *115*, 7625-7632.
17. Marshall, A. G.; Roe, D. C. *J. Chem. Phys.* 1980, *73*, 1581-1590.
18. Spartan ’08 for Macintosh; Wavefunction, Inc.: Irvine, CA.
19. (a) Becke, A. D. *J. Chem. Phys.* 1993, *98*, 5648−5652.
(b) Lee, C.; Yang, W.; Parr, R. G. *Phys. Rev. B* 1988, *37*, 785−789.
20. Dunning, Jr., T. H. *J. Chem. Phys.* 1989, *90*, 1007-1023.
21. Frisch, M. J.; et al. *Gaussian 09*; Gaussian, Inc.: Pittsburgh, PA, 2009.
22. (a) Zhao, Y.; Truhlar, D. G. *J. Phys. Chem. A* 2008, *112*, 1095−1099.
(b) Zhao, Y.; Truhlar, D. G. *Theor. Chem. Acc*. 2008, *120*, 215−241.
(c) Zhao, Y.; Truhlar, D. G. *Acc. Chem. Res*. 2008, *41*, 157−167.
23. MØller, C.; Plesset, M. S. *Phys. Rev*. 1934, *46*, 618-622.
24. (a) Hampel, C.; Peterson, K.; Werner, H. -J. *Chem. Phys. Lett*. 1992, *190*, 1-12.
(b) Deegan, M. J. O.; Knowles, P. J. *Chem. Phys. Lett.* 1994, *227*, 321-326.
(c) Knowles, P. J.; Hampel, C.; Werner, H. -J. *J. Chem. Phys*. 1993, *99*, 5219-5227; erratum: *J. Chem. Phys.* 2000, *112*, 3106.
25. Papajak, E.; Truhlar, D. G. *J. Chem. Theory Comput.* 2010, *6*, 597−601.
26. For similar scaling factors, see: Scerba, M. T.; DeBlase, A. F.; Bloom, S.; Dudding, T.; Johnson, M. A. *J. Phys. Chem. A* 2012, *116*, 3556-3560.
27. Linder, R.; Nispel, M.; Häber, T.; Kleinermanns, K. *Chem. Phys. Lett.* 2005, *409*, 260-264.
28. Rudolph, A. S.; Crowe, J. H. *Biophys. J.* 1986, *50*, 423-430.
29. Czinki, E.; Császár, A. G. *Chem. Eur. J.* 2003, *9*, 1008-1019.
30. Strong bands at 2477 and 2480 cm^{-1} are also predicted, but these frequencies are too small to be observed with our apparatus.
31. A similar value of 18.9 kcal mol^{-1} was obtained at the shorter distance by carrying out M06-2X/maug-cc-pVT(+d)Z single-point energy determinations.
32. (a) Prell, J. S.; Chang, T. M.; O'Brien, J. T.; Williams, E. R. *J. Am. Chem. Soc.* 2010, *132*, 7811-7819.
(b) Prell, J. S.; Correra, T. C.; Chang, T. M.; Biles, J. A.; Williams, E. R. *J. Am. Chem. Soc.* 2010, *132*, 14733-14735.

(c) Prell, J. S.; Chang, T. M.; Biles, J. A.; Berden, G.; Oomens, J.; Williams, E. R. *J. Phys. Chem. A* 2011, *115*, 2745-2751.[2]

---

[1] Generous support from the National Science Foundation and the Minnesota Supercomputer Institute for Advanced Computational Research are gratefully acknowledged. Supporting Information Available: Computed structures (xyz coordinates) and energies, complete ref. 21 and the predicted IRPD spectrum of N3 are provided (zz pgs). This information is available free of charge via the internet at http://pubs.acs.org.

Bibliography

1. Accardi, A., Miller, C., *Nature,* 2004, *427,* 803-807.
2. Aflatooni, K.; Hitt, B.; Gallup, G. A.; Burrow, P. D. *J. Chem. Phys.* 2001, *115*, 6489-6494.
3. Aikens, C. M.; Gordon, M. S. *J. Am. Chem. Soc*. 2006, *128*, 12835–12850.
4. Armentrout, P. B.; Rodgers, M. T.; Oomens, J.; Steill, J. D. *J. Phys. Chem. A* 2008, *112*, 2248-2257.
5. Arnett, E. M.; Moe, K. D. *J. Am. Chem. Soc*. 1991, *113*, 7288-7293.
6. Arnett, E. M.; Moriarity, T. C.; Small, L. E.; Rudolph, J. P.; Quirk, R. P. *J. Am. Chem. Soc*. 1973, *95*, 1492-1495.
7. Bachrach, S. M. *J. Phys. Chem. A* 2008, *112*, 3722-3730.
8. Becke, A. D. *J. Chem. Phys.* 1993, *98*, 5648-5652.
9. Blondel, C.; Cacciani, P.; Delsart, C.; Trainham, R., *Phys. Rev. A*, 1989, 40, 3698.
10. Bondi, A. *J. Phys. Chem.* 1964, 68, 441-451.
11. Bordwell, F. G.; Bartmess, J. E.; Drucker, G. E.; Margolin, Z.; Matthews, W. S. *J. Am. Chem. Soc.* 1975, *97*, 3226-3227.
12. Broadus, K. M.; Kass, S. R. *J. Am. Chem. Soc*. 2000, *122*, 9014-9018.
13. Brotherhood, P. R.; Davis, A. P. Chem. Soc. Rev. 2010, 39, 3633-3647.
14. Buhlmann, P.; Chen, L. D. Supramolecular Chemistry: From Molecules to Nanomaterials, Steed, A. W., Gale, P. A., Eds., Wiley: New York, 2012, Vol. 5, pp 2539-2580.
15. Burt, M. B.; Decker, S. G. A.; Atkins, C. G.; Rowsell, M.; Peremans, A.; Fridgen, T. D. *J. Phys. Chem. B* 2011, *115*, 11506-11518.
16. Burt, M. B.; Fridgen, T. D. *Eur. J. Mass Spectrom.* 2012, *18*, 235-250.
17. Busenlehner, L. S.; Armstrong, R. N. *Arch. Biochem. Biophys*. 2005, *433*, 34-46.
18. Bush, M. F.; O'Brien, J. T.; Prell, J. S.; Saykally, R. J.; Williams, E. R. *J. Am. Chem. Soc*. 2007, *129*, 1612-1622.
19. Bush, M. F.; O'Brien, J. T.; Prell, J. S.; Saykally, R. J.; Williams, E. R. *J. Am. Chem. Soc.* 2007, *129*, 1612-1622.
20. Bush, M. F.; Oomens, J.; Saykally, R. J.; Williams, E. R. *J. Am. Chem. Soc.* 2008, *130*, 6463-6471.
21. Bush, M. F.; Oomens, J.; Saykally, R. J.; Williams, E. R. *J. Phys. Chem. A* 2008, *112*, 8578-8584.
22. Bush, M. F.; Saykally, R. J.; Williams, E. R. *ChemPhysChem* 2007, *8*, 2245-2253.
23. Carl, D. R.; Cooper, T. E.; Oomens, J.; Steill, J. D.; Armentrout, P. B. *Phys. Chem. Chem. Phys.* 2010, *12*, 3384-3398.
24. Chapo, C. J.; Paul, J. B.; Provencal, R. A.; Roth, K.; Saykally, R. J. *J. Am. Chem. Soc*. 1998, 120, 12956.
25. Chen, X.; Fang, L.; Liu, J.; Zhan, C. G. *Biochemistry* 2012, *51*, 1297−1305.
26. Chmielewski, M.J., Jurczak, J., *Chem. Eur. J*. 2005, *11*, 6080–6094.

27. Chomicz, L.; Rak, J.; Paneth, P.; Sevilla, M.; Ko, Y. J.; Wang, H.; Bowen, K. H. *J. Chem. Phys*. 2011, *135*, 114301/1-114301/7.
28. Chu, T. M.; Jusaitis, M.; Aspinall, D.; Paleg, L. G. *Physiol. Plant.* 1978, *43*, 254-260.
29. Citir, M.; Hinton, C. S.; Oomens, J.; Steill, J. D.; Armentrout, P. B. *J. Phys. Chem. A* 2012, *116*, 1532-1541.
30. Citir, M.; Stennett, E. M. S.; Oomens, J.; Steill, J. D.; Rodgers, M. T.; Armentrout, P. B. *Int. J. Mass Spectrom.* 2010, *297*, 9-17.
31. Cleland, W. W. *Biochemistry* 1992, 31, 317– 319.
32. Corral, I.; Lamsabhi, A. M.; Mo, O.; Yanez, M. *Int. J. Quant. Chem*. 2012, *112*, 2126-2134.
33. Czinki, E.; Császár, A. G. *Chem. Eur. J.* 2003, *9*, 1008-1019.
34. Davis, J. T.; Okunola, O.; Quesada, R. Chem. Soc. Rev. 2010, 39, 3843-3862.
35. Deegan, M. J. O.; Knowles, P. J. *Chem. Phys. Lett.* 1994, *227*, 321-326.
36. Deward, M. J. S. *Enzyme* 1986, *36*, 8-20.
37. Diken, E. G.; Hammer, N. I.; Johnson, M. A. *J. Chem. Phys.* 2004, *120*, 9899-9902.
38. Ding, Y.; Krogh-Jesperson, K. *Chem. Phys. Lett.* 1992, *199*, 261-266.
39. Dole, M., Mack, L.L., Hines, R.L. Mobley, R.C., Ferguson, L.D., Alice, M.B., *J. Chem. Phys.* 1968, 49, 2240-2249.
40. Doyle, A. G.; Jacobsen, E. N. *Chem. Rev.* 2007, 107, 5713-5743.
41. Drayss, M. K.; Armentrout, P. B.; Oomens, J.; Schäfer, M. *Int. J. Mass Spectrom.* 2010, *297*, 18-27.
42. Drayss, M. K.; Blunk, D.; Oomens, J.; Gao, B.; Wyttenbach, T.; Bowers, M. T.; Schäfer, M. *J. Phys. Chem. A* 2009, *113*, 9543-9550.
43. Drayss, M. K.; Blunk, D.; Oomens, J.; Schäfer, M. *J. Phys. Chem. A* 2008, *112*, 11972-11974.
44. Dunbar, R. C.; Polfer, N. C.; Oomens, J. *J. Am. Chem. Soc.* 2007, *129*, 14562-14563.
45. Duncan, M.A.*,* Int. Rev. Phys. Chem. 2003*,* 22, 407*.*
46. Dunning, Jr., T. H. *J. Chem. Phys.* 1989, *90*, 1007-1023.
47. Dutzler, R., Campbell, E. B., Cadene, M., Chait, B. T., MacKinnon, R. *Nature* 2002, 415, 287−294.
48. Dutzler, R., Campbell, E. B., MacKinnon, R. *Science* 2003, 300, 108−112.
49. Dutzler, R., Campbell, E.B., Cadene, M., Chait, B.T., MacKinnon, R., *Nature* 2002, *415,* 287-294.
50. Dutzler, R., Campbell, E.B., MacKinnon, R., *Science,* 2003, *300,* 108-112.
51. Engen, J. R.; Smith, D. L. *Anal. Chem*. 2001, *73*, 256A-265A.
52. Englander, S. W. *J. Am. Soc. Mass Spectrom*. 2006, *17*, 1481-1489.
53. Esteban-Gomez, D., Fabbrizzi, L., Licchelli, M., *J. Org. Chem.* 2005, *70* 5717–5720.
    Lee, K.H., Hong, H.I., *Tetrahedron Lett.* 2000, *41* 6083–6087.
54. Ferreira da Silva, F.; Denifl, S.; Maerk, T. D.; Ellis, A. M.; Scheier, P. *J. Chem. Phys*. 2010, *133*, 214306/1-214306/6.

55. Flammang, R.; Dechamps, N.; Pascal, L.; Van Haverbeke, Y.; Gerbaux, P.; Nam, P. C.; Nguyen, M. T. *Lett Org Chem*. 2004, *1*, 23-30,
56. Frisch, M. J.*, et al. Gaussian 09*, Gaussian, Inc., Wallingford, CT, 2009.
57. Fujio, M.; McIver, R.T., Jr.; Taft, R.W., *J. Am. Chem. Soc.* 1981, 103, 4017.
58. Gale, P. A. *Acc. Chem. Res*. 2011, *44*, 216-226.
59. Gale, P. A. Coord. Chem. Rev. 2006, 250, 2939-2951.
60. Garcia-Garrido, S.E., Caltagirone, C., Light, M.E., Gale, P.A., *Chem. Commun*. 2007, 1450–1452.
61. Gerlt, J. A.; Gassman, P. G. *Biochemistry* 1993, 32, 11943– 11952.
62. Gerlt, J. A.; Gassman, P. G. *J. Am. Chem. Soc.* 1993, 115, 11552– 11568.
63. Godfrey, P.D., Brown, R.D., *J. Am. Chem. Soc*. 117 1995, 2019.
64. Gordon, M.; Jensen, J., *J. Am. Chem. Soc.* 1995, *117*, 8159-8170.
65. Grandori, R. *Curr. Org. Chem*. 2003, *7*, 1589-1603.
66. Greene, J. R.; Francisco, J. S.; Huang, J.; Xu, D.; Jackson, W. M. *J. Chem. Phys.* 2004, *121*, 5868-5873.
67. Gronert, S.; Simpson, D. C.; Conner, K. M. *J. Am. Soc. Mass Spectrom.* 2009, *20*, 2116-2123.
68. Guthrie, J. P*. Chem. Biol.* 1996, 3, 163– 170.
69. Hampel, C.; Peterson, K.; Werner, H. -J. *Chem. Phys. Lett*. 1992, *190*, 1-12.
70. Harel, M.; Quinn, D. M.; Nair, H. K.; Silman, I.; Sussman, J. L. *J. Am. Chem. Soc*. 1996, *118*, 2340-2346.
71. Haynes, C. J. E.; Gale, P. A. *Chem. Commun*. 2011, *47,* 8203-8209.
72. Hoffmann, E. K. *Biochem. Biophys. Acta* 1986, *864,* 1-31.
73. Hofstetter, T. E.; Howder, C.; Berden, G.; Oomens, J.; Armentrout, P. B. *J. Phys. Chem. B* 2011, *115*, 12648-12661.
74. Hunter, E. P. L.; Lias, S. G. "Proton Affinity Evaluation" and "Ionization Energy Evaluation" in *NIST Chemistry WebBook, NIST Standard Reference Database Number 69* (Eds.: Linstrom, P. J.; Mallard, W. G.), June 2005, National Institute of Standards and Technology, Gaithersburg MD, 20899 (http://webbook.nist.gov).
75. Iribarne, J.V., Thomson, B.A., *J. Chem. Phys.*1976, 64, 2287-2294.
76. Jencks, W. P. *Acc. Chem. Res.* 1976, 9, 425– 432.
77. Jencks, W. P. *Adv. Enzymol. Relat. Areas Mol. Biol.* 1975, 43, 219– 410.
78. Jensen, J. H.; Gordon, M. S. *J. Am. Chem. Soc.* 1995, *117*, 8159-8170.
79. Jones, C. M.; Bernier, M.; Carson, E.; Colyer, K. E.; Metz, R.; Pawlow, A.; Wischow, E. D.; Webb, I.; Andriole, E. J.; Poutsma, J. C. *Int. J. Mass Spectrom.* 2007, *267*, 54-62.
80. Kamariotis, A.; Boyarkin, O. V.; Mercier, S. R.; Beck, R. D.; Bush, M. F.; Williams, E. R.; Rizzo, T. R. *J. Am. Chem. Soc.* 2006, *128*, 905-916.
81. Kang, S.O., Begum, R.A., Bowman-James, K., *Angew. Chem., Int. Ed*. 2006, *45,* 7882–7894.
82. Kapota, C.; Lemaire, J.; Maitre, P.; Ohanessian, G. *J. Am. Chem. Soc.* 2004, *126*, 1836-1842.
83. Kass, S. R. *J. Am. Chem. Soc.* 2005, *127*, 13098-13099.

84. Kavallieratos, K., Bertao, C.M., Crabtree, R.H., *J. Org Chem*. 1999, *64*, 1675-1683.
85. Kavallieratos, K., de Gala, S.R., Austin, D.J., Crabtree, R.H., *J. Am Chem. Soc.* 1997, *119*, 2325-2326.
86. Kayi, H.; Kaiser, R. I.; Head, J. D. *Phys. Chem. Chem. Phys.* 2012, *14*, 4942-4958.
87. Kebarle, P., McMahon, T. B. *J. Am. Chem. Soc.* 1977, 99, 2222-2230.
88. Kebarle, P.; Davidson, W. R.; French, M.; Cumming, J. B.; McMahon, T. B. *Faraday Trans*. 1977, *64*, 220-229.
89. Kebarle, P.; McMahon, T. B. *J. Am. Chem. Soc.* 1977, *99*, 2222-2230.
90. Knowles, P. J.; Hampel, C.; Werner, H. -J. *J. Chem. Phys*. 1993, *99*, 5219-5227; erratum: *J. Chem. Phys.* 2000, *112*, 3106.
91. Knowles, R. R.; Jacobsen, E. N. *Proc. Natl. Acad. Sci. USA* 2010, *107*, 20678-20685.
92. Laufer, D. A.; Gelb, R. I.; Schwartz, L. M. *J. Org. Chem*. 1984, *49*, 691-696.
93. Lee, C. T.; Yang, W. T.; Parr, R. G. *Phys. Rev. B* 1988, *37*, 785-789.
94. Lemoff, A. S.; Bush, M. F.; Williams, E. R. *J. Phys. Chem. A* 2005, *109*, 1903-1910.
95. Levy, D. *Physiol. Plant.* 1983, *57*, 169-173.
96. Li, X.; Wang, H.; Bowen, K. H.; Martinez, A.; Salpin, J.-Y.; Schermann, J.-P. *J. Chem. Phys*. 2010, *133*, 084303/1-084303/6.
97. Linder, R.; Nispel, M.; Häber, T.; Kleinermanns, K. *Chem. Phys. Lett.* 2005, *409*, 260-264.
98. Lo, Y. C.; Lin, S. C.; Shaw, J. F.; Liaw, Y. C. *J. Mol. Biol*. 2003, *330*, 539–551.
99. MacArthur, M.; Thornton, J. M. *J. Mol. Biol*. 1991, *218*, 397-412.
100. Machajewski, T. D.; Wong, C.H. *Angew. Chem. Int. Ed*. 2000, *39*, 1352-1374.
101. Maciel G. E.; Traficante, D. D. J. Phys. Chem. 1965, *69*, 1030-1033.
102. Maier, C. S.; Deinzer, M. L. *Methods Enzymol*. 2005, *402*, 312-360.
103. Marshall, A. G.; Roe, D. C. *J. Chem. Phys.* 1980, *73*, 1581-1590.
104. Martinez, C.; Nicolas, A.; van Tilbeurgh, H.; Egloff, M. P.; Cudrey, C.; Verger, R.; Cambillau, C. *Biochem.* 1994, 33, 83-89.
105. McLafferty, F. W. *J. Am. Chem. Soc*. 2005, *127*, 4076-4083.
106. Merenbloom, S. I.; Flick, T. G.; Daly, M. P.; Williams, E. R. *J. Am. Soc. Mass Spectrom.* 2011, *22*, 1978-1990.
107. Meyer, M. M. Ph.D. Thesis, University of Minnesota, Minneapolis, MN, 2010.
108. Meyer, M. M.; Chan, B.; Radom, L. Kass, S. R. *Angew. Chemie. Int. Ed. Eng*. 2010, *49*, 5161-5164.
109. Middlemiss, N. E.; Harrison, A. G. *Can. J. Chem.* 1979, *57*, 2827-2833.
110. Miller, C., *Nature* 2006, 440, 484−489.
111. Milner, E. M.; Nix, M. G.; Dessent, C. E. *J. Phys. Chem. A* 2012, *116*, 801-809.
112. MØller, C.; Plesset, M. S. *Phys. Rev*. 1934, *46*, 618-622.
113. Nachon, F.; Asojo, O. A.; Borgstahl, G. E. O.; Masson, P.; Lockridge, O. *Biochemistry* 2005, *44,* 1154-1162.

114. O'Brien, J. T.; Prell, J. S.; Berden, G.; Oomens, J.; Williams, E. R. *Int. J. Mass Spectrom.* 2010, *297*, 116-123.
115. Oh, H.-B.; Lin, C.; Hwang, H. Y.; Zhai, H.; Breuker, K.; Zabrouskov, V.; Carpenter, B. K.; McLafferty, F. W. *J. Am. Chem. Soc*. 2005, *127*, 4076-4083.
116. O'Hair, R. A. J.; Bowie, J. H.; Gronert, S. *Int. J. Mass Spectrom. Ion Proc.* 1992, *117*, 23-36.
117. Olah, G. A.; White, A. M. J. Am. Chem. Soc. 1967, *89*, 7072-7075.
118. Oomens*, J.,* van Roij*, A.J.A.,* Meijer*, G.,* von Helden, G.*,* Astrophys. J. 2000*,* 542, 404–410*.*
119. Oomens, J.; Sartakov, B. G.; Meijer, G.; Helden, G. v. *Int. J. Mass Spectrom.* 2006, *254*, 1-19.
120. Papajak, E.; Truhlar, D. G. *J. Chem. Theory Comput.* 2010, *6*, 597−601.
121. Pappas, C. G.; Tzakos, A. G.; Gerothanassis, I. P. *J. Amino Acids* 2012, *2012*, 1-11.
122. Pasker, F. M.; Solca, N.; Dopfer, O. *J. Phys. Chem. A* 2006, *110*, 12793-12804,
123. Paterson, Y.; Nemethy, G.; Scheraga, H. A. *Ann. N. Y. Acad. Sci.* 1981, *367*, 132-150.
124. Pflugrath, J.W., Quiocho, F.A., *Nature,* 1985, *314,* 257-260.
125. Pihko, P. M. Ed., *Hydrogen Bonding in Organic Synthesis*, Wiley-VCH: Weinheim, 2009.
126. Polfer, N. C.; Oomens, J. *Mass Spectrom. Rev.* 2009, *28*, 468-494.
127. Prell, J. S.; Chang, T. M.; Biles, J. A.; Berden, G.; Oomens, J.; Williams, E. R. *J. Phys. Chem. A* 2011, *115*, 2745-2751.
128. Prell, J. S.; Chang, T. M.; O'Brien, J. T.; Williams, E. R. *J. Am. Chem. Soc.* 2010, *132*, 7811-7819.
129. Prell, J. S.; Correra, T. C.; Chang, T. M.; Biles, J. A.; Williams, E. R. *J. Am. Chem. Soc.* 2010, *132*, 14733-14735.
130. Prell, J. S.; O'Brien, J. T.; Williams, E. R. *J. Am. Soc. Mass Spectrom*. 2010, *21*, 800-809.
131. Price, W.D., Schnier, P.D., Williams, E.R., *Anal. Chem.*, 1996, 68 (5), 859–866.
132. Raghavan, A.; Sheik, T.; Graham, B. H.; Craigen, W. J. *Biochim. Biophys. Acta, Biomembranes* 2012, *1818*, 1477-1485.
133. Ranashinghe, A.; Cooks, R. G.; Sethi, S. Org. Mass Spectrom. 1992, *27*, 77-88.
134. Rawal, V. H.; Thadani, A. N. *Asymmetric Synthesis – The Essentials*, 2nd Edition; Christmann, M., Brase, S., Eds., Wiley-VCH: Weinheim, 2008, pp. 144-148.
135. Reed, D. R., Ph.D. Thesis, University of Minnesota, 2001; pp 71–87.
136. Reisman, S. E.; Doyle, A. G.; Jacobsen, E. N. *J. Am. Chem. Soc.* 2008, *130*, 7198-7199.
137. Richardson, J. S.; Richardson, D. C. *Sci*ence 1988, *240*, 1648-1652.
138. Ritchie, C. D.; Uschold, R. E. *J. Am. Chem. Soc*. 1968, *90*, 2821-2834.
139. Robin, M.B.; Kuebler, N.A., *J. Electron Spectrosc. Relat. Phenom*. 1973, 1, 13.
140. Rodgers, M. T.; Armentrout, P. B. *Acc. Chem. Res*. 2004, *37*, 989-998.
141. Rudolph, A. S.; Crowe, J. H. *Biophys. J.* 1986, *50*, 423-430.

142. Russo, N.; Toscano, M.; Grand, A.; Mineva, T. *J. Phys. Chem. A* 2000, *104*, 4017-4021.
143. Scerba, M. T.; DeBlase, A. F.; Bloom, S.; Dudding, T.; Johnson, M. A. *J. Phys. Chem. A* 2012, *116*, 3556-3560.
144. Schmidt, J.; Meyer, M. M.; Spector, I.; Kass, S. R. *J. Phys. Chem. A* 2011, *115*, 7625-7632.
145. Schobert, B. *J. Theor. Biol.* 1977, *68*, 17-26.
146. Schreiner, P. R. *Chem. Soc. Rev*. 2003, *32*, 289-296.
147. Schreiner, P. R.; Wittkopp, A. *Org. Lett.* 2002, *4*, 217-220.
148. Schutz, C.N., Warshel, A., *Proteins*. 2004, 55, 711-723.
149. Sessler, J. L.; Gale, P. A.; Cho, W. S. In Anion Receptor Chemistry (*Monographs in Supramolecular Chemistry*), Stoddart, J. F. Ed.; RSC: Cambridge, 2006; pp 1-413.
150. Sessler, J.L., Camiolo, S., Gale, P.A., *Coord. Chem. Rev*. 2003, *240,* 17–55.
151. Shokri, A., Abedin, A., Fattahi, A., Kass, R. *J. Am. Chem. Soc.*, 2012, 134 (25), 10646–10650
152. Shokri, A., Schmidt, J., Wang, X., Kass, S. *J. Am. Chem. Soc.*, 2012, 134 (4), 2094–2099.
153. Simon, L., Goodman, J.M., *J. Org. Chem.,* 2010, *75,* 1831-1840.
154. Simóna, L.; Muñiza, F. M.; Sáeza, S.; Raposob, C.; Morána, J. R. *ARKIVOC* 2007, 47-64.
155. Spartan '08 for Macintosh; Wavefunction, Inc.: Irvine, CA.
156. Steill, J. D.; Oomens, J. *J. Am. Chem. Soc.* 2009, *131*, 13570-13571.
157. Stephen, J. C. *Chem. Eur. J.* 2006, *12*, 5418–5427.
158. Stewart, G. R.; Lee, J. A. *Planta* 1974, *120*, 279-289.
159. Stover, M. L.; Jackson, V. E.; Matus, M. H.; Adams, M. A.; Cassady, C. J.; Dixon, D. A. *J. Phys. Chem. B* 2012, *116,* 2905-2916.
160. Taft, R.W.; Bordwell, F.G., *Acc. Chem. Res*. 1988, 21, 463.
161. Takemoto, Y. *Org. Biomol. Chem*. 2005, *3*, 4299-4306.
162. Taylor, M. S., Jacobsen, E. N., *Angew. Chem. Int. Ed.* 2006, *45*, 1520-1543.
163. Taylor, S. S.; Yang, J.; Wu, J.; Haste, N. M.; Radzio-Andzelm, E.; Anand, G. *Biochimica Biophysica Acta, Proteins Proteomics* 2004, *1697*, 259-269.
164. Thorne, L. R.; Beauchamp, J. L. In *Gas Phase Ion Chemistry*; Bowers, M. T., Ed.; Academic Press: New York, 1984; Vol. 3, pp 41-97.
165. Tian, Z., Fattahi, A., Lis, L., Kass, S.R., *J. Am. Chem. Soc.*, 2009, *131*, 16984-16988.
166. Tian, Z.; Kass, S. R. *Angew. Chemie, Int. Ed. Engl*. 2009, *48*, 1321-1323.
167. Tian, Z.; Kass, S. R. *J. Am. Chem. Soc*. 2008, *130*, 10842-10843.
168. Tian, Z.; Wang, X. B.; Wang, L. S.; Kass, S. R. *J. Am. Chem. Soc*. 2009, *131*, 1174-1181.
169. Tse, Y. C.; Newton, M. D.; Vishveshwara, S.; Pople, J. A. *J. Am. Chem. Soc.* 1978, *100*, 4329-4331.
170. Turecek, F. *Mass Spectrom. Rev.* 2007, *26*, 563-582.

171. Uddin, K. M.; Warburton, P. L.; Poirier, R. A. *J. Phys. Chem. B* 2012, *116*, 3220-3234.
172. Uggerud, E. *Top. Curr. Chem*. 2003, *225*, 3-36.
173. Walsh, C. *Enzymatic Reaction Mechanisms*; W. H. Freeman: San Francisco, 1979.
174. Wang, X. B.; Broadus, K. M.; Wang, L. S.; Kass, S. R. *J. Am. Chem. Soc.* 2000, *122*, 8305-8306.
175. Williams, E. R.; Jurchen, J. C.; Garcia, D. E.; Lemoff, A. S.; Bush, M. F. *Adv. Mass Spectrom.* 2004, *16*, 79-94.
176. Wyttenbach, T.; Bowers, M. T. *Chem. Phys. Lett.* 2009, *480*, 1-16.
177. Xu, S.; Nilles, J. M.; Bowen, Jr., K. H. *J. Chem. Phys.* 2003, *119*, 10696-10701.
178. Yang, G.; Zu, Y.; Liu, C.; Fu, Y.; Zhou, L. *J. Phys. Chem. B* 2008, *112*, 7104-7110.
179. Yu, D.; Armstrong, D. A.; Rauk, A. *Can. J. Chem.* 1992, *70*, 1762-1772.
180. Zhang, X. X.; Oscarson, J. L.; Izatt, R. M.; Schuck, P. C.; Li, D. *J. Phys. Chem*. *B* 2000, *104*, 8598-8605.
181. Zhang, Y.; Kua, J.; McCammon, J. A. *J. Am. Chem. Soc*. 2002, *124*, 10572-10577.
182. Zhang, Z.; Schreiner, P. R. *Chem. Soc. Rev.* 2009, *38*, 1187-1198.
183. Zhao, Y.; Truhlar, D. G. *Acc. Chem. Res.* 2008, *41*, 157-167.
184. Zhao, Y.; Truhlar, D. G. *J. Phys. Chem. A* 2008, *112*, 1095-1099.
185. Zhao, Y.; Truhlar, D. G. *Theor. Chem. Acc.* 2008, *120*, 215-241.
186. Zhu, H.; Blom, M.; Compagnon, I.; Rijs, A. M.; Roy, S.; von Helden, G.; Schmidt, B. *Phys. Chem. Chem. Phys.* 2010, *12*, 3415-3425.
187. Zhu, X.; Larsen, N. A.; Basran, A.; Bruce, N. C.; Wilson, I. A. *J. Biol. Chem.* 2003, *278*, 2008-2014.